Microcontroller (MCU) Based Simplified Optimal Trajectory Control (SOTC) for High-Frequency LLC Resonant Converters

Chao Fei

Thesis submitted to the Faculty of the
Virginia Polytechnic Institute and State University
in partial fulfillment of the requirements for the degree of

Master of Science
in
Electrical Engineering

Qiang Li, Chair
Fred C. Lee, Co-chair
Dong S. Ha

May 1st, 2015
Blacksburg, Virginia

Keywords: Digital control, optimal trajectory control, LLC resonant converter, Microcontroller

Microcontroller (MCU) Based Simplified Optimal Trajectory Control (SOTC) for High-Frequency LLC Resonant Converters

Chao Fei

(Abstract)

The LLC resonant converter has been widely used as a DC-DC converter due to its high efficiency, high power density and hold-up capability in power supplies for communication systems, computers and consumer electronics. Use of the high-frequency LLC converter has also been increasing in recent years due to its high power density and integrated magnetics, which reduce the total cost. With the fast development of wideband gap devices and novel magnetic materials, the trend of pushing switching frequency higher continues.

However, the control characteristics of the LLC resonant converter are much more complex than that of the PWM converter due to the dynamics of the resonant tank. This paper employs state-trajectory analysis to describe and analyze the behavior of the resonant tank. Control methods based on state-trajectory analysis were used to solve the challenges in the control of the LLC resonant converter, including unpredictable dynamics, burst mode for light-load efficiency, soft start-up and short circuit protection.

Additionally, digital controllers are gradually taking the place of analog controllers in the control of the LLC resonant converter due to the advantages of the digital controllers over the analog controllers, such as their ability to be flexible and re-configurable, capable of non-linear

control, and able to communicate with other controllers. Among the digital controllers, cost-effective microcontrollers (MCU) are preferred for industrial applications. Because of the advantages of the state-trajectory control and the industrial preference in the cost-effective digital controllers, it would be of great benefit to apply state-trajectory control to high-frequency LLC converters with cost-effective digital controllers.

This thesis investigates the impact of digital delay on state-trajectory control. Simplified Optimal Trajectory Control (SOTC) for LLC converters is further simplified so that SOTC can be achieved with cost-effective digital controllers. Furthermore, the limitations caused by digital controller are explained in detail, and methods are proposed to apply the SOTC to high frequency LLC converter is proposed. A detailed analysis of fast load transient response, soft start-up, burst mode for light-load efficiency and synchronous rectification (SR) driving is provided.

Multi-step SOTC for fast load transient response is proposed to apply cost-effective digital controllers to high-frequency LLC converters; SOTC for soft start-up with only sensing Vo is proposed to minimized the impact of digital delay on state-trajectory control; SOTC for burst mode with multi-step is proposed to eliminate the limitation of minimum off-time caused by digital controllers in constant burst-on time control; a generalized adaptive SR driving method using the ripple counter concept is proposed to significantly reduce controller resource utilization for the SR control of high-frequency LLC converters.

The whole control system is demonstrated on a 500kHz 1kW 400V/12V LLC converter with a 60MHz MCU, which integrates all the proposed control methods.

Acknowledgments

First I would like to express my sincere gratitude to my advisor, Dr. Qiang Li, for his guidance and encouragement. It is he that helped me go through the most difficult time at the beginning of my research. His passion towards research always inspires me. I am also very grateful to my co-advisor, Dr. Fred C. Lee, who offered me the opportunity to study at Center for Power Electronics Systems (CPES), Virginia Tech, and always shares a great amount of knowledge, suggestions, and experience with me.

Special thanks to Dr. Weiyi Feng, from whom, I learnt all the details about state-trajectory control. Special thanks to Dr. Daocheng Huang for the help in the design of the resonant converters.

I would also like to thank all the great staff in CPES: Ms. Teresa Shaw, Ms. Marianne Hawthorne, Ms. Teresa Rose, Ms. Linda Long, Mr. David Gilham, and Dr. Wenli Zhang.

It is a great pleasure to work with the talented colleagues in the Center for Power Electronics Systems (CPES). Without your help, this work cannot be accomplished. I would like to thank Dr. Mingkai Mu, Dr. Yingyi Yan, Mr. Shu Ji, Mr. Sizhao Lu, Dr. Pei-Hsin Liu, Dr. Yipeng Su, Mr. Zhongsheng Cao, Mr. Xuebing Chen, Mr. Mohamed Ahmed, Mr. Syed Bari, Mr. Junjie Feng, Dr. Dongbin Hou, Mr. Xiucheng Huang, Dr. Weijing Du, Mr. Zhengrong Huang, Mr.Yang Jiao, Mr. Bin Li, Ms. Virginia Li, Mr. Tao Liu, Mr. Zhengyang Liu, Ms. Yincan Mao, Mr. Shuilin Tian, Mr. Yuchen Yang, Mr. Wei Zhang. I cherish the wonderful time together and the great friendship.

With much love and gratitude, I want to thank my parents: my father Yongqing Fei and my mother Lijun Bai for their love, encouragement, and support throughout twenty years of school.

Special thanks to the CPES PMC mini-consortium members for the funding of my research.

Table of Contents

List of Figures

List of Tables

Chapter 1. Introduction

1.1 Introduction to LLC Resonant Converter

Efforts to increase efficiency and power have been constant drivers of the development of energy conversion technology over the past decades. With the fast development of information technology, the distributed power system (DPS) architecture has been widely adopted as an industry practice. Different system architecture and design considerations are investigated to improve the efficiency and power density [1][2][3][4][5].

Currently, most existing front-end converters in distributed power systems (DPS) adopt the two-stage approach shown in Fig. 1.1. The first stage of the front-end converter consists of EMI and PFC, providing power factor correction (PFC); and the second stage, which is an isolated DC/DC converter, provides isolation and tight regulation of the dc output. The output of the front-end converter is connected to different kinds of point-of-load (POL) converters. Hence the design of each stage in the front-end converter is critical to the performance of the whole system.

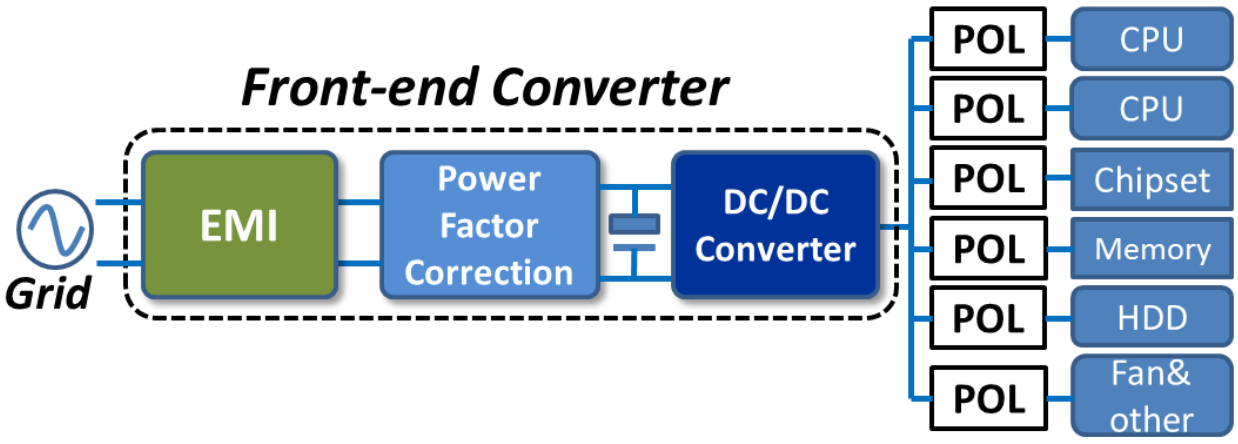

Fig. 1.1. Front-end converter in power supply for server applications

Due to economic and environmental consideration, efficiency is always a key factor to evaluate the design of a front-end converter. The pursuit of higher efficiency is even more desirable for datacenter applications, in which higher efficiency means a significant reduction of cost [6][7][8]. The 80 Plus certification program is used to classify converters based on efficiency and to promote efficient energy use in computer power supply units (PSUs) [9], as shown in Fig. 1.2. It certifies products that have more than 80% energy efficiency at 20%, 50% and 100% of the rated load, and a power factor of 0.9 or greater at 100% load. The green curve in Fig. 1.2 is the industry benchmark which uses the LLC resonant converter as the DC/DC converter.

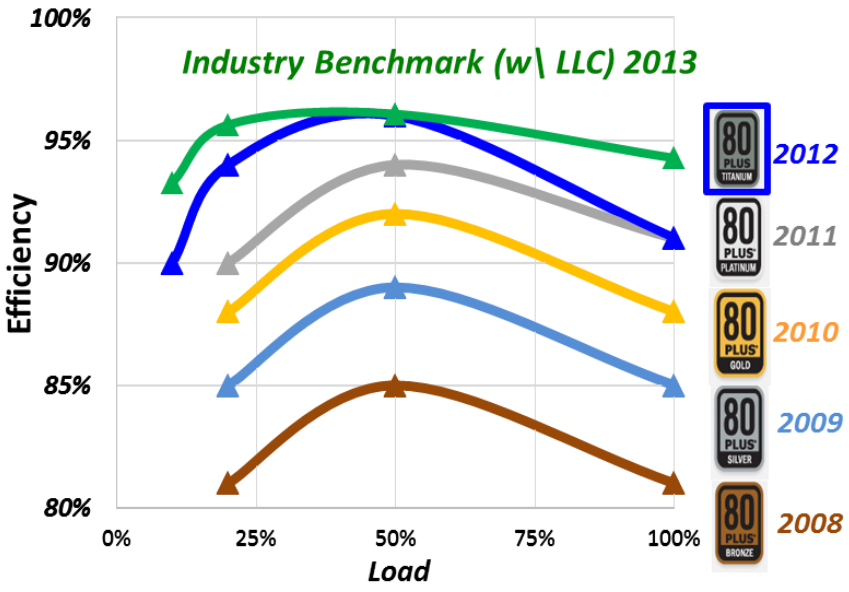

Fig. 1.2. Efficiency requirement of 80 Plus certification program

In addition to the efficiency requirements, the power density of front-end converters keeps increasing with the development of new components and materials [4]. Higher power density will eventually reduce the total converter cost and accommodate more equipment in the existing infrastructures. Over the past ten years, the power density of front-end commercial converters

has increased sevenfold, as shown in Fig. 1.3. This trend will continue with the development of novel semiconductor devices and magnetic materials [10][11][12][13][14].

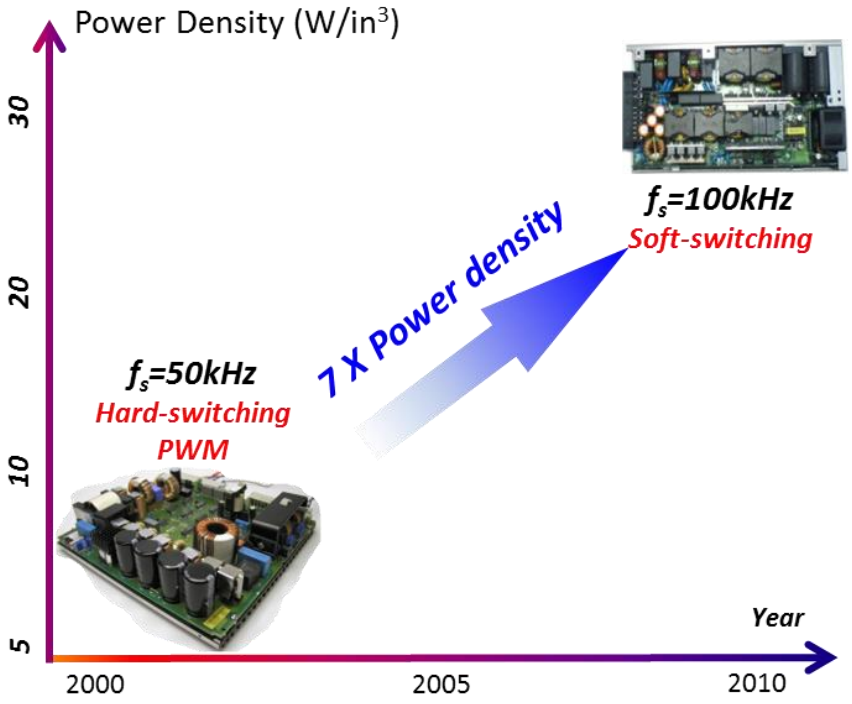

Fig. 1.3. Trend in power density of front-end converters

Another important consideration in the design of the front-end converters is the hold-up capability, which requires the converter to maintain the regulated output voltage for about 20ms when the input ac line is lost. As shown in Fig. 1.4, during the hold-up time, all the energy transported to the load comes from the holdup capacitor C_{hold}, which is the output capacitor in the PFC stage. The requirements of C_{hold} are determined by the system power level and the input voltage range of the DC/DC converter stage. A wider DC/DC stage input voltage range means better hold-up capability and fewer bulky hold-up capacitors. Therefore, the DC/DC converter must be able to operate within a wide range of input voltages to improve the power density of the whole front-end converter.

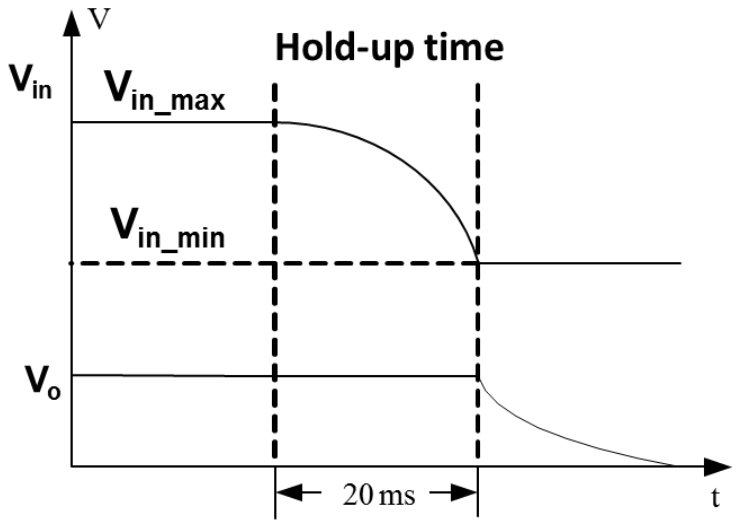

Fig. 1.4. Hold-up requirement for front-end converter

For the DC/DC converter in the front-end converter, a hard-switching PWM converter cannot achieve high efficiency and high power density at the same time, because the switching loss increases as the switching frequency is increased to improve power density. Soft-switching PWM converters, such as the phase-shift full-bridge PWM converter and the asymmetrical half-bridge PWM converter, have been used as the DC/DC stage for a long time [15][16][17][18]. However, the soft-switching PWM converters have to sacrifice normal operation efficiency to extend their input voltage range for hold-up purpose. If the converter is designed to achieve high gain for hold-up, which means a larger duty cycle at low line, the duty cycle at normal operation would become much smaller, leading to a larger primary-side RMS current.

A promising candidate for use in the DC/DC stage is the resonant converter. Resonant converters can achieve very low switching loss because they use soft-switching, and are thus able to operate at high switching frequencies while still maintaining good efficiency[19][20][21]. Among the resonant converters, the LLC resonant converter shown in Fig. 1.5, has been widely used as the DC/DC stage in the front-end converter [22][23][24][25][26]. The LLC resonant

converter is able to achieve both high gain for hold-up purpose and good efficiency for normal operation [27][28].

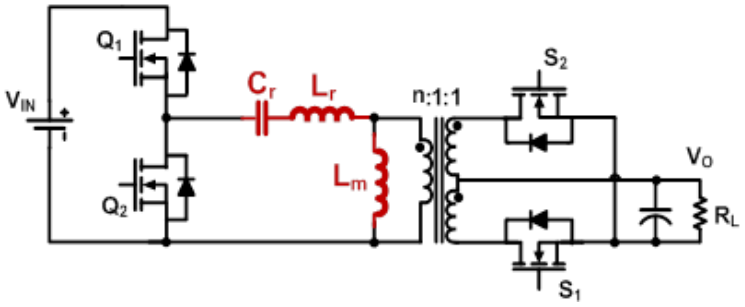

Fig. 1.5. LLC resonant converter

The DC characteristic of the LLC converter is shown in Fig. 1.6. During normal operation, the LLC converter operates around the resonant frequency ($f_S = f_O$), which is the optimal point because it can achieve zero-voltage-switching (ZVS) for the primary switches and zero-current-switching (ZCS) for the synchronous rectifiers (SR). In addition, the voltage gain at resonant frequency is always 1 for different load condition, which means converter design can be optimized to achieve good efficiency for a wide load range. During the hold-up time, the switching frequency is reduced to achieve high gain without sacrificing efficiency during normal operation.

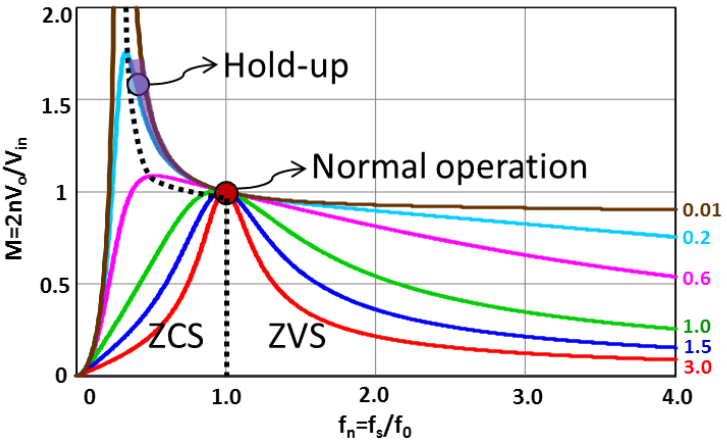

Fig. 1.6. Gain curve of the LLC resonant converter

Although the LLC converter is already popular for use in the front-end converter, there are still some challenges in the control of the LLC resonant converter due to the dynamic behavior of the resonant tank.

1.2 Challenges in Control of LLC Resonant Converter

Challenges in the control of the LLC resonant converter include large current/voltage stresses during start-up, unpredictable dynamic behavior, burst mode for light load efficiency, and driving the synchronous rectifiers (SRs).

The start-up is the most critical process in the control of the LLC resonant converter. There will be very large current and voltage stresses if the process is not well controlled. Fig. 1.7(a) shows the start-up waveform of a commercial controller, and Fig. 1.7(b) shows the frequency trajectory on the gain curve during start-up. Fig. 1.7 shows that the controller's start-up frequency is 1.5 times the resonant frequency. Since the start-up frequency is not high enough, the stresses are very large at the beginning.

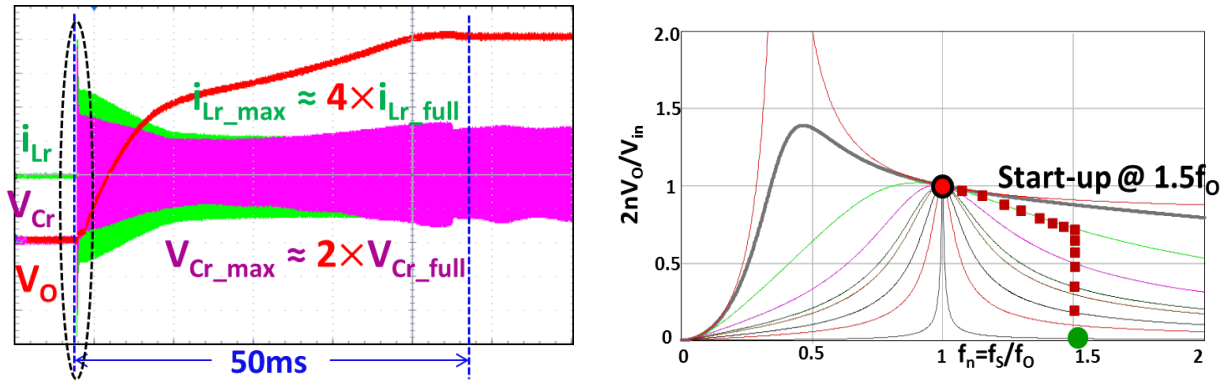

(a) Time-domain waveform (b) Frequency trajectory on gain curve

Fig. 1.7. Start-up of a commercial LLC controller which starts at $1.5 \cdot f_O$

Even if the start-up frequency is sufficient high, there are still large stresses during the start-up with a commercial controller, as shown in Fig. 1.8. The start-up frequency is five times the resonant frequency, and at the beginning, the voltage and current stresses are small. However, during the soft start-up process, the switching frequency decreases too quickly, and the large voltage and current stresses still occur, which triggers the over-current protection. Then the switching frequency increases a little to limit the stresses, but there are still large stresses and it takes a long time to start up.

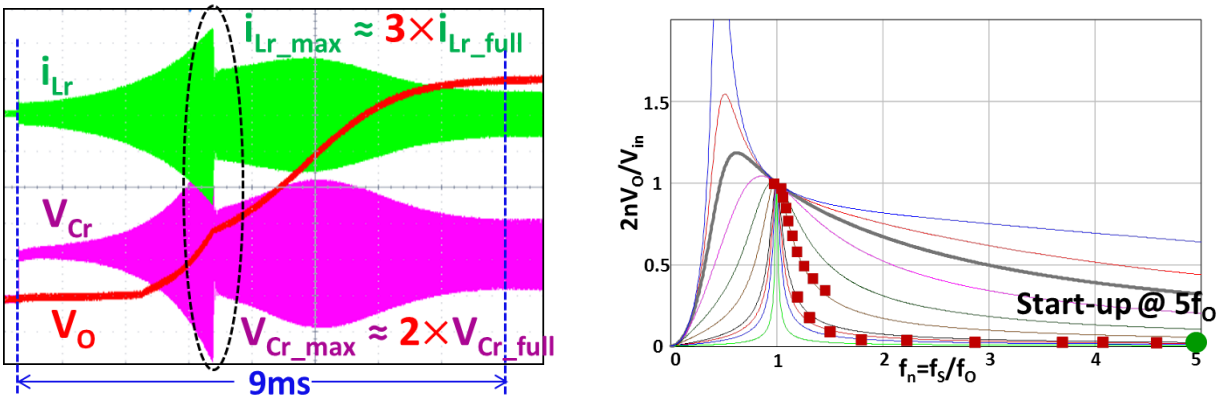

(a) Time-domain waveform (b) Frequency trajectory on gain curve

Fig. 1.8. Start-up of a commercial LLC controller which starts at $5 \cdot f_O$

Besides start-up, unpredictable dynamic behavior is also a challenge in the control of the LLC converter. Conventional LLC controllers employ a linear compensator, and control the switching frequency to regulate the output voltage. The control scheme used in conventional LLC controllers is shown in Fig. 1.9(a). Due to the complex dynamic behavior and small-signal mode of resonant converter, the bandwidth of the closed-loop control for the resonant converter cannot use high-bandwidth design for the whole operation range [22][29][30][31][32]. The transient performance with conventional LLC controllers is quite poor, and the dynamic oscillation and settling time are both large. The state-trajectory under a load transient with a conventional LLC

controller is shown in Fig. 1.9(b). State-trajectory analysis is used to describe the steady-state and transient behaviors of the resonant converter. By normalizing the resonant capacitor voltage V_{Cr} with the voltage factor V_{IN}, and resonant current i_{Lr} with the current factor V_{IN}/Z_O (Z_O is the characteristic impedance of resonant tank, $Z_O = \sqrt{\frac{L_r}{C_r}}$), the state-trajectory can be drawn with an x-axis of normalized V_{Cr} and an y-axis of normalized i_{Lr}, as shown in Fig. 1.9(b).

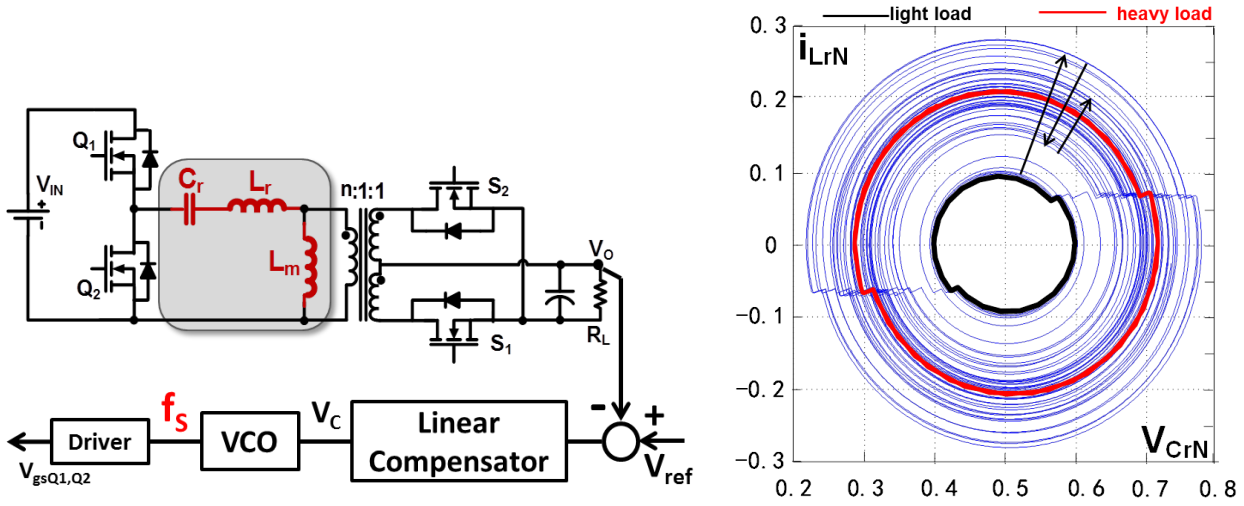

(a) Control scheme (b) State-trajectory under load transient

Fig. 1.9. Conventional linear control of the LLC converter

Light-load efficiency is also very important for power conversion as the efficiency requirements become higher and higher, and burst mode is widely used to improve the light-load efficiency [33]. Variable frequency control methods have already been adopted to improve light-load efficiency in PWM converters [34][35]. The intent of using variable frequency control is to decrease the switching frequency to reduce these load-independent losses. For the LLC converter, burst-mode control is also used to improve light-load efficiency by periodically blocking the switch gate driving signals [36]. Burst mode in LLC converters is a highly dynamic process and difficult to control, since the resonant tank rapidly changes between idle mode and

high-power mode periodically. It is actually very difficult to fix to the optimal efficiency point during burst on-time, as shown in Fig. 1.10. The resonant current shrinks during burst on-time, and in terms of state-trajectory, the energy in the resonant tank is becoming smaller and smaller, and cannot be fixed to a given circle.

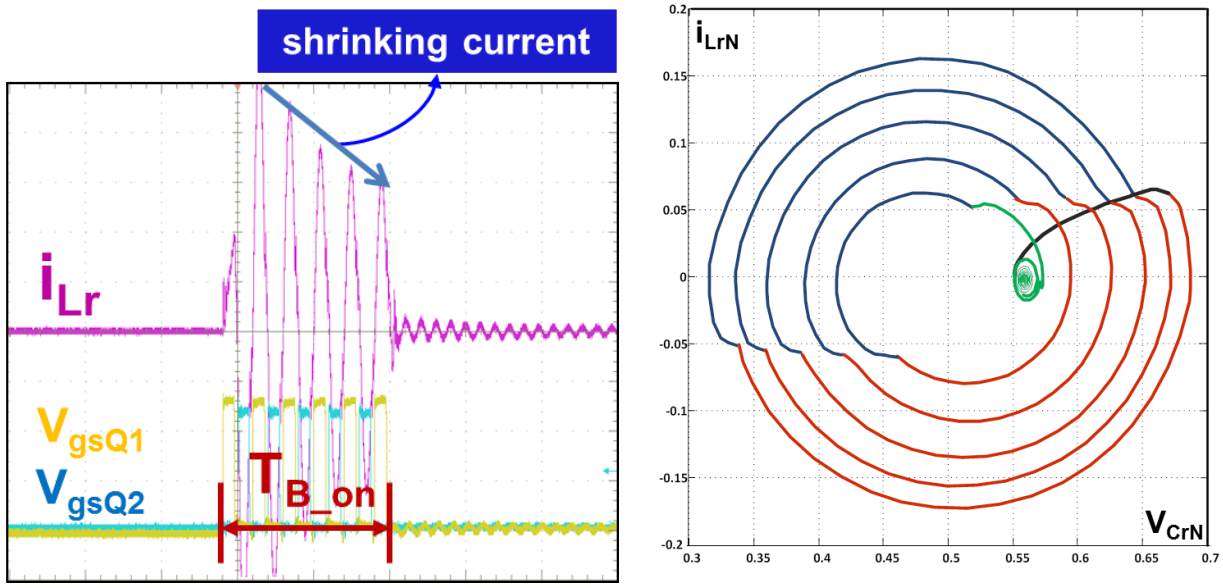

(a) Time-domain waveform (b) State-trajectory

Fig. 1.10. Conventional burst mode for LLC converter

To guarantee high efficiency for large-output-current applications such as servers and telecom applications, synchronous rectifiers (SR) are necessary to reduce the conduction loss. However, the efficiency optimization of the SR is highly dependent on the SR driving signals. The desired SR gate-driving signals for the LLC resonant converter are shown in Fig. 1.11. Although the turn-on of the SR is synchronous with the primary switch, the turn-off of the SR is not in phase with the primary driving signal. When the switching frequency is below the resonant frequency, the SR should be turned off earlier than the main switch. Otherwise, there will be energy circulating through the SR, and the RMS current will increase. When the switching frequency is

above the resonant frequency, the SR should be turned off a bit later than the main switch. Otherwise, there will be a large current going through the paralleled body diode.

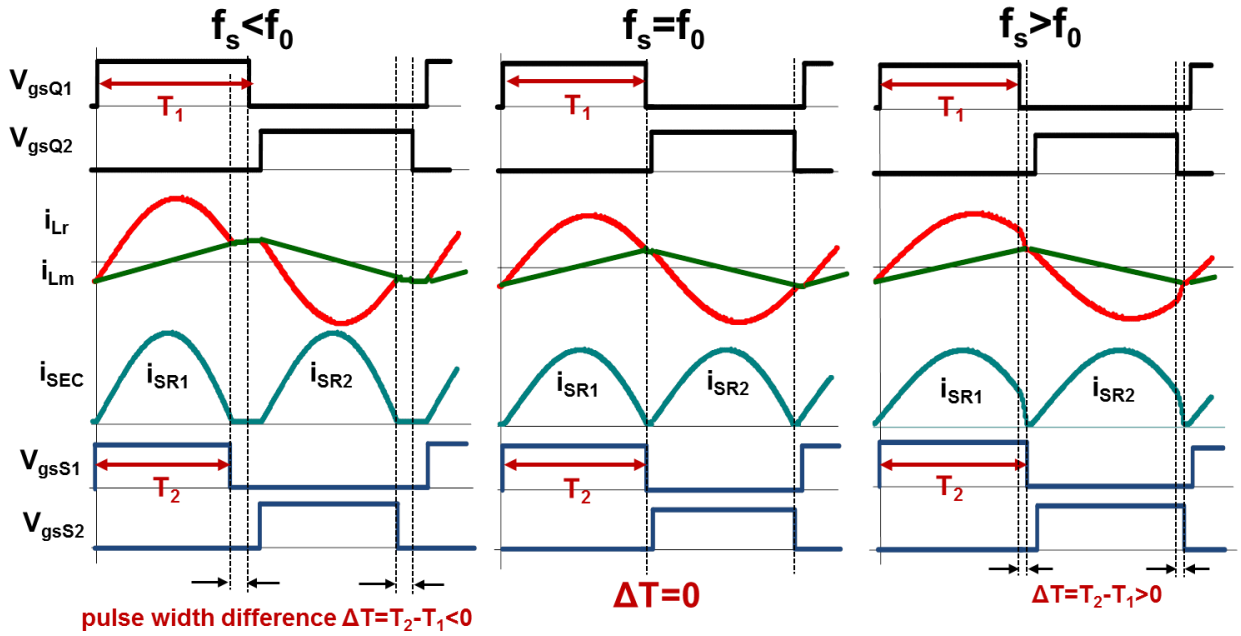

Fig. 1.11. Desired SR driving signal under different switching frequency

These challenges in the control of the LLC resonant converter are critical for the converter performance. They are related to either the stress of the converter, which may break down the whole system if not well controlled; or the efficiency of the converter, which is keeps drawing more and more attention.

1.3 Optimal Trajectory Control (OTC) for Series Resonant Converter

Due to the unpredictable dynamic behavior of the resonant tank and the complex small-signal model of the resonant converter, state-trajectory analysis and control were employed to describe and analyze the behavior of the resonant tank for the series resonant converter (SRC) in [37] and [38]. The optimal trajectory control was employed to control the SRC to achieve the optimal

transient performance. The control scheme is shown in Fig. 1.12(a) and the state-trajectory under control step change is shown in Fig. 1.12(b). When the control has a step change, the state-trajectory can be controlled from a heavy-load trajectory (the brown trajectory) to a light-load trajectory (the black trajectory) within one switching cycle (the red trajectory).

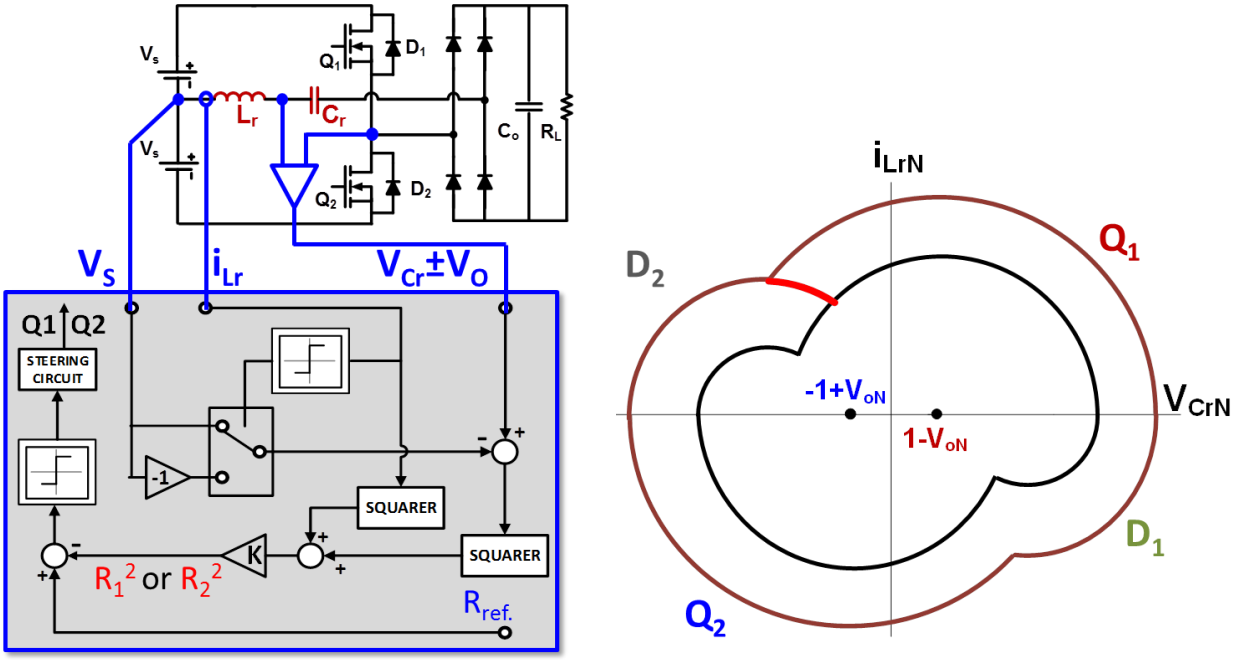

(a) Control scheme (b) State-trajectory of control step change

Fig. 1.12. The optimal trajectory control for SRC

However, the LLC resonant converter has three resonant elements. If the concept of sensing all state variables and controlling the exact trajectory is applied to the LLC converter, the control of the LLC converter would be even more complex than SRC. Moreover, the additional sensing of a magnetizing inductor is required for the LLC converter, which may cause a loss of integration. Furthermore, since OTC controls the radius of the trajectory, the LLC has a fast load transient response and inherent start-up and short-circuit protection. However, there has been no method defined for using state-trajectory control to solve the challenges in burst mode.

1.4 Simplified Optimal Trajectory Control (SOTC) for LLC Resonant Converters

Simplified optimal trajectory control (SOTC) for LLC resonant converters is used to simplify the control scheme and improve the transient performance [40]. The same concept is used for the soft start-up and the burst mode of the LLC converter [41][42].

The SOTC for the LLC resonant converter senses the load current and modifies the pulse widths of the primary-side driving signals, which works as a load current feed-forward loop and significantly improves transient response. The control scheme is quite simple compared with the OTC, as shown in Fig. 1.13(a), and the transient response improvement is significant, as shown in Fig. 1.13(b).

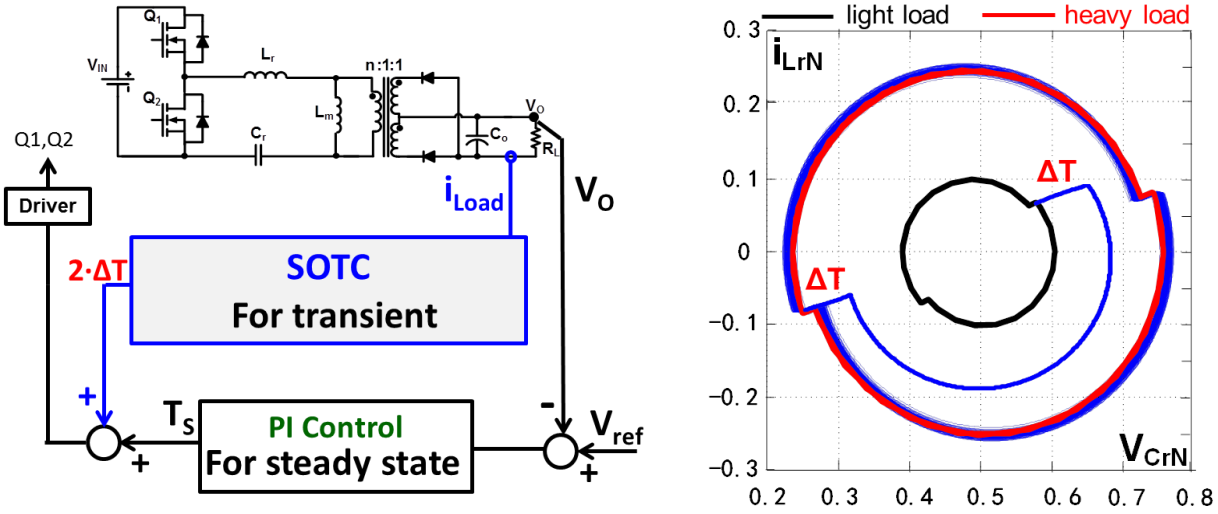

(a) Control scheme (b) State-trajectory of load step-up

Fig. 1.13. Simplified optimal trajectory control (SOTC) for the LLC converters

The OTC for soft start-up of LLC converter is divided into three stages, as shown in Fig. 1.14. Stage 1 sets an asymmetrical current-limiting band to settle resonant voltage to half of input

voltage (for half bridge LLC converter). Stage 2 sets a symmetrical current-limiting band to optimize energy delivery. Stage 3 simply decreases the switching frequency until V_O reaches the reference voltage.

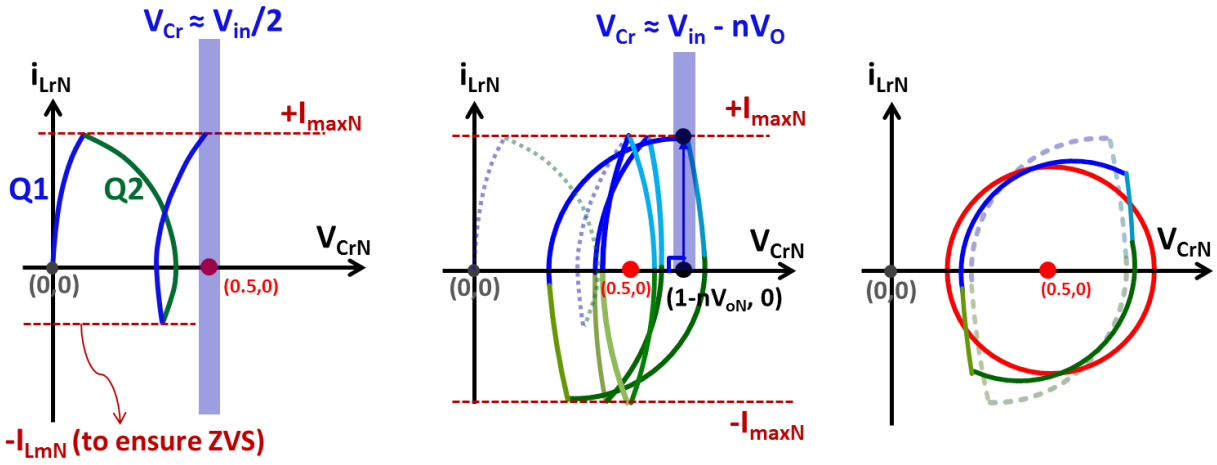

(a) Stage 1 (b) Stage 2 (c) Stage 3

Fig. 1.14. The optimal trajectory control for soft start-up of LLC converter

The OTC for soft start-up is based on the graphical state-trajectory analysis of the resonant tank. hence it can minimize the resonant tank stresses, thus ensuring a safe start-up process and optimizing energy delivery. Fig. 1.15 shows the simulation results of the optimal trajectory control for soft start-up. The simulation results show that the maximum resonant current during the whole start-up process is only a little bit larger than the full-load steady state, and the start-up frequency trajectory on the gain curve is smooth.

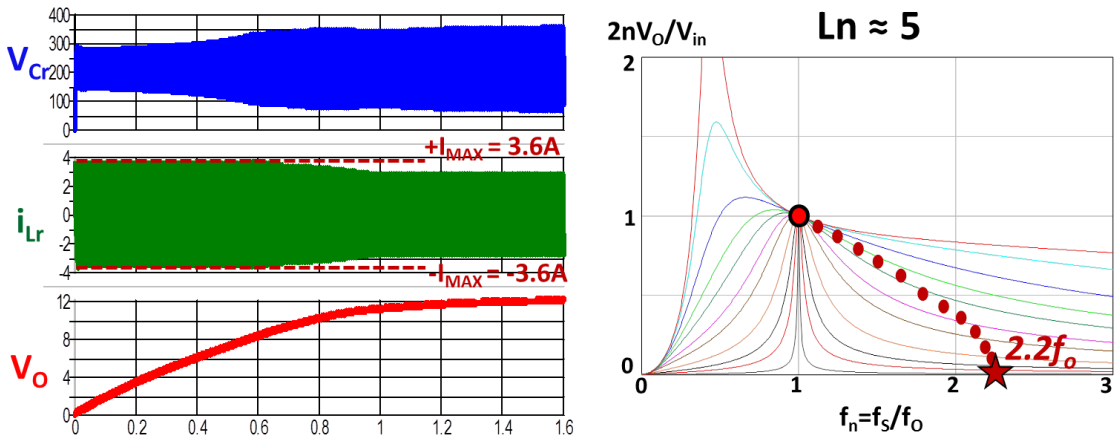

(a) Simulated time-domain waveform (b) Frequency trajectory on gain curve

Fig. 1.15. Simulation of the optimal trajectory control for soft start-up

For burst-mode control, the optimal trajectory control employs a three-pulse switching pattern during the burst on-time. By optimizing the first pulse width, the state variables are settled to the steady state of the highest efficiency load, and then the next two pulse operation follows this steady-state trajectory to achieve high burst efficiency. Moreover, with constant burst on-time control, even when the load changes, the burst on-time with the optimal three-pulse switching pattern can still be maintained by modulating the burst off-time. The time-domain waveform and corresponding trajectory are shown in Fig. 1.16.

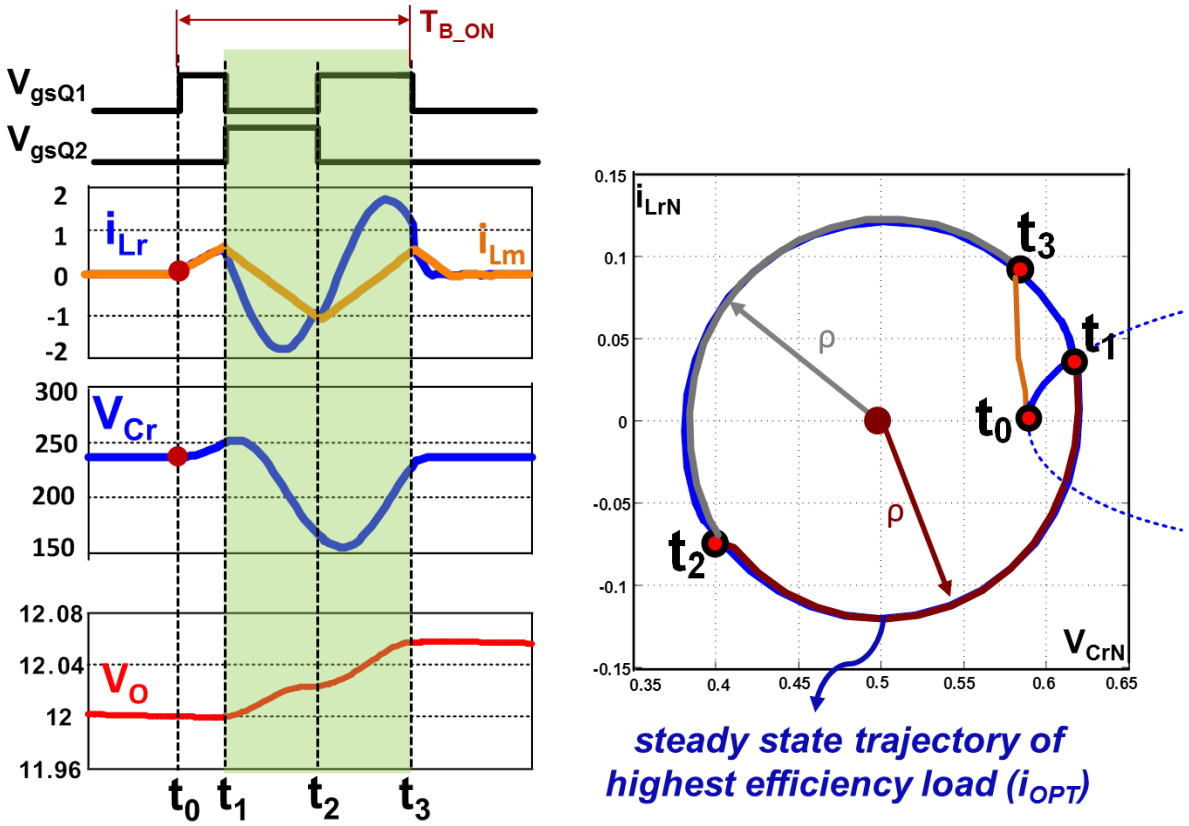

(a) Time-domain waveform (b) State-trajectory

Fig. 1.16. The optimal trajectory control of burst mode for LLC converter

Digital controllers are becoming more and more popular, and among the digital controllers, cost-effective microcontrollers are preferred in power supplies for telecom applications, servers and other applications [43][44][45]. The high-frequency LLC converter has increased in popularity in recent years because of its high power density and integrated magnetics, which reduce the total cost.

Furthermore, although different functions of state-trajectory control have been proposed and proved to have overwhelming performance over the linear control methods, state-trajectory control requires a very high-performance digital controller combined with an analog controller to implement the state-trajectory control functions. Thus it is important to investigate how to

implement SOTC using low-cost microcontrollers, as shown in Fig. 1.17, and furthermore, to integrate all the functions within one cost-effective microcontroller.

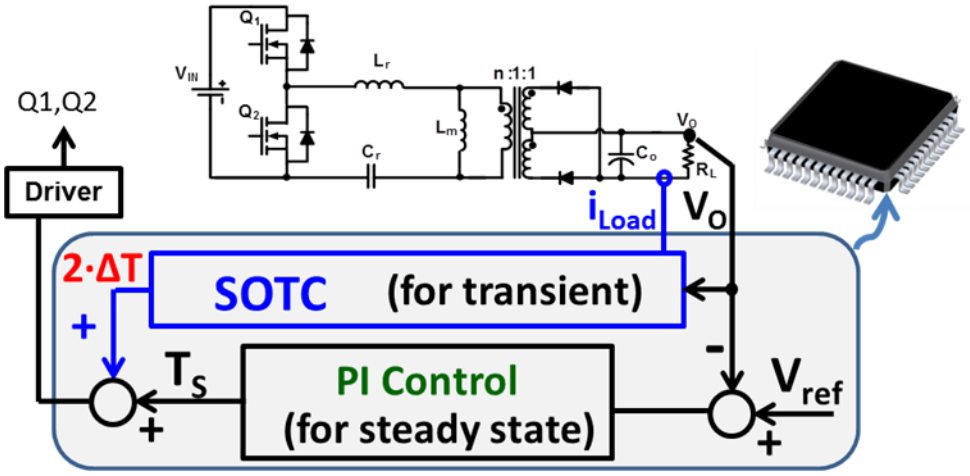

Fig. 1.17. SOTC implemented by microcontroller

1.5 Thesis Outline

The main objective of this thesis is to achieve simplified optimal trajectory control (SOTC) for an LLC resonant converter with a cost-effective digital controller, and develop methodology to apply the SOTC to the high-frequency LLC converter.

In Chapter 1, the applications, benefits and future trends of the LLC resonant converter are introduced. The LLC converter is widely used as the DC/DC converter in front-end converters for the IT industry due to its hold-up capability, high efficiency and high power density. However, there are several challenges in the control of the LLC converter caused by the complexity of the resonant tank. Optimal trajectory control (OTC) can solve these challenges, but it requires high-performance digital controllers, which are not feasible for industrial applications. Hence it is necessary to investigate how to achieve optimal trajectory control with cost-effective digital controllers.

In Chapter 2, SOTC is investigated and improved to increase the maximum switching frequency limitation for a given cost-effective controller. Then the multi-step SOTC is proposed to further solve the maximum switching frequency limitations. With multi-step SOTC, low-cost controllers can be used to control high-frequency LLC converters with state-trajectory control. The number of steps in the multi-step SOTC is determined by the speed of the controllers and the switching frequency of the LLC converter.

Chapter 3 investigates the implementation of OTC for soft start-up with a commercial low-cost MCU. SOTC for soft start-up of LLC converter with only sensing Vo is proposed. OTC for soft start-up is universally applicable but requires an additional analog circuit and proper PWM module configuration. SOTC for soft start-up doesn't need additional circuits and only needs to sense V_O, but requires a case-by-case look-up table for different power stages. Both methods can achieve optimal trajectory control for soft start-up with a low-cost MCU.

Chapter 4 explores the use of OTC for the burst mode of the LLC converter, and its limitations in the high-frequency LLC converter with digital implementation are explained in detail. The use of SOTC for burst mode with adaptive burst on-power and adaptive multi-step control is proposed to extend the burst operation range. In addition, the optimized transition process between burst mode and normal operation is proposed to combine burst mode with normal operation.

In Chapter 5, adaptive SR-driving for the LLC converter is investigated and its limitations with digital implementation are explained in detail. The adaptive SR driving method based on ripple detection and the adaptive SR driving method based on the ripple counter concept are proposed. The first proposed method is suitable for conventional LLC converters where the resonant frequency is below 150kHz. The second proposed method is suitable for high-frequency

LLC converters. Both methods can be achieved with low-cost digital controllers and very little CPU utilization.

Chapter 6 presents the summary of work done in this thesis and explores options for future work.

Chapter 2. Multi-step Simplified Optimal Trajectory Control (SOTC) for LLC Converters Implemented by Microcontroller

2.1 Introduction

The LLC resonant converter has been widely used as a DC-DC converter due to its high efficiency and hold-up capability. However, compared with PWM converter, the control characteristics of the resonant converter are much more complex due to the dynamics of the resonant tank. It is still a challenge to improve the load transient response of the LLC converter.

Several approaches have been tried to describe the control characteristics and improve the transient response of the resonant converters. One approach is using small-signal model of the resonant converter [29][30][31]. However, since the switching frequency of the resonant converter is around the resonant frequency, it is hard for small-signal model to describe the dynamics of the resonant converters of the whole operating range. For LLC converter, the simulation-based small-signal model has been employed, showing that the transfer function is quite complex under different operating points [22]. Recently, another approach based on current-mode control was proposed to improve the transient response of resonant converter [46][47][48]. The variation of control-to-output transfer function of current-mode control under different operating points is smaller than the conventional voltage-mode control due to the feedback from resonant tank. However, the implementation of this approach is quite complex, requiring additional logic circuits and sensing circuits to control the switching instants of primary-side switches.

Different from the small-signal approach, state-trajectory analysis and control can better describe and analyze the behavior of the resonant tank. It is first applied to the series resonant converter (SRC) [37][38][39]. The Optimal Trajectory Control (OTC) for SRC can control the resonant tank of SRC to follow the desired trajectory exactly. However, the LLC resonant converter has three resonant elements, which causes the analysis and control of the LLC converter to be more complex than the SRC. Simplified Optimal Trajectory Control (SOTC) was proposed to improve the transient response of the LLC converter [40].

In this chapter, firstly, the implementation of Simplified Optimal Trajectory Control (SOTC) and its improvement are introduced. Secondly, the multi-step Simplified Optimal Trajectory Control (SOTC) is proposed to achieve fast load transient response of the LLC converter with low-cost digital controllers. The proposed Multi-step SOTC consists of two main concepts: the first concept is calculating trajectory based on only output voltage and load current, which simplifies the whole control scheme; the second concept is settling the resonant tank within multi-step, which allows low-cost controllers to control the high frequency LLC converters. The number of steps in multi-step SOTC is determined by the speed of controller and the switching frequency of LLC converter. Finally, experimental results on a 500kHz LLC converter are presented.

2.2 Implementation of Simplified Optimal Trajectory Control (SOTC) and Its Improvement

Different from previous state-trajectory control methods, the Simplified Optimal Trajectory Control (SOTC) calculates the trajectory based on only the output voltage and the load current, rather than the resonant current and/or the resonant voltage. This is because the steady-state

trajectory is determined by the output voltage and the load current under certain input voltage range, regardless of switching frequency.

Fig. 2.1 is an example of the state-trajectory of LLC converter operating at around resonant frequency. The x-axis is normalized resonant current, and the y-axis is normalized resonant voltage. The current normalizing factor is $V_{in}/\sqrt{L_r/C_r}$, and the voltage normalizing factor is V_{in}. Firstly, the centers of trajectory are determined by the output voltage. When the high-side switch is on, the voltage across resonant tank is $V_{in} - nV_o$, which is $O_1(1 - nV_{oN}, 0)$ in the state-plane. When the low-side switch is on, the voltage across resonant tank is nV_o, which is $O_2(nV_{oN}, 0)$ in the state-plane. The radius R of the trajectory is determined by the load current. Take switching frequency at around resonant frequency as an example, R is expressed as

$$\boldsymbol{R = \frac{\sqrt{2}\cdot I_{Lr\_RMS}}{V_{in}/\sqrt{L_r/C_r}}} \tag{2.1}$$

In which, I_{Lr_RMS} is the RMS value of the resonant current, expressed as:

$$I_{Lr\_RMS} = \frac{1}{4\sqrt{2}}\sqrt{\frac{n^4 {V_O}^2 T^2}{{L_m}^2} + 4\pi^2\left(\frac{I_{Load}}{n}\right)^2} \tag{2.2}$$

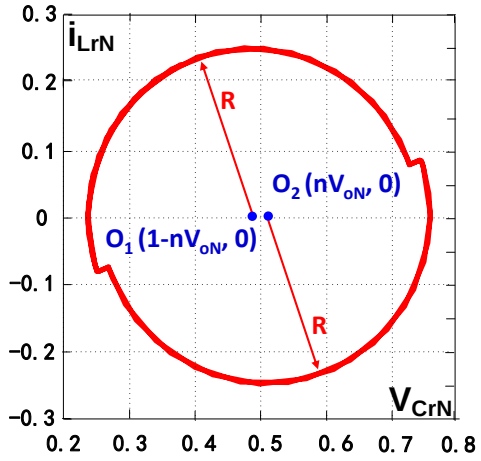

Fig. 2.1 State-trajectory of LLC converter operating at around resonant frequency

The Simplified Optimal Trajectory Control (SOTC) uses linear regulator to eliminate the steady-state error during steady state, and uses SOTC to achieve fast response during load transient. Based on the output voltage and load current, the steady-state trajectory before and after load transient can be calculated, then the required pulse width of primary driving signal during load transient can be obtained by SOTC. The control scheme of SOTC is shown in Fig. 2.2.

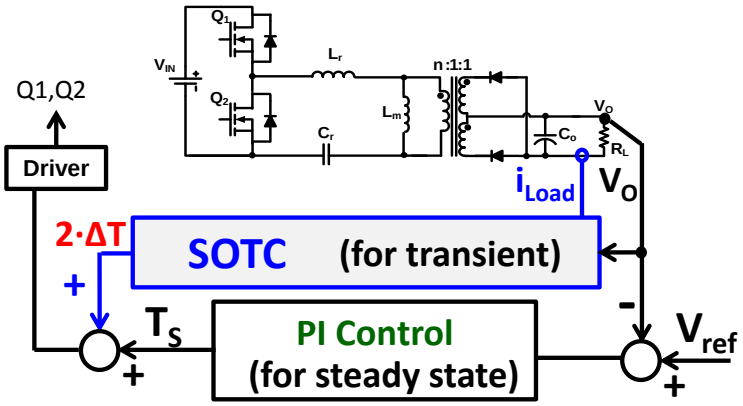

Fig. 2.2. Control scheme of SOTC

The state-trajectory during load step-up with SOTC is shown in Fig. 2.3. Initially, the converter runs at light load condition, corresponding to the black circle in the state-plane. Immediately after load step-up, SOTC would increase primary driving signal by ΔT_{UP} to boost resonant tank energy. Then the linear regulator eliminates the steady-state error and the converter is stable at heavy load, corresponding to the red circle in the state-plane.

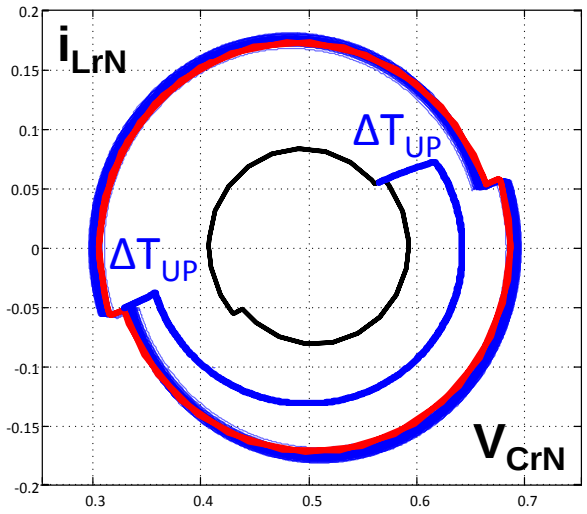

Fig. 2.3. State-trajectory during load step-up with SOTC

Since digital delay is a key factor impacting transient performance, sampling and calculation time is allocated within one switching cycle to optimize the transient response. Fig. 2.4 is an example of sampling and calculation during load step-up for implementation of SOTC with one switching cycle digital delay. Fig. 2.5 shows the comparison of ideal SOTC and MCU based SOTC.

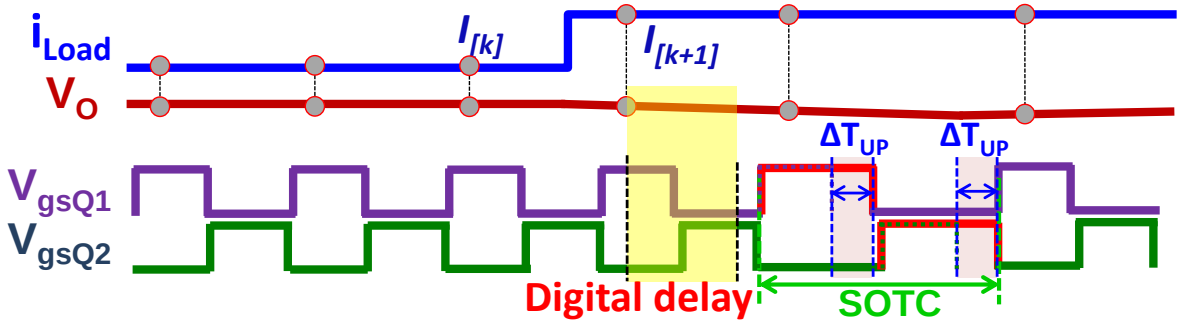

Fig. 2.4. Sampling and calculation during load step-up for implementation of SOTC with one switching cycle digital delay

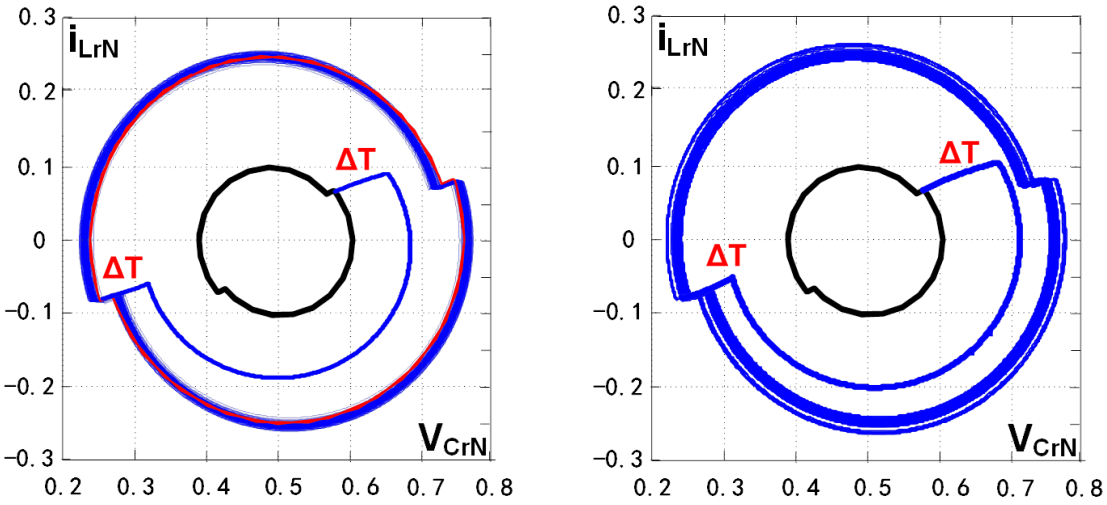

(a) Ideal SOTC without delay; (b) MCU based SOTC (one switching cycle delay)

Fig. 2.5. Comparison of ideal SOTC and MCU based SOTC

It is shown clearly in Fig. 2.5 that less delay mean better load transient performance. However, for digital control, the delay is discrete so there is no need to use the best controller to minimize the delay. For industrial application, the switching frequency of power stage is around 100kHz and delay can be limited within 1 switching cycle using simplified calculation proposed above when implementing by a cost-effective MCU.

In Fig. 2.4, the digital delay consists of A/D delay and calculation time. Take TI's digital controller TMS320F28027 as an example, the total digital delay is 7.2us, which means that the maximum switching frequency suitable for SOTC is 140kHz. If we want to further increase this maximum switching frequency limitation, the implementation of SOTC must be improved by reducing digital delay in SOTC.

The first step to reduce digital delay is to re-allocate the sampling time and calculation time as shown in Fig. 2.6. The A/D conversion for output voltage is finished before the beginning of present switching cycle, and then PI calculation starts at the beginning of present switching cycle

since PI calculation only needs output voltage. At the same time of PI calculation, load current is sampled and converted, and then SOTC calculation follows immediately after PI calculation, since SOTC calculation only needs load current. With the first improvement, the digital delay consists of only calculation time. With digital controller TMS320F28027, the digital delay now becomes 6.7us, and the maximum switching frequency suitable for SOTC is increased to 150kHz.

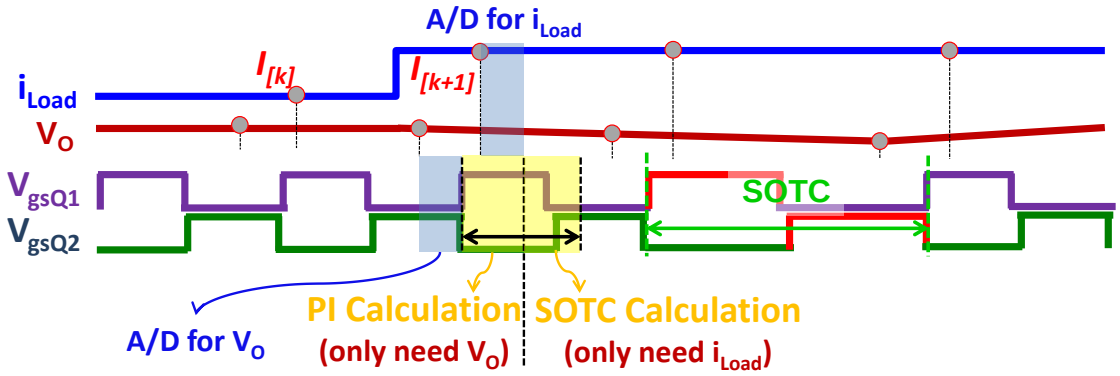

Fig. 2.6. Step 1 to improve implementation of SOTC by re-allocating sampling and calculation time

The second step to reduce digital delay is to use look-up table for SOTC calculation instead of real-time calculation. In previous implementation, the equations for ΔT_{UP} in load step-up and ΔT_{DOWN} in load step-down are expressed below:

$$\Delta \boldsymbol{T_{UP}} = \frac{\boldsymbol{L_m}\cdot\left(\boldsymbol{I_{[k]}}-\boldsymbol{I_{[k-1]}}\right)}{\boldsymbol{n}\cdot\boldsymbol{V_{in}}} \tag{2.3}$$

$$\Delta \boldsymbol{T_{DOWN}} = -\left(\mathbf{1}-\sqrt{\frac{\boldsymbol{I_{[k]}}}{\boldsymbol{I_{[k-1]}}}}\right)\cdot\frac{\boldsymbol{T}}{\mathbf{4}} \tag{2.4}$$

The real-time calculation can be replaced by look-up table to reduce the calculation time. Take a 500kHz LLC converter as an example, the look-up table is shown in Fig. 2.7. It is 3-demension table, with x-axis of $(k-1)^{th}$ sampling, y-axis of k^{th} sampling, and z-axis of ΔT.

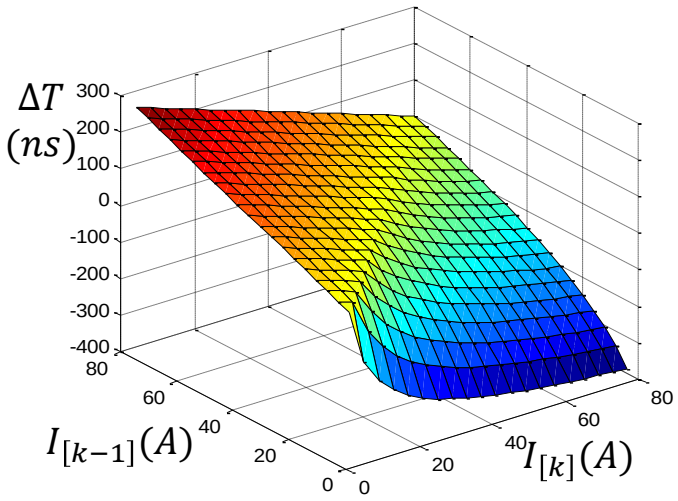

Fig. 2.7. Look-up table for ΔT calculation in SOTC for a 500kHz LLC converter

The result from look-up table is the same with that from real-time calculation, but the required CPU cycles for calculation is reduced from around 400 CPU cycles to around 240 CPU cycles. And the table occupies the RAM space equivalent to only 121 integers, which is only around 3% RAM space of TMS320F28027. With look-up table to reduce digital delay, the digital delay is reduced to 4us, and the maximum switching frequency suitable for SOTC is increased to 250kHz. Although the evaluations above are based on given controller, same analogy applies to other digital controllers.

After these steps, the implementation of SOTC is improved by optimizing the sampling points and using look-up table to reduce calculation time. With these improvements, the maximum switching frequency suitable for SOTC is improved from 140kHz to 250kHz with TMS320F28027. But there is still limitation if we want to further increase switching frequency

2.3 Proposed Multi-step Simplified Optimal Trajectory Control (SOTC)

Although the implementation of SOTC is optimized and improved, there is still a maximum switching frequency limitation with given controller. Adaptive Multi-step SOTC is proposed to further increase this maximum switching frequency limitation with given controller.

The concept of SOTC is to settle resonant tank within 2-step, which is the optimal way to settle 3 resonant elements: resonant inductor Lr, resonant capacitor Cr and magnetizing inductor Lm in the LLC resonant converter. However, due to this 2-step limitation, the maximum switching frequency with given controller is also limited. If we want to further increase this maximum switching frequency limitation, this 2-step solution is not suitable any more.

Instead of trying to achieve the optimal performance, multi-step SOTC can be used to settle resonant tank within more than 2 steps as shown in Fig. 2.8. The number m of steps in Multi-step SOTC is determined by the speed of digital controller and switching frequency of power stage. For example, 2-step SOTC with TMS320F28027 is suitable for up to 250kHz switching frequency; then 4-step SOTC with same controller would be suitable for up to 500kHz switching frequency; same analogy applies to the cases with more steps.

Even Multi-step SOTC uses more steps to settle resonant tank, it can still achieve the benefit of SOTC, which means there is no oscillation in resonant tank during load transient. This is because Multi-step SOTC is still much faster than linear regulator, and resonant tank is first settle to around final steady state; than the linear regulator takes very little effort to eliminate steady state error. For given high frequency power stage and low-cost digital controller, the benefit of SOTC can still be achieved by using Multi-step SOTC.

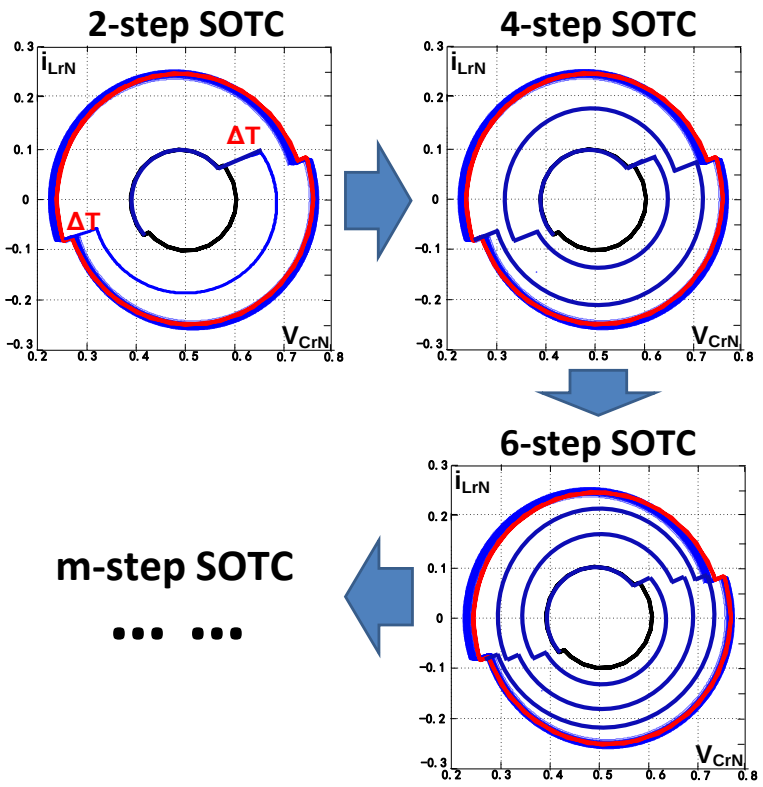

Fig. 2.8. Proposed adaptive Multi-step SOTC

Fig. 2.9 shows the implementation of 6-step SOTC. The output voltage and load current are sampled every third switching cycle. After load transient happens, the controller would have 3 switching cycles (equivalent to 6 steps) to accommodate calculation time. Then the controller uses 6-step to settle resonant tank. So the same controller can be applied to higher switching frequency with Multi-step SOTC compared with the case using 2-step SOTC.

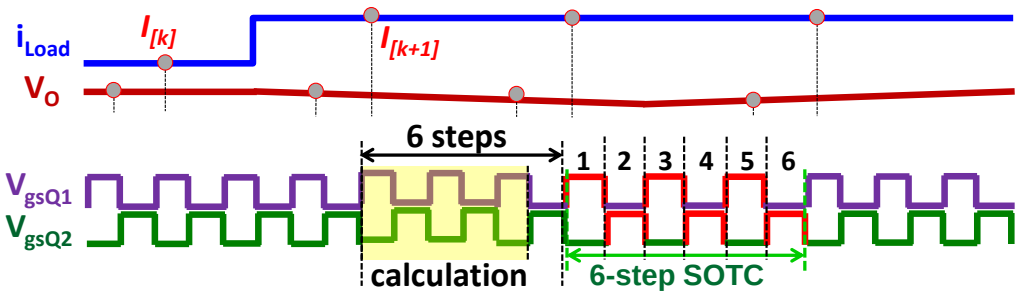

Fig. 2.9. Implementation of 6-step SOTC

The calculation of ΔT in SOTC will be briefly summarized. Then based on the derivation of ΔT in SOTC, calculation for ΔT' in Multi-step SOTC is derived in the followings.

Fig. 2.10 is an example illustrating load step-up. The length of AB equals to that of CD, since the ΔTs for two steps in SOTC are always the same to ensure that the magnetizing current is settled no matter during load step-up or load step-down. The converter is assumed to run at around resonant frequency. Light load current is I_{light} and heavy load current is I_{heavy}. Then the coordinates of point A and point E are expressed as:

$$\boldsymbol{A}: \left(\frac{\pi}{2} \frac{I_{light}}{n} \frac{1}{V_{in}/Z_o} + \mathbf{0.5}\,,\ \frac{nV_o}{L_m} \frac{T}{4} \frac{1}{V_{in}/Z_o} \right) \tag{2.5}$$

$$\boldsymbol{E}: \left(\frac{\pi}{2} \frac{I_{heavy}}{n} \frac{1}{V_{in}/Z_o} + \mathbf{0.5}\,,\ \frac{nV_o}{L_m} \frac{T}{4} \frac{1}{V_{in}/Z_o} \right) \tag{2.6}$$

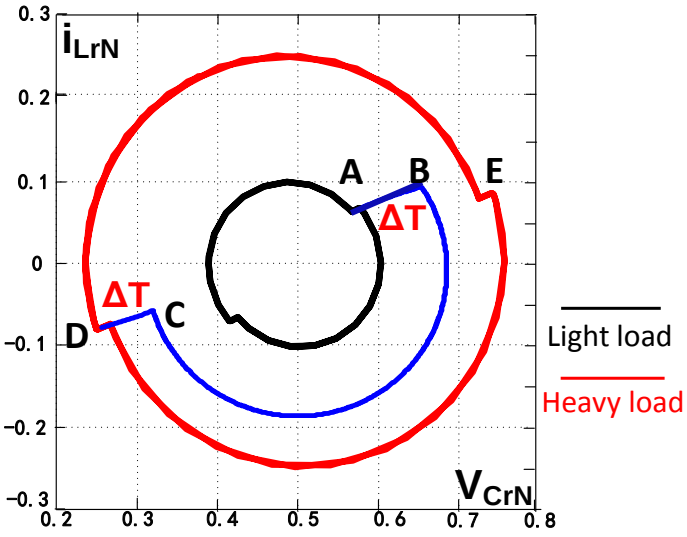

Fig. 2.10. Calculation of ΔT_{UP} in SOTC for load step-up

Since the length of AB equals that of CD, point B is approximately in the middle of point A and point E. And during AB, the magnetizing current I_{Lm} is approximately constant, expressed as:

$$I_{Lm} = \frac{V_{in}/2}{L_m} \cdot \frac{T}{4} \tag{2.7}$$

And the resonant capacitor voltage is charged by the magnetizing current I_{Lm} during AB. Then ΔT_{UP} can be derived:

$$\Delta T_{UP} = \frac{C_r \cdot (V_B - V_A)}{I_{Lm}} = \frac{L_m \cdot (I_{heavy} - I_{light})/n}{V_{in}} \tag{2.8}$$

The ΔT' in Multi-step SOTC for load step-up is derived iteratively based on the conclusion from SOTC. Firstly, the ΔT's in the multi steps are always the same since this ensures the magnetizing current are balanced and PWM cannot be updated every switching cycle. Take 4-step SOTC for load step-up as an example, shown in Fig. 2.11.

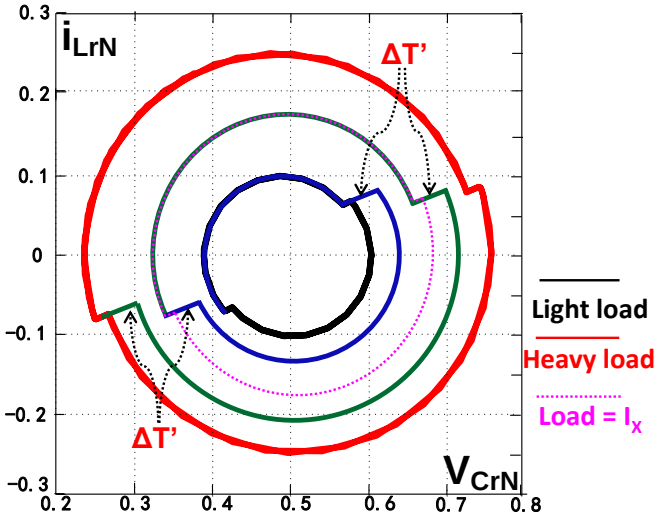

Fig. 2.11. Calculation of ΔT_{UP_4}' in 4-step SOTC for load step-up

In 4-step SOTC, assume the first 2-step settles resonant tank from I_{light} equivalent trajectory to I_X equivalent trajectory, then ΔT_{UP_4}' can be expressed as

$$\Delta T_{UP\_4}' = \frac{L_m \cdot (I_X - I_{light})/n}{V_{in}} \tag{2.9}$$

The next 2-step will settle resonant tank from I_X equivalent trajectory to I_{heavy} equivalent trajectory. So anther expression of ΔT_{UP_4}' is:

$$\Delta T_{UP\_4}' = \frac{L_m \cdot (I_{heavy} - I_x)/n}{V_{in}} \tag{2.10}$$

Expression of ΔT_{UP_4}' can be derived by combining equation (9) and equation (10) as below:

$$\Delta T_{UP\_4}' = \frac{L_m \cdot (I_{heavy} - I_{light})/n}{2 \cdot V_{in}} \tag{2.11}$$

By iteration, ΔT_{UP_m}' of m-step SOTC for load step-up can be derived as below:

$$\Delta T_{UP\_m}' = \frac{L_m \cdot (I_{heavy} - I_{light})/n}{(m/2) \cdot V_{in}} \tag{2.12}$$

Fig. 2.12 is an example illustrating load step-down. The angle of α_1 equals to that of α_2, since the ΔTs for two steps in SOTC are always the same to ensure that the magnetizing current is settled.

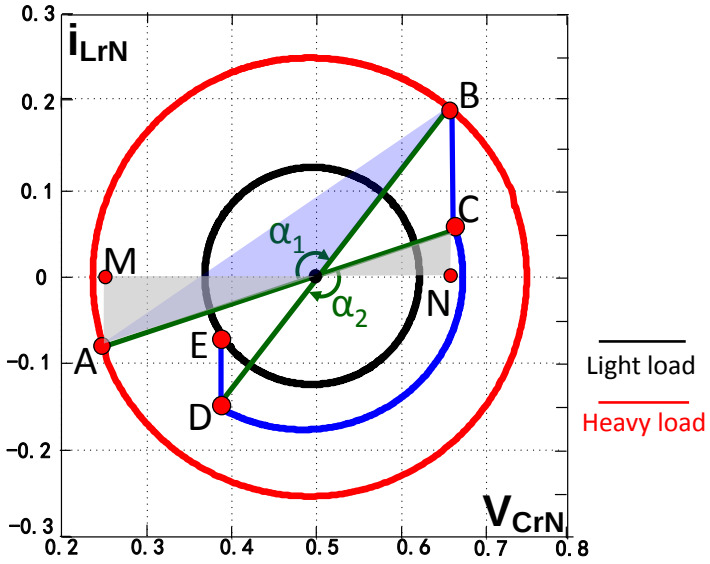

Fig. 2.12. Calculation of ΔT_{DOWN} in SOTC for load step-down

The length of AO equals to that of BO, and the length of CO equals to that of DO. So ΔABO and ΔCDO are similar triangles, then:

$$\frac{V_{CN}-0.5}{0.5-V_{AN}}=\frac{0.5-V_{DN}}{V_{BN}-0.5} \tag{2.13}$$

In the equation (13), V_{XN} means normalized resonant voltage at point X. With $V_{BN} = V_{CN}$ and $V_{DN} = V_{EN}$, then:

$$V_{CN}=\sqrt{(0.5-V_{AN})\cdot(0.5-V_{EN})}+0.5 \tag{2.14}$$

The coordinates of point A and point E are expressed as:

$$A:\left(-\frac{\pi}{2}\frac{I_{heavy}}{n}\frac{1}{V_{in}/Z_o}+0.5\ ,\ -\frac{nV_o}{L_m}\frac{T}{4}\frac{1}{V_{in}/Z_o}\right) \tag{2.15}$$

$$E:\left(-\frac{\pi}{2}\frac{I_{light}}{n}\frac{1}{V_{in}/Z_o}+0.5\ ,\ -\frac{nV_o}{L_m}\frac{T}{4}\frac{1}{V_{in}/Z_o}\right) \tag{2.16}$$

With equations (14) – (16), V_{CN} is expressed as:

$$V_{CN}=\frac{\pi}{2}\frac{\sqrt{I_{heavy}\cdot I_{light}}}{n}\frac{1}{V_{in}/Z_o}+0.5 \tag{2.17}$$

Since ΔAMO and ΔCNO are similar triangles, then:

$$\frac{I_{CN}}{I_{AN}}=-\frac{V_{CN}-0.5}{0.5-V_{AN}}=-\sqrt{\frac{I_{light}}{I_{heavy}}} \tag{2.18}$$

I_{AN} is y-coordinate of point A, which is expressed in equation (15), so resonant current at point C is expressed as:

$$I_C=\sqrt{\frac{I_{light}}{I_{heavy}}}\cdot\left(\frac{V_{in}/2}{L_m}\cdot\frac{T}{4}\right) \tag{2.19}$$

Since the duration from point B to point C is a negligible time compare with the duration from point A to point B on the heavy load trajectory. In the time from point A to point B, magnetizing inductor is clamped by the output voltage. So duration from point A to point B is approximately expressed as:

$$T_{AB} = \frac{L_m \cdot (I_C - I_A)}{V_{in}/2} = \left(1 + \sqrt{\frac{I_{light}}{I_{heavy}}}\right)\frac{T}{4} \tag{2.20}$$

Since the converter runs at around resonant frequency, so the ΔT_{DOWN} of SOTC for load step-down is:

$$\Delta T_{DOWN} = T_{AB} - \frac{T}{2} = -\left(1 - \sqrt{\frac{I_{light}}{I_{heavy}}}\right)\frac{T}{4} \tag{2.21}$$

The ΔT' in Multi-step SOTC for load step-down is derived iteratively based on the conclusion from SOTC. Firstly, the ΔT's in the multi steps are always the same since this ensures the magnetizing current are balanced and PWM cannot be updated every switching cycle. Take 4-step SOTC for load step-down as an example, shown in Fig. 2.13.

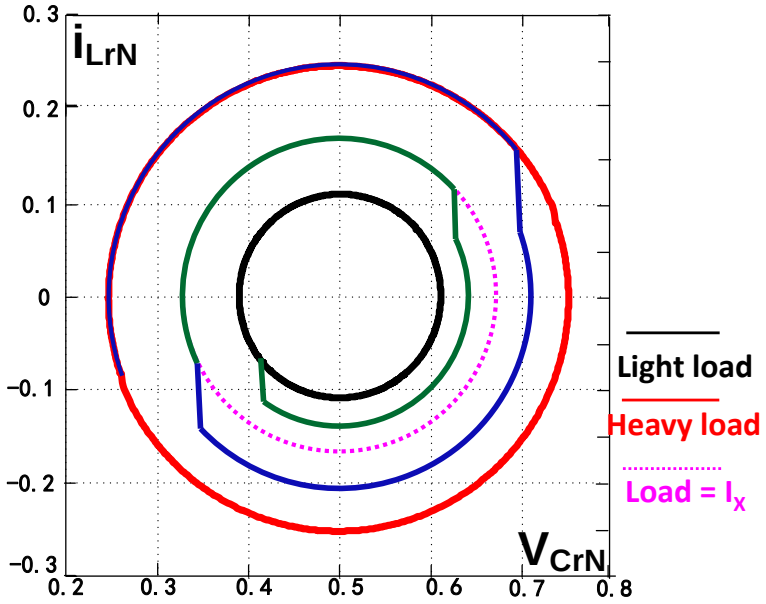

Fig. 2.13. Calculation of ΔT_{DOWN_4}' in 4-step SOTC for load step-down

In 4-step SOTC, assume the first 2-step settles resonant tank from I_{heavy} equivalent trajectory to I_X equivalent trajectory, then ΔT_{DOWN_4}' can be expressed as

$$\Delta \boldsymbol{T_{DOWN\_4}}' = -\left(\mathbf{1} - \sqrt{\frac{\boldsymbol{I_X}}{\boldsymbol{I_{heavy}}}}\right)\frac{\boldsymbol{T}}{\mathbf{4}} \tag{2.22}$$

The next 2-step will settle resonant tank from I_X equivalent trajectory to I_{light} equivalent trajectory. So anther expression of ΔT_{DOWN_4}' is:

$$\Delta \boldsymbol{T_{DOWN\_4}}' = -\left(\mathbf{1} - \sqrt{\frac{\boldsymbol{I_{light}}}{\boldsymbol{I_X}}}\right)\frac{\boldsymbol{T}}{\mathbf{4}} \tag{2.23}$$

Expression of ΔT_{DOWN_4}' can be derived by combining equation (22) and equation (23) as below:

$$\Delta \boldsymbol{T_{DOWN\_4}}' = -\left(\mathbf{1} - \sqrt[4]{\frac{\boldsymbol{I_{light}}}{\boldsymbol{I_{heavy}}}}\right)\frac{\boldsymbol{T}}{\mathbf{4}} \tag{2.24}$$

By iteration, ΔT_{DOWN_m}' of m-step SOTC for load step-down can be derived as below:

$$\Delta \boldsymbol{T_{DOWN\_m}}' = -\left(\mathbf{1} - \sqrt[\boldsymbol{m}]{\frac{\boldsymbol{I_{light}}}{\boldsymbol{I_{heavy}}}}\right)\frac{\boldsymbol{T}}{\mathbf{4}} \tag{2.25}$$

In this section, the adaptive Multi-step SOTC is proposed so that SOTC can be applied to high frequency LLC converter with low-cost digital controllers. The number of steps in Multi-step SOTC is selected based on the speed of the controller and the switching frequency of the power stage. Furthermore, the required ΔT' for Multi-step SOTC is derived based on the conclusion from SOTC.

2.4 Experimental Results of Load Transient

The SOTC is verified on TI's demo board TMDSHVRESLLCKIT as shown in Fig. 2.14, which is a 130kHz 300W 380V/12V half-bridge LLC resonant converter with the following circuit parameters: L_r = 55uH, C_r = 24nF, L_m = 280uH, C_O = 1.32mF.

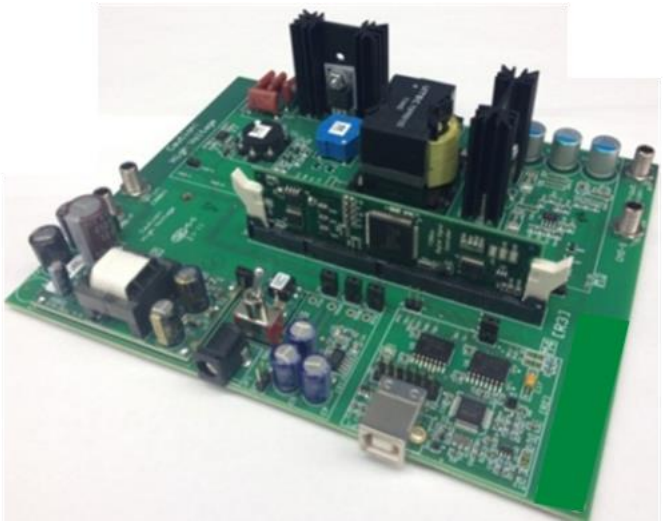

Fig. 2.14. The 130kHz LLC converter (TI's demo board TMDSHVRESLLCKIT)

Fig. 2.15 is the experimental results of SOTC for load transient. Fig. 2.15(a) is load step up from 5A to 15A, and Fig. 2.15(b) is load step down from 15A to 5A. There is almost no dynamic oscillation in resonant tank during load transient.

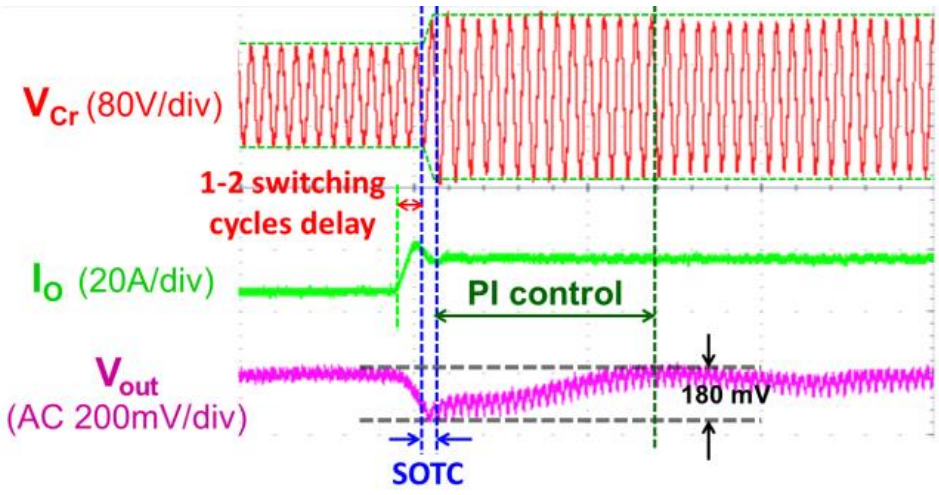

(a)

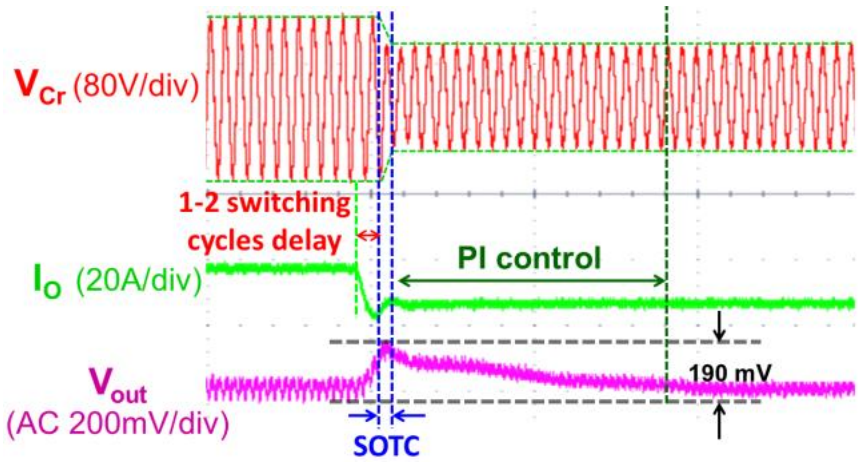

(b)

Fig. 2.15. SOTC for load transient (a) step up from 5A to 15A; (b) step down from 15A to 5A

The Multi-step SOTC is verified on a 500kHz LLC converter. The 500kHz LLC converter is designed based on Matrix Transformer for LLC Resonant Converters [14], which was originally a 1MHz 1kW 390V/12V unregulated DCX with GaN devices. Here the LLC converter is a 500kHz 1kW 390V/12V regulated DC/DC converter with Si devices. The parameters of the 500kHz LLC converter is: Lr = 4.5uH, Cr = 22nF, Lm = 22uH. The hardware of the 500kHz LLC converter is shown in Fig. 2.16, with the efficiency curve shown in Fig. 2.17.

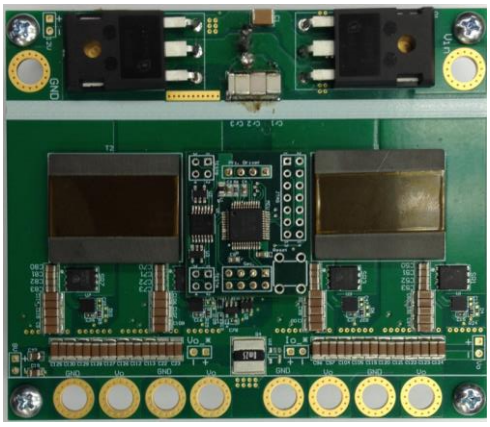

Fig. 2.16. The 500kHz LLC converter hardware

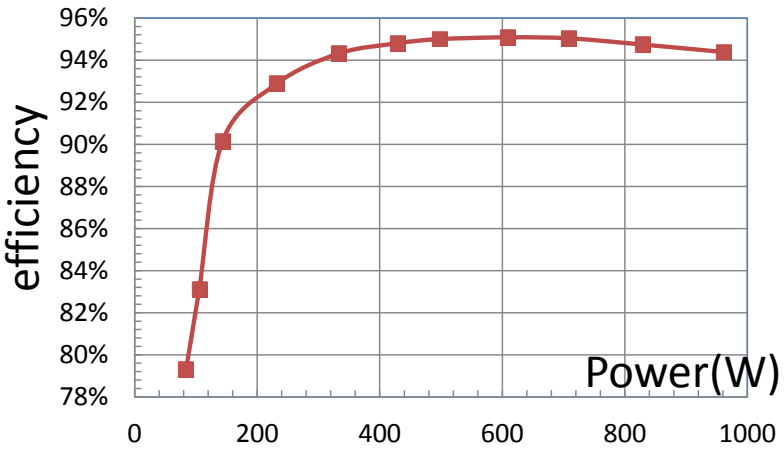

Fig. 2.17. Efficiency curve of the 500kHz LLC converter

To control the 500kHz LLC converter, a 60MHz MCU (TMS320F28027) is selected, which is popular in industrial application for power supply of server and telecom. However, in industrial application, the switching frequency of power converter is normally below 130kHz.

The experimental results of load step-up from 40A to 80A and load step-down are shown in Fig. 2.18 and Fig. 2.19 respectively. The output capacitor is totally 5mF ceramic capacitor (X5R), whose capacitance drops to 10% at 12V DC bias. So the actual output capacitance is only around 500uF. The overshoot for both load step-up and load step-down are within 600mV (5% V_O), and there is no oscillation in resonant tank.

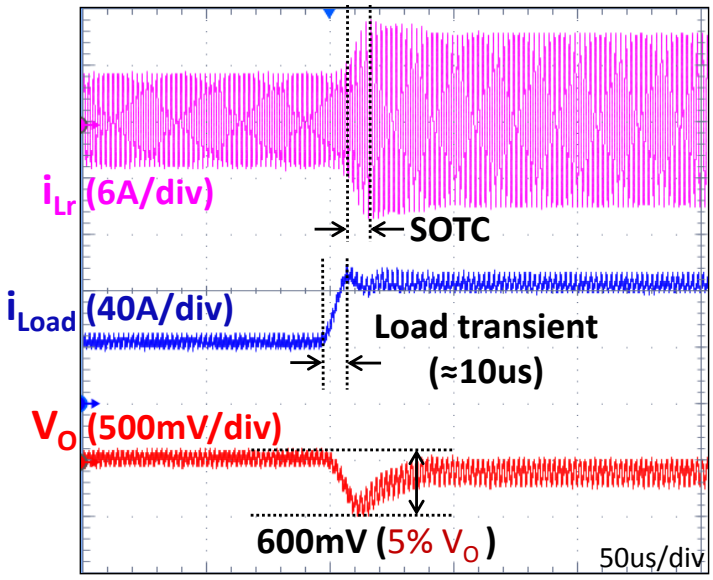

Fig. 2.18. Multi-step SOTC for load step-up (from 40A to 80A)

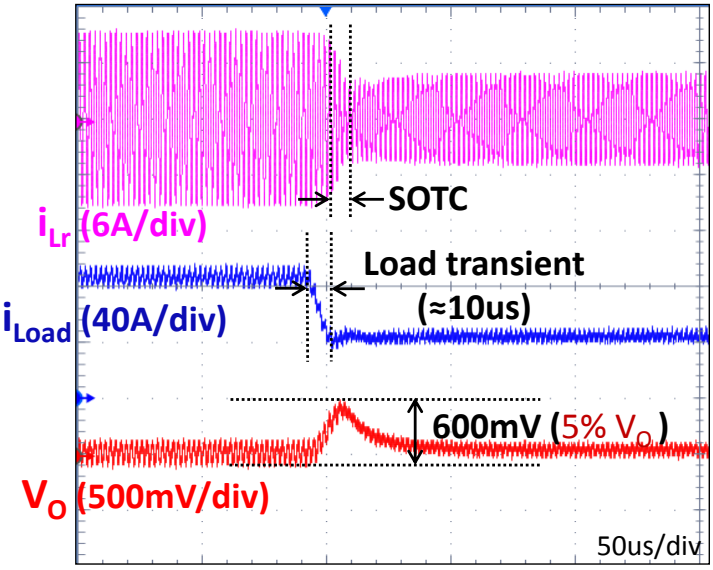

Fig. 2.19. Multi-step SOTC for load step-down (from 80A to 40A)

2.5 Conclusions

In this chapter, the Simplified Optimal Trajectory Control (SOTC) is investigated and improved to increase the maximum switching frequency limitation for given controller, and

SOTC can be implemented by low-cost controllers to achieve fast load transient response. Then the Multi-step Simplified Optimal Trajectory Control (SOTC) is proposed to further increase the maximum switching frequency limitation, which calculates trajectory based on only output voltage and load current, and settles resonant tank within multi-step. With Multi-step SOTC, low-cost controllers can be used to control high frequency LLC converter with state-trajectory control. The number of steps in Multi-step SOTC is determined by the speed of the controllers and the switching frequency of the LLC converter. Experimental results are demonstrated on 500kHz 1kW 400V/12V LLC converter with 60MHz microcontroller (TMS320F28027). Fast load transient response is achieved by using 6-step SOTC.

Chapter 3. Simplified Optimal Trajectory Control (SOTC) for Soft Start-up of LLC Resonant Converters Based on Only Output Voltage

3.1 Introduction

Start-up is the most critical process in the control of the LLC resonant converter. There would be very large current and voltage stresses if the process is not well controlled. Fig. 3.1(a) is the start-up waveform of a commercial controller. And Fig. 3.1(b) is the frequency changing trajectory on the gain curve.

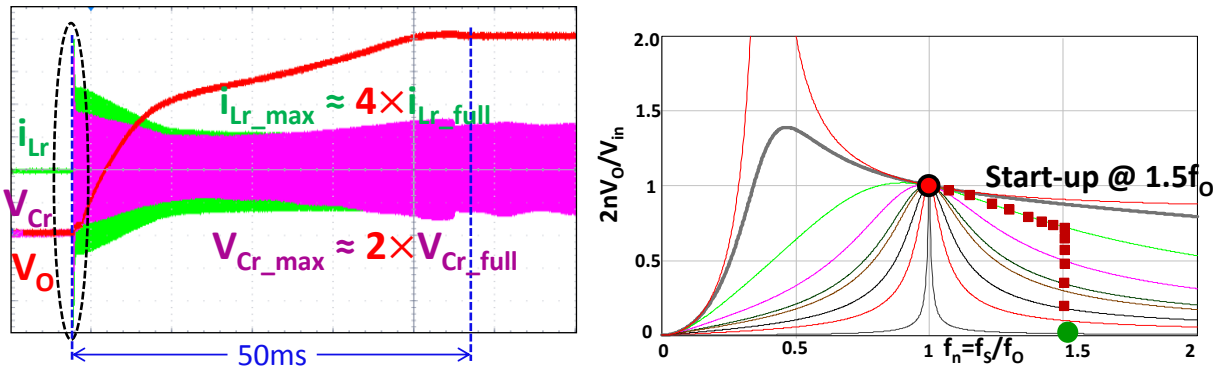

(a) (b)

Fig. 3.1. Start-up of a commercial controller which start-up @ $1.5f_O$: (a) experimental waveforms; (b) frequency changing trajectory on the gain curve

It is shown in Fig. 3.1 that the controller's start-up frequency is 1.5 times resonant frequency. Since the start-up frequency is not high enough, the stresses are very large at the beginning.

Even if the start-up frequency is high enough, there are still large stresses during the start-up with a commercial controller as shown in Fig. 3.2. The start-up frequency is 5 times resonant

frequency, and at the beginning, the voltage and current stresses are small. However, during the soft start-up process, switching frequency decreases too quickly, and large voltage and current stresses still happen, which triggers the over-current protection. Then switching frequency increases a little to limit stress. There are still large stresses and it takes a long time to start up.

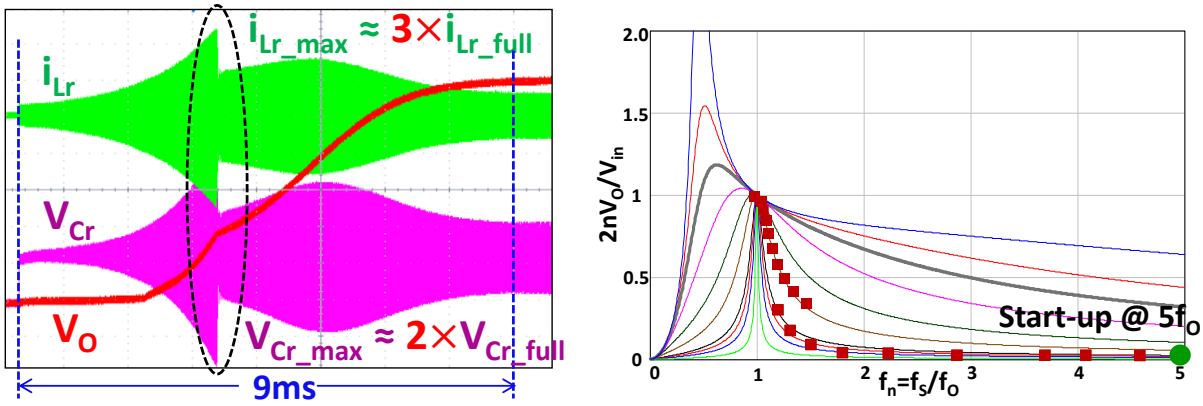

Fig. 3.2. Start-up of a commercial controller which start-up @ $5f_O$: (a) experimental waveforms; (b) frequency changing trajectory on the gain curve

Commercial controllers spend a lot of effort in solving the challenge of start-up from the perspective of gain curve, but there are still large current and voltage stresses.

3.2 Optimal Trajectory Control (OTC) for Soft Start-up

The optimal trajectory control (OTC) for soft start-up is first proposed in [41] to solve the challenge in start-up. The whole start-up process is divided into 3 stages as shown in Fig. 3.3. Stage 1 sets asymmetrical current limiting band to settle resonant voltage to half of input voltage (for half bridge LLC converter). Stage 2 sets symmetrical current limiting band to optimized energy delivery. Stage 3 simply decreases switching frequency until V_O reaches 12V.

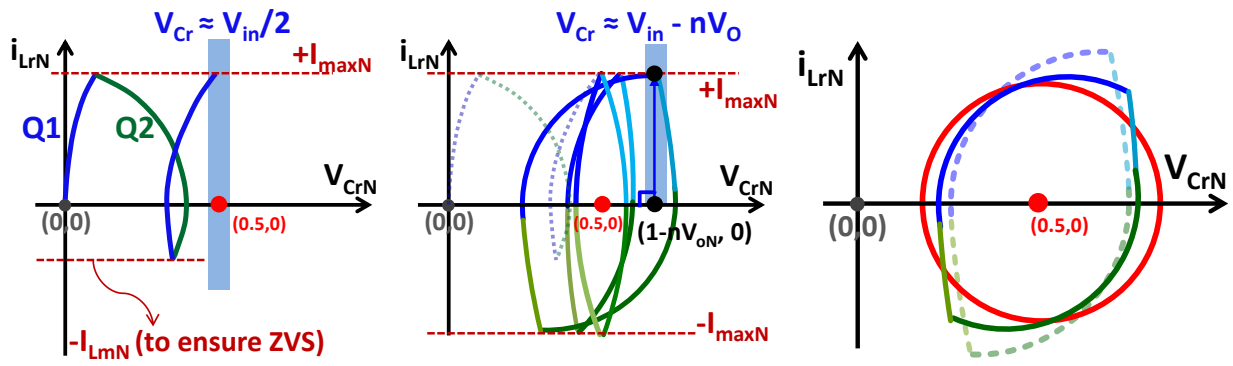

(a) (b) (c)

Fig. 3.3. optimal trajectory control for soft start-up (a) Stage1: asymmetrical current limiting band; (b) Stage2: symmetrical current limiting band; (c) Stage3: decrease f_S gradually until V_O = 12V

The OTC for soft start-up is based on the graphical state-trajectory analysis of resonant tank. So it can minimize resonant tank stress, thus ensuring a safe start-up process and optimizing energy delivery.

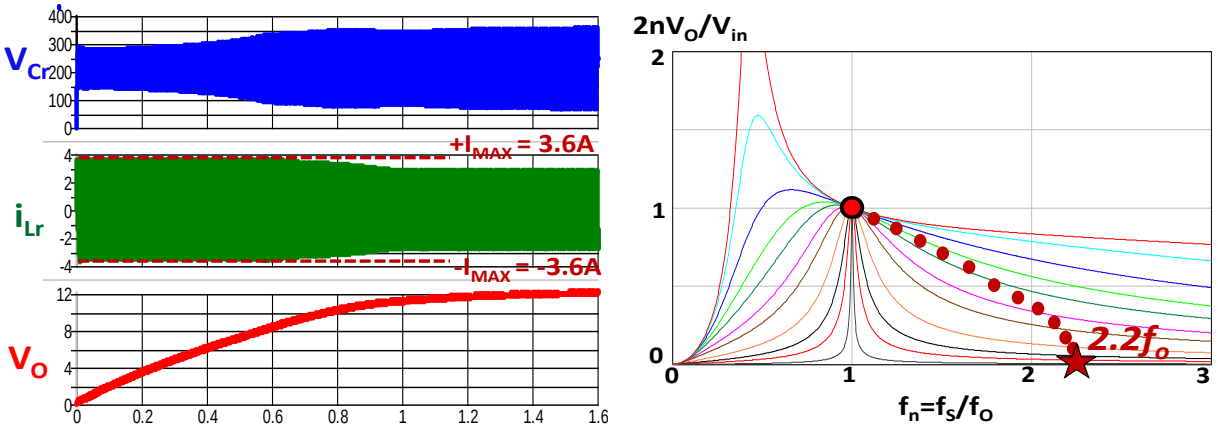

(a) (b)

Fig. 3.4. Simulation of optimal trajectory control for start-up: (a) experimental waveforms; (b) frequency changing trajectory on the gain curve

Fig. 3.4 is the simulation result of the optimal trajectory control for soft start-up. The parameter of the LLC is: Lr = 55uH, Cr = 24nF, Lm = 280uH. The simulation result shows that the maximum resonant current during the whole start-up process is only a little bit larger than the full load steady state. The start-up frequency changing on the gain curve is smooth. It is obvious that OTC for soft start-up has overwhelming advantages than other control methods. So it is meaningful to investigate how to implement OTC for soft start-up.

As introduced in previous chapters, the digital controllers are gradually taking the place of the analog controllers in control of the LLC resonant converter, and the cost-effective digital controllers are preferred in the industrial applications among those digital controllers. But the digital delay caused by the analog-to-digital converter (ADC) and the calculation will have large impact on the performance of resonant converter, especially during start-up, in which energy in the resonant tank changes very fast.

If a microcontroller (MCU) is employed directly to implement the OTC for soft start-up, as show in Fig. 3.5(a), there would be very large current stress. Take TMS320F28027 as an example, which is a low-cost MCU and widely used in power supply for server. All the required state variables are sensed through the ADC and processed by the CPU. In Stage 1 of the start-up, the MCU senses the resonant current i_{Lr} and compare it with the current limiting band, and there would be a total digital delay of 0.8us. The impact of this 0.8us digital delay will cause very large current stress as shown in Fig. 3.5(b).

In Fig. 3.5(b), the dash line is the desired trajectory, and the solid line is the trajectory with digital delay. Since switching frequency at the beginning of start-up is very high, even very small digital delay will cause very large current stress. 0.8us digital delay will cause current stress to be 2 times I_{max} for 130kHz LLC and larger than 3 times I_{max} for 500kHz LLC.

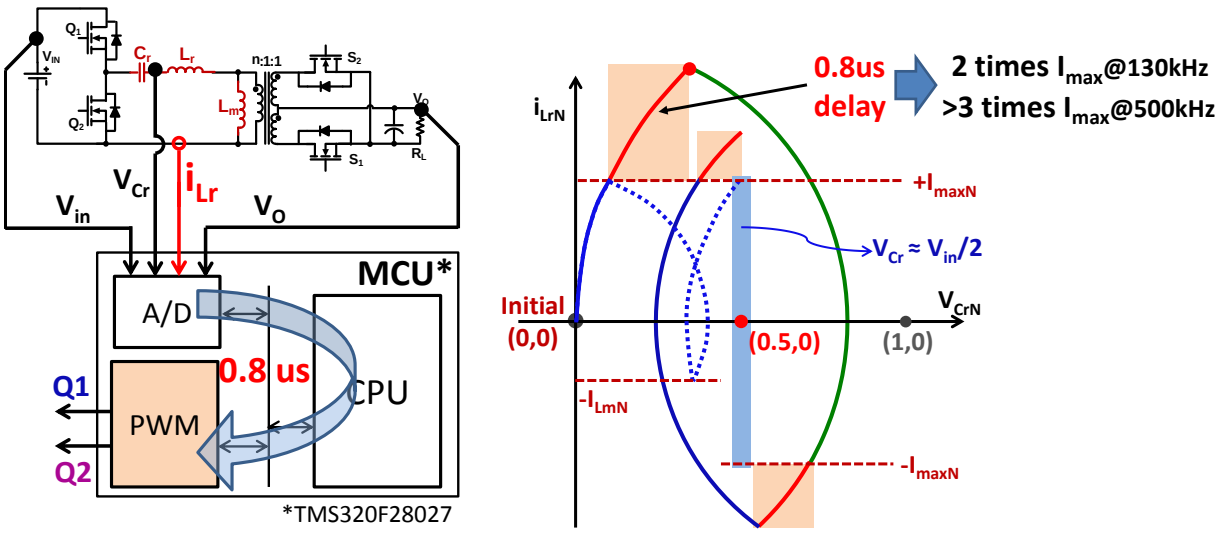

(a) (b)

Fig. 3.5. Use MCU to implement the optimal trajectory control for soft start-up directly: (a) system scheme; (b) state-trajectory of Stage 1 with digital delay

Since the OTC for soft start-up has overwhelming advantages than other control methods and the digital controllers have superior advantages over analog controllers, further efforts need to be spent on how to reduce the impact of the digital delay so that soft start-up can be implemented with the commercial digital controllers. Two methods are proposed in this chapter to solve this problem.

To solve the digital delay caused by the ADC and the calculation. The first proposed method is mixed-signal implementation as shown in Fig. 3.6(a). In addition to the MCU, there are two comparators in the analog part. The resonant current i_{Lr} is sensed as the positive input of Comparator 1 and the negative input of Comparator 2. The positive band is set to be I_{MAX} as the negative input of Comparator 1. And the negative band is controlled by the MCU, which is $-I_{LM}$ in Stage 1 and $-I_{MAX}$ in Stage 2. The outputs of the two comparators are directly fed back to the PWM module in the MCU. Since the PWM module is configured before the control loop starts

running and the propagation delay of the comparators is negligible, the delay of the whole control loop is very small, thus suitable for the optimal trajectory control for soft start-up.

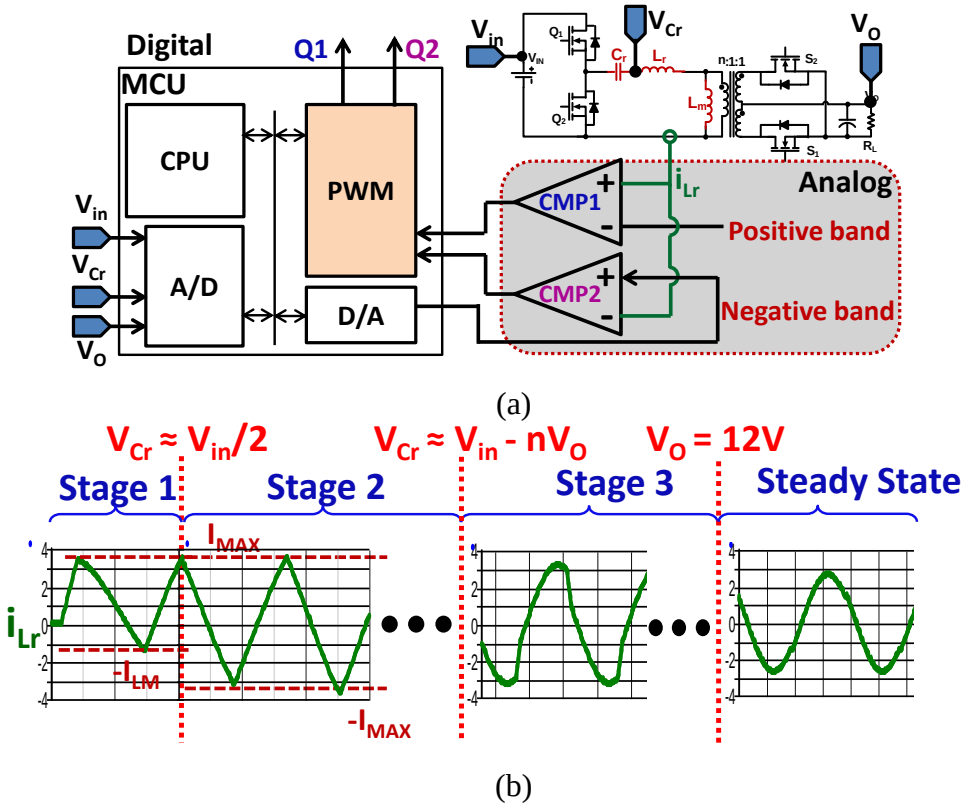

Fig. 3.6. Mixed-signal implementation of the optimal trajectory control for soft start-up: (a) control scheme; (b) waveforms illustrating the control strategy

Fig. 3.6(b) is the time-domin waveforms illustrating the control strategy. In Stage 1 and Stage 2, when i_{Lr} touches the positive current limiting band, the PWM module will turn off the high-side switch and turn on the low-side switch; and when i_{Lr} touches the negative current limiting band, the PWM module will turn on the high-side switch and turn off the low-side switch. The MCU controls the negative current limiting band to be $-I_{LM}$ in Stage 1. When $V_{Cr} \approx V_{in}/2$, the MCU sets the negative current limiting band to be $-I_{MAX}$ and enters Stage 2. When $V_{Cr} \approx V_{in} -$

nV_O at the high-side switching instants, the MCU enters Stage 3 and turns into frequency control, decreasing the switching frequency gradually until V_O = 12V.

Method 1 can be implemented with the low-cost MCUs for the optimal trajectory control of soft start-up, and is universal applicable for different power stage design, but requires two additional comparators and the corresponding configuration of the PWM module.

3.3 Simplified Optimal Trajectory Control (SOTC) for Soft Start-up

Another proposed method is based on the concept of Simplified Optimal Trajectory Control (SOTC) with only sensing output voltage, which can be implemented by low-cost digital controllers with look-up table as shown in Fig. 3.7. The table in Fig. 3.7 is based on the parameters of a 130kHz LLC power stage.

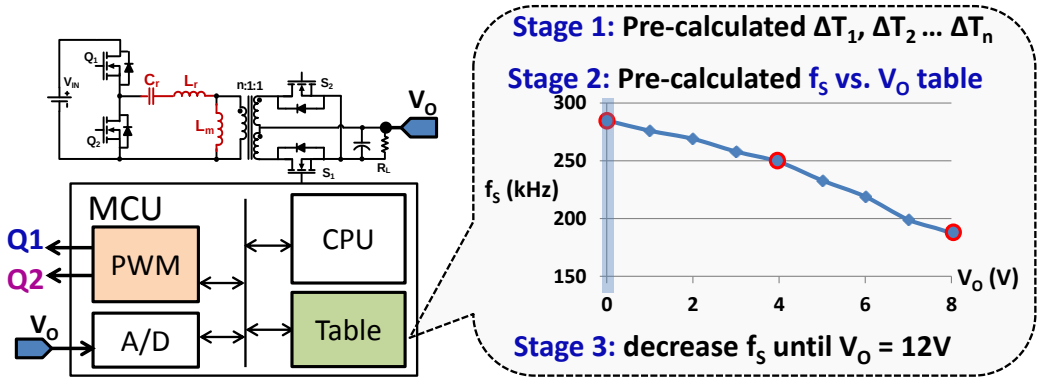

Fig. 3.7. Simplified Optimal Trajectory Control (SOTC) for soft start-up with look-up table

When the input voltage reaches around 400V (means that the PFC is ready), the MCU will start the soft start-up process. In Stage 1, the pre-calculated ΔT_1, ΔT_2 … ΔT_n are generated consequently. In stage 2, the MCU senses V_O and controls the switching frequency based on the

pre-calculated f_S vs. V_O table. In Stage 3, the MCU decreases the switching frequency gradually until V_O = 12V. Detailed derivation for the table will be presented in the followings.

In Stage 1, the output voltage is considered to be approximately 0V because the output capacitor is very large and there are only several switching pulses in Stage 1. And the initial condition is: $V_{Cr} = 0$ and $i_{Lr} = 0$ because there is no energy in the resonant tank before start-up.

The calculation for ΔT_1 and ΔT_2 is shown in Fig. 3.8. ΔT_1 is calculated as follows:

$$\boldsymbol{\alpha_1 = sin^{-1}\left(\frac{I_{maxN}}{\rho_1}\right)} \tag{3.1}$$

$$\boldsymbol{\Delta T_1 = \frac{\alpha_1}{\omega_o}} \tag{3.2}$$

In which $\omega_o = \frac{1}{\sqrt{L_r \cdot C_r}}$. And ΔT_2 is calculated as follows:

$$\boldsymbol{\alpha_2 = sin^{-1}\left(\frac{I_{maxN}}{\rho_2}\right) + sin^{-1}\left(\frac{I_{LmN}}{\rho_2}\right)} \tag{3.3}$$

$$\boldsymbol{\Delta T_2 = \frac{\alpha_2}{\omega_o}} \tag{3.4}$$

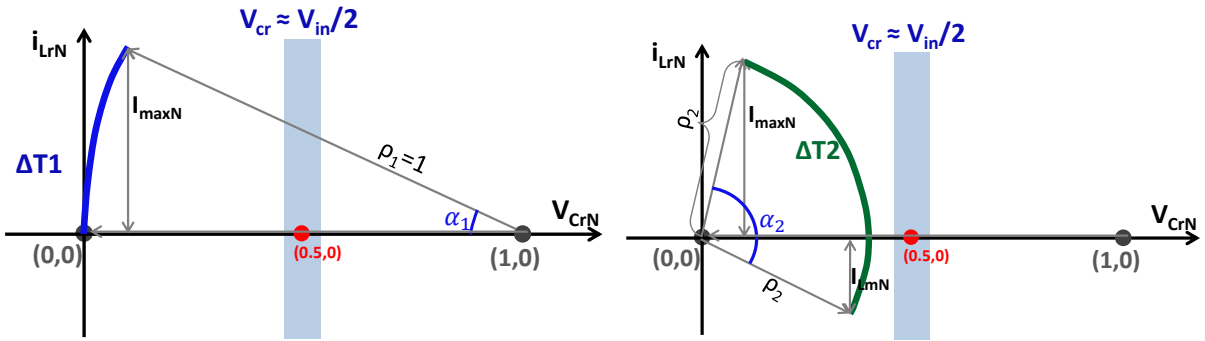

(a) (b)

Fig. 3.8. The calculation of the table for Stage 1: (a) ΔT_1; (b) ΔT_2

ΔT_1, ΔT_2 … ΔT_n are calculated step by step until it comes to the very step that V_{Cr} comes into the region around Vin/2. Then the calculation for Stage 1 ends and starts Stage 2. In Stage 2, the

switching frequency is given based on the pre-calculated table. The assumptions for this method to work are that the converter runs at above resonant frequency, and that within several switching cycles, both the input and the output can be considered as constant voltage sources. These assumptions are always true because during the start-up, the output voltage is very low and converter always runs at above resonant frequency to avoid entering ZCS region; and both the input capacitor and the output capacitor are very large for the hold-up time and load transient purpose.

Under these conditions, for given input and output voltage, one switching frequency corresponds to one maximum i_{Lr}. The I_{MAX} for i_{Lr} is pre-set, then for different V_O, the corresponding switching frequency to limit i_{Lr} within I_{MAX} under the nominal Vin can be obtained. The f_S vs. V_O table is piece-wise-linearized and stored in the MCU. The calculation for the table of Stage 2 is shown in Fig. 3.9. Given V_O, the corresponding trajectory within I_{MAXN} can be drawn as shown in Fig. 3.9.

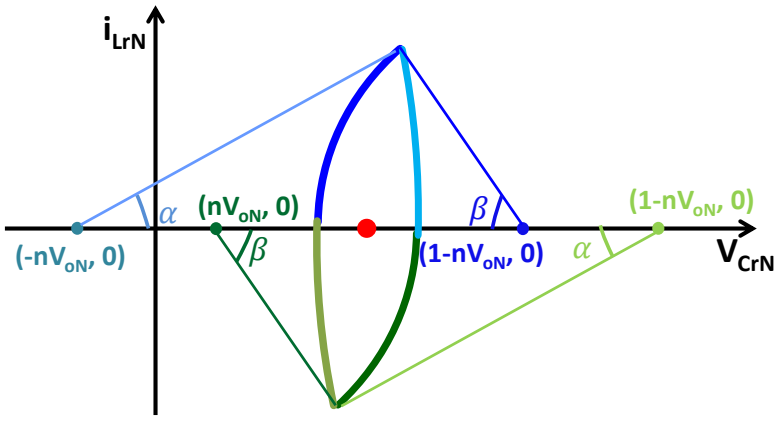

Fig. 3.9. f_S vs. V_O table calculation for given V_O

For given V_O, the switching period is calculated as follows:

$$\boldsymbol{\alpha = sin^{-1}\left(\frac{I_{maxN}}{\rho_1}\right);\ \beta = sin^{-1}\left(\frac{I_{maxN}}{\rho_2}\right)} \tag{3.5}$$

$$\boldsymbol{T_s = \frac{2(\alpha+\beta)}{\omega_o}} \tag{3.6}$$

Stage 3 for this method is same as previous, just decreasing f_S gradually until V_O = 12V. This method is applicable for different load condition because even under different load, the output can still be considered as a constant voltage source within several switching cycles. The load condition has impact on the duration of the whole start-up process, but will not have impact on current stress.

However, since this method is calculated based on nominal Vin and given Lr, Cr value, the impact of Vin and the tolerance of Lr and Cr need to be considered. The ΔT table and the f_S vs. V_O table are calculated based on normalized current band:

$$\boldsymbol{I_{maxN} = \frac{I_{max}}{Vin/\sqrt{L_r/C_r}}} \tag{3.7}$$

For given power stage parameters, the ΔT table and the f_S table, the normalized trajectory and I_{maxN} are the same. But under different input voltage condition, the current stress is different, which is expressed as below:

$$\boldsymbol{I_{Stress}(Vin) = I_{maxN} \cdot \frac{Vin}{\sqrt{L_r/C_r}}} \tag{3.8}$$

From the equation above, it is clear that the current stress is proportional to the input voltage. Since the input voltage is within a certain range (normally ±5%), current stress variation under the certain range of Vin is also very small.

The impact of the tolerance of Lr and Cr is estimated by simulation as shown in Fig. 3.10. The start-up condition is Vin =390V and load = 25A. The table is calculated based on Lr = 60uH and Cr = 24nF. Fig. 3.10(a) is the case without tolerance, and the I_{MAX} = 3.60A as designed. Fig. 3.10(b) is the case with positive 5% tolerance for both Lr and Cr, and the I_{MAX} = 3.40A. Fig.

3.10(c) is the case with negative 5% tolerance for both Lr and Cr, and the I_{MAX} = 3.91A. It is clear that ±5% tolerance of resonant tank will only result in the current stress variation of less than 10%.

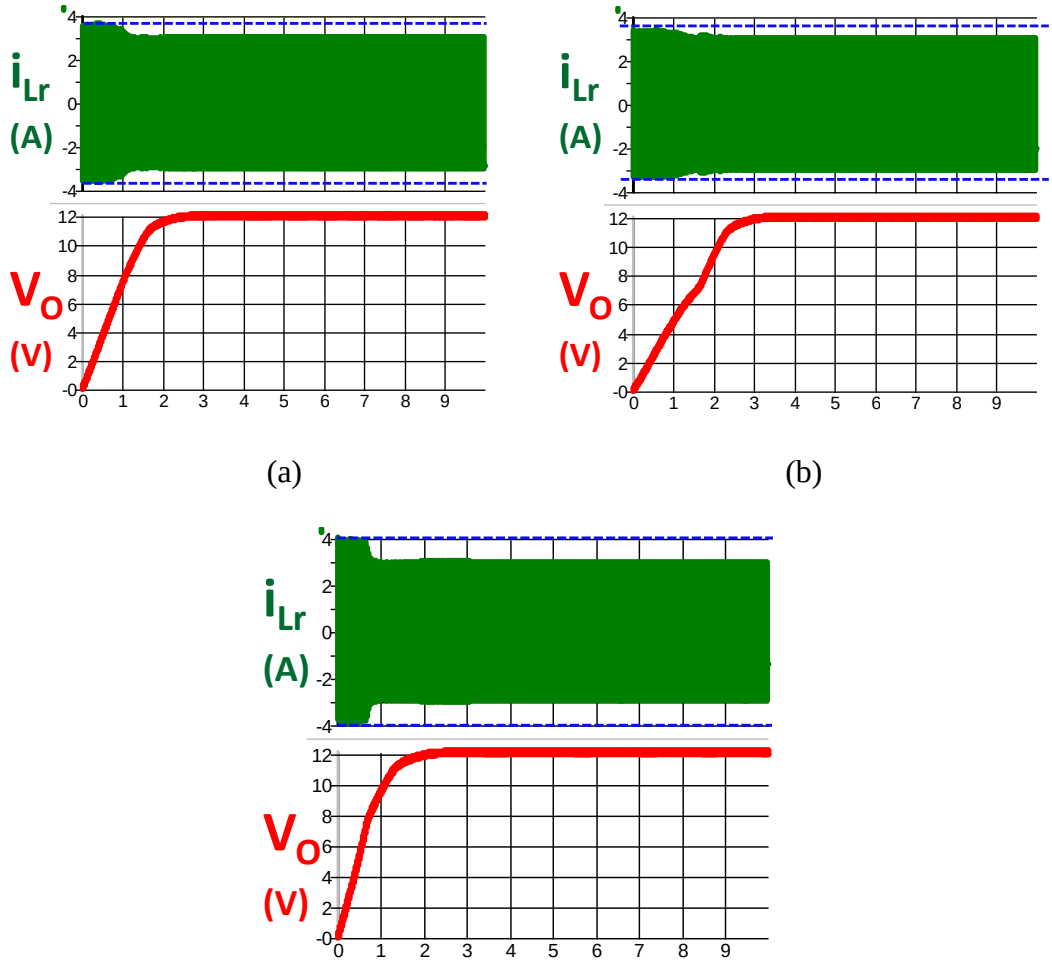

Fig. 3.10. Simulation of Method 2 for soft start-up using look-up table: (a) Lr and Cr have no tolerance; (b) both Lr and Cr have positive 5% tolerance; (c) both Lr and Cr have negative 5% tolerance

The control scheme of SOTC for soft start-up is very simple. And the table is derived for given power stage parameters and input voltage.

3.4 Implementation of SOTC for Soft Start-up of High Frequency LLC Converter

For SOTC for soft start-up with look-up table, the switching instants are controlled by the CPU of the MCU, there is limitation in the switching frequency with given performance of CPU. This section mainly discusses how to apply the SOTC for soft start-up to high frequency LLC converter.

Firstly, a suitable MCU is selected. Among the MCUs provided by Texas Instrument, TMS320F28027 is widely used in the power supply for server and telecom applications. So TMS320F28027 is selected as the controller to implement Method 2. Among the commercial product, this MCU is used to control the LLC converter with resonant frequency of around 70kHz – 130kHz. Below is analysis of how to use the MCU for LLC converter with resonant frequency of above 500kHz.

With MCU TMS320F28027, in each switching cycle, it takes 25 CPU cycles to update ΔT_1, $\Delta T_2 \ldots \Delta T_n$ for Stage 1; and 130 CPU cycles to update the f_S according to V_O for Stage 2; and 180 CPU cycles to update the f_S according to V_O for Stage 3. When the system is reset, the MCU would generate ΔT_1, $\Delta T_2 \ldots \Delta T_n$ consequently for Stage 1, so it actually takes only a few CPU cycles to execute Stage 1; and then the MCU sense V_O to determine the f_S for Stage 2; for Stage 3, it takes a few more CPU cycles than Stage 2 because the MCU needs to gradually merge with the closed-loop control.

The duration of switching instants for Stage 1 is shown in Table 3.1. And the relationship between the f_S and the V_O for Stage 2 and Stage 3 is shown in Fig. 3.11. These analyses are based on a 130kHz LLC converter with Ln ≈ 5, but the same methodology and the relative

relationship between the f_S and the V_O during start-up applies to the power stage with different designs.

Switching instant	ΔT1	ΔT2	ΔT3	ΔT4
Duration	808ns	2096ns	1163ns	1646ns
Equivalent T_S (f_S)	2904ns (344kHz)		2809ns (356kHz)	

Table 3.1. ΔT1, ΔT2 … ΔTn for Stage 1 (130kHz LLC converter)

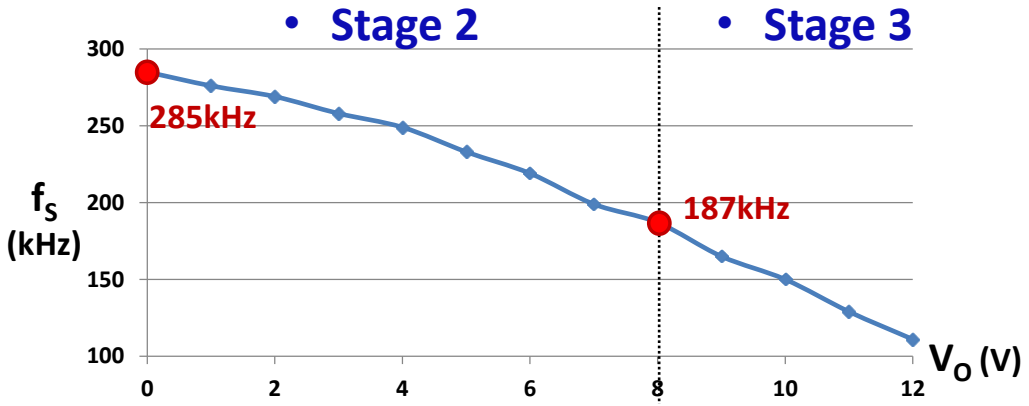

Fig. 3.11. The relationship between switching frequency and output voltage for Stage 2 and Stage 3 (130kHz LLC converter)

Since the maximum f_S of Stage 2 is much higher than that of Stage 3, and it takes much more CPU cycles for Stage 2 than Stage 1, the limitation for the soft start-up is the beginning of Stage 2. To ensure that there is enough time for the CPU to execute the instructions, the PWM module can be configured to be updated every n^{th} switching cycle (n = 1, 2, 3 …). The maximum start-up frequency must satisfy:

$$\frac{n}{f_{s\_max}} > \frac{130}{60MHz} \tag{3.9}$$

The summary for the maximum start-up frequency under different PWM updating speed is listed in Table 3.2.

MCU PWM updating speed	Max. start-up frequency
Within 1 switching cycle	460kHz
Within 2 switching cycles	920kHz
Within 3 switching cycles	1.38MHz
Within 4 switching cycles	1.84MHz

Table 3.2. Maximum start-up frequency under different PWM updating speed

For the 130kHz LLC converter, the maximum start-up frequency is around 300kHz, so the PWM is updated within 1 switching cycle. For the 500kHz LLC converter with Ln = 5 and certain current limit, the maximum start-up frequency is around 1.1MHz, so the PWM is updated within 3 switching cycles.

If the switching frequency is further pushed to even above MHz, then for Method 2, either an MCU with a higher-performance CPU is needed; or it required more switching cycles to update PWM. For Method 1, the impact of the propagation delay of analog circuit and the PWM module on current stress during the start-up will become significant as the switching frequency continues to increase, so proper comparators and MCUs need to be selected accordingly.

3.5 Experimental Results of Soft Start-up

The SOTC for soft start-up is verified on the 500kHz LLC converter referred in Chapter 2. Fig. 3.12 is the experimental result of the soft start-up for the 500kHz LLC converter with 385V input voltage and 0.178Ω resistive load (81% load). Then the soft start-up under 400V input voltage and 80A electrical load (96% load) is shown in Fig. 3.13. Since the output voltage changes much faster than the tracking speed of the electrical load during the soft start-up process, the electrical load cannot keep to 80A for the whole process. This is why the waveforms don't

look as smooth as the previous case with resistive load. However, the maximum current is still within the desired current limiting band even the output is electrical load.

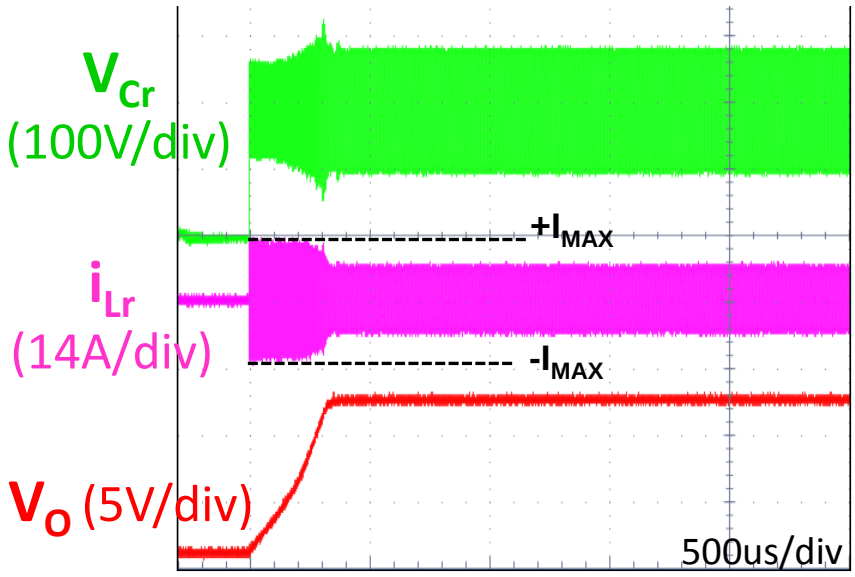

Fig. 3.12. Soft start-up for 500kHz LLC converter under 385V input voltage and 0.178Ω resistive load

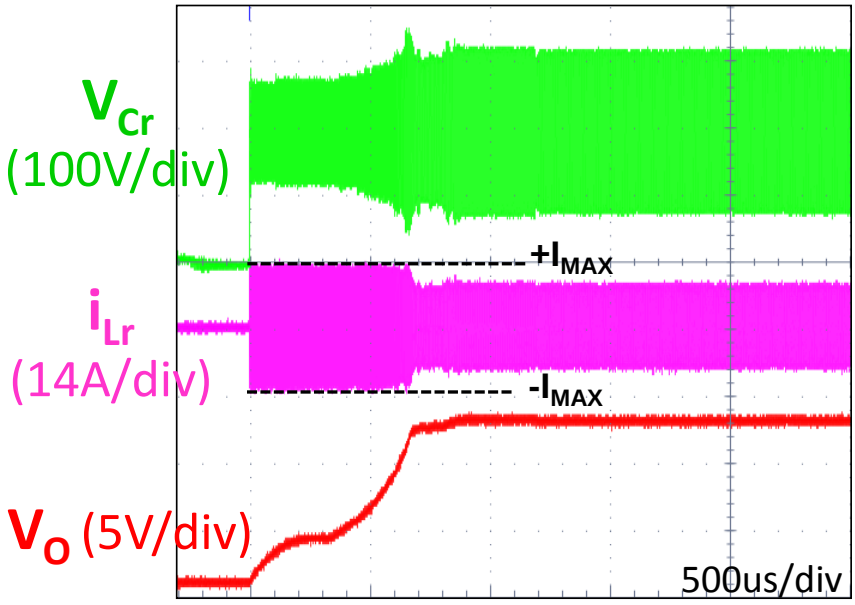

Fig. 3.13. Soft start-up for 500kHz LLC converter with 400V input voltage and 80A electrical load

3.6 Conclusions

In this chapter, how to implement the Optimal Trajectory Control (OTC) for soft start-up with the commercial low-cost MCU is investigated. Simplified Optimal Trajectory Control (SOTC) for soft start-up of LLC converter with only sensing Vo is proposed. And SOTC for soft start-up is verified on a 500kHz LLC converter using 60MHz MCU. OTC for soft start-up is universal applicable but requires additional analog circuit and proper PWM module configuration. SOTC for soft start-up doesn't need additional circuit and only needs to sense V_O, but requires case-by-case look-up table for different power stage design. Both methods can achieve the optimal trajectory control for soft start-up with low-cost MCU.

Chapter 4. Simplified Optimal Trajectory Control (SOTC) for Burst Mode of LLC Resonant Converters

4.1 Introduction

Burst mode is widely used to improve the light load efficiency of the LLC resonant converter. The concept of burst mode is to switch the converter between ON and OFF mode. During the burst-ON time, the converter runs at the efficiency-optimal point. While during the burst-OFF time, the converter is shut down and there is no energy delivered to the load. The average power of the whole burst period equals to the power required by the load so that output voltage is stabilized around the reference. The comparison of the conventional frequency control and the burst mode control is shown in Fig. 4.1.

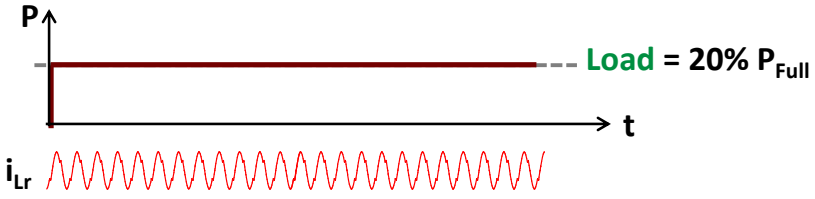

(a)

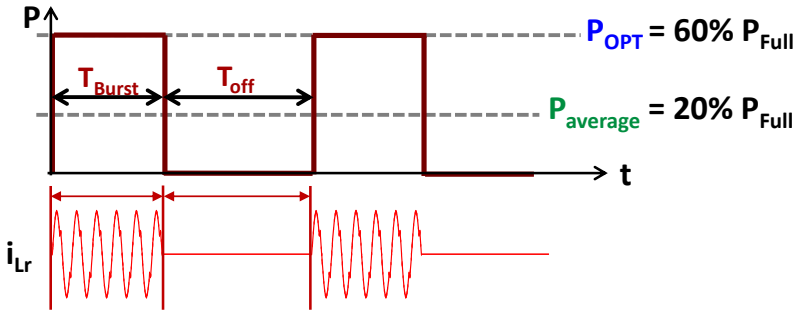

(b)

Fig. 4.1. Comparison of frequency control (a) and burst mode control (b)

The burst mode on-time is defined as T_{burst}, and off-time is defined as T_{off}. P_{OPT} is the power delivered to the secondary side during burst on-time. Then the burst duty cycle D_{burst} and average power $P_{average}$ during burst mode is expressed as below:

$$\boldsymbol{D_{Burst}} = \frac{\boldsymbol{T_{Burst}}}{\boldsymbol{T_{Burst}+T_{off}}} \tag{4.1}$$

$$\boldsymbol{P_{Average}} = \boldsymbol{P_{OPT}} \cdot \boldsymbol{D_{Burst}} \tag{4.2}$$

Ideally, burst mode can boost the light efficiency to the optimal efficiency by settling resonant tank to the efficiency-optimal state during burst-ON time. However, it is challenging to control the resonant converter during burst on-time due to the complex control characteristics caused by the dynamics of the resonant tank.

Several approaches have been tried to control the burst mode of the LLC resonant converter. Some controllers use hysteresis control: since the output voltage increases at light load, when it reaches the positive threshold, the controllers would enter burst-OFF; and when the output voltage decreases to the negative threshold, the controllers would start burst-ON again [49][50]; so the output could be controlled around the reference. Another controller limits the maximum switching frequency to realize burst mode: when the compensator required switching frequency is above the positive threshold, the controller would enter burst-OFF until the compensator required switching frequency is below the negative threshold [51]. Another controller senses load current to determine whether operating in burst mode or not: if load current is below the threshold, the controller would enter into a Missing Cycle (MC) mode, where every two out of five switching cycles are removed [52]. Another burst mode control method proposed in paper [36] uses constant burst frequency and variable burst duty cycle depending on load condition; while the switching frequency during burst on-time is controlled by the compensator. With these

burst mode control methods, since the switching frequency is controlled by the compensator rather than optimized for the resonant tank and their output voltage ripple during burst mode is too large, they have the problem of being not able to fix to the highest-efficiency status during burst on-time.

The concept of state-trajectory analysis and control was extended to the burst mode of the LLC resonant converter in [42]: the problems of the previous burst mode control methods are analyzed and the Optimal Trajectory Control (OTC) of burst mode for the LLC resonant converter is proposed.

However, the OTC of burst mode was based on very high-performance digital controller, which is not feasible for industrial application. To improve the light load efficiency of the high frequency LLC resonant converter, it is very important to investigate the limitation of the OTC for burst mode with low-cost digital controllers, and solve the challenge in the burst mode of high frequency LLC converter without sacrificing the performance and increasing the cost.

4.2 Implementation of Optimal Trajectory Control (OTC) for Burst Mode and Its Limitation in High Frequency LLC Converter

The previous burst mode control methods have the problem of being not able to fix to the highest-efficiency status during burst on-time since the switching frequency is controlled by the compensator rather than optimized for the resonant tank and the output voltage ripple is very large. To solve this problem, Optimal Trajectory Control (OTC) of burst mode for LLC converter uses fixed 3-pulse pattern for burst on-time and constant burst-on time implementation for closed-loop control.

Fig. 4.2 is the illustration of fixed 3-pulse pattern in OTC for burst mode with time-domain waveforms in Fig. 4.2(a) and corresponding state-trajectory in Fig. 4.2(b). In the fixed 3-pulse pattern in OTC, the first pulse settles resonant tank from burst mode initial point to the highest efficiency load equivalent trajectory; then the second and the third pulse would follow the highest efficiency load equivalent trajectory; after the third pulse, all the switches are turned off, and the state-trajectory comes to burst mode initial point after a little oscillation cause by energy in magnetizing inductor.

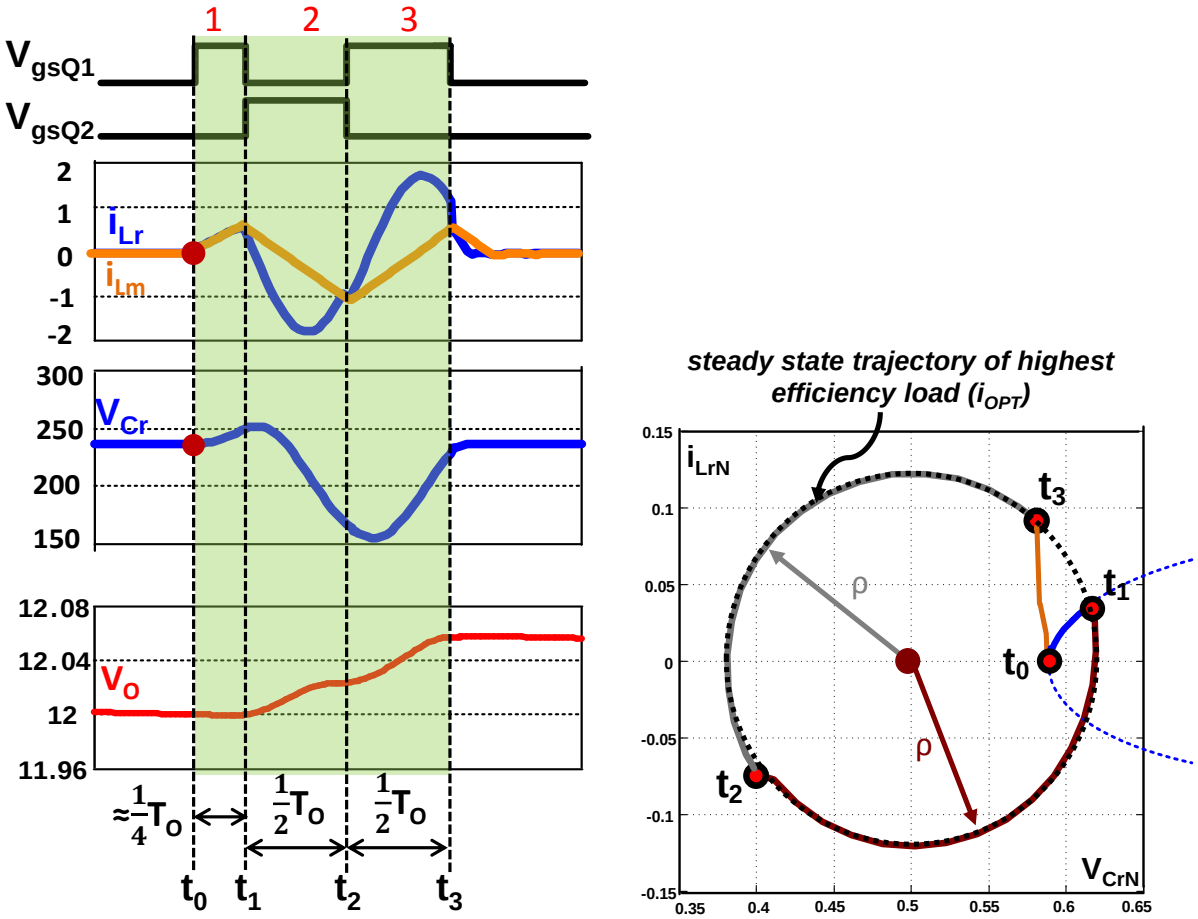

(a) (b)

Fig. 4.2. Fixed 3-pulse pattern in OTC for burst mode: (a) time-domain waveform; (b) state-trajectory

With the calculation in [42], the length of the first pulse is normally around $\frac{1}{4}T_o$, in which T_O is the resonant period; the length may have some variation for different power stage designs. Since the second and the third pulse follow the highest efficiency load equivalent trajectory, both their lengths are around the half of the resonant period. The third pulse may be a little bit smaller than the half of the resonant period in order to settle resonant tank to burst mode initial point, but it can still be treated approximately as the half of the resonant period in the following analysis.

An example of digital implementation of OTC for burst mode based on MCU (TMS320F28027) is shown in Fig. 4.3. The basic control scheme is constant burst-on time control. When the output voltage is below the reference, which is 12V in this example, the controller would generate the fixed 3-pulse pattern. After that, there would a 1us blanking time to avoid noise from oscillation. Then the controller would sample output voltage, compare with reference and determine if updating PWM for the next burst on-time. The control loop in off-time is executed every 2us. The sampling includes load current for system power management consideration and the control loop includes over-current monitor and transition to normal operation.

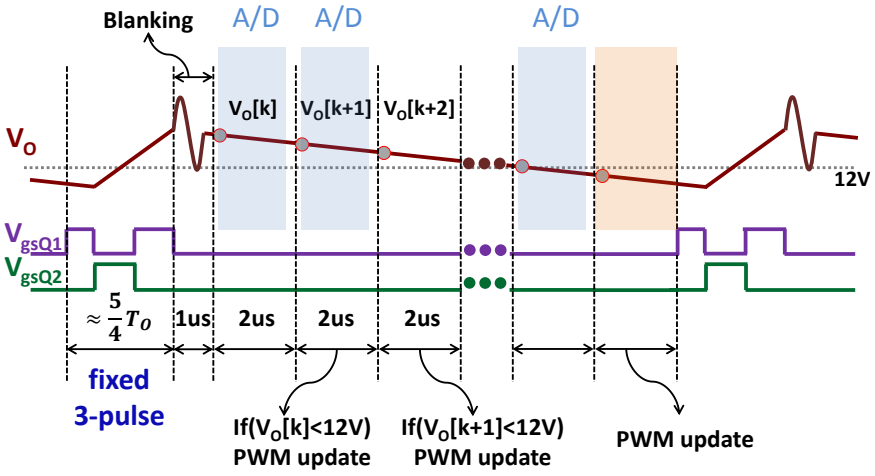

Fig. 4.3. Digital implementation of OTC for burst mode

The off-time in the constant on-time control is variable and dependent on load condition. When the load condition becomes lighter, the off-time is increased so that the average power is decreased. When the load condition becomes heavier, the off-time decreases. While the on-times for different conditions are always the same to ensure small output voltage ripple.

For the digital implementation of OTC for burst mode, there would be a minimum off-time limitation, an example of which based on MCU (TMS320F28027) is shown in Fig. 4.4. The case of minimum off-time happens when the first sampling of output voltage, which is just after the 1us blanking time, is equal to or below the reference. The first control loop execution after the 1us blanking time is just the sampling and A/D conversion of the output voltage and output current. The second control loop updates PWM for burst on-time. The first pulse of the 3-pulse pattern is also classified as off-time in the following analysis, since there the first pulse is used to settle resonant tank and there is no energy delivered to the secondary side within the first pulse.

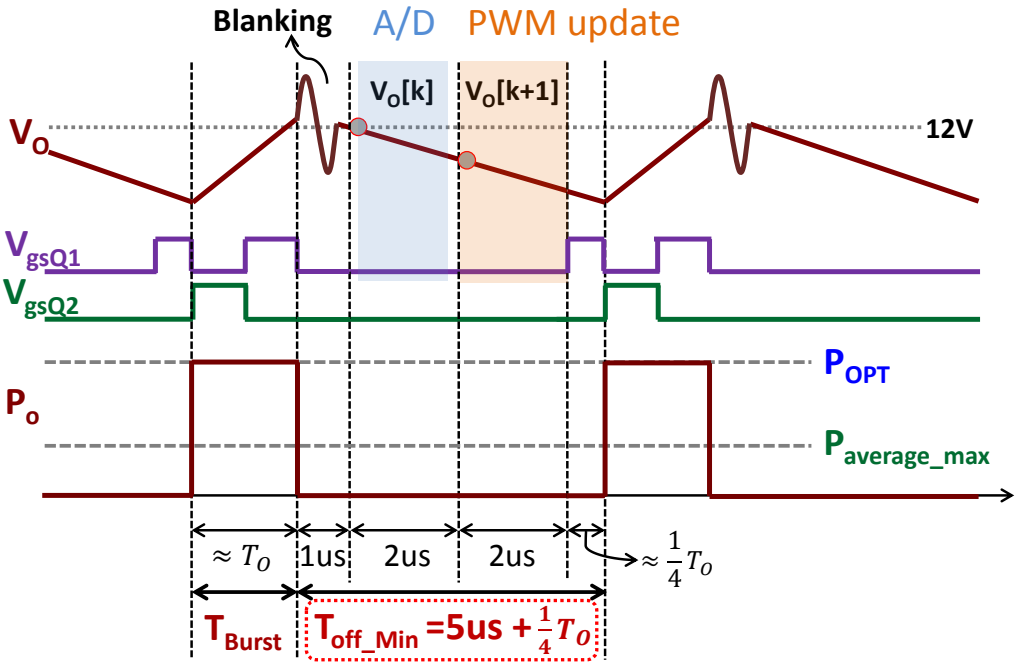

Fig. 4.4. Minimum off-time limitation in the digital implementation of OTC for burst mode

Deriving from the analysis above, the minimum off-time consists of 1us blanking time, twice execution of control loop, first pulse of fixed 3-pulse pattern. And the on-time is later 2 pulses in the fixed 3-pulse pattern. Corresponding to the minimum off-time, the maximum burst duty cycle and maximum average power is expressed as below

$$\boldsymbol{D_{Burst\_max}} = \frac{\boldsymbol{T_{Burst}}}{\boldsymbol{T_{Burst}+T_{off\_min}}} = \frac{\boldsymbol{T_O}}{\frac{5}{4}\boldsymbol{T_O}+5\boldsymbol{us}} \tag{4.3}$$

$$\boldsymbol{P_{Average\_max}} = \boldsymbol{P_{OPT}} \cdot \boldsymbol{D_{Burst\_max}} \tag{4.4}$$

With the equation for maximum burst duty cycle D_{Burst_max} and resonant period T_O referred above, the relationship between D_{Burst_max} and resonant frequency f_O is shown in Fig. 4.5. In which D_{Burst_max} for 130kHz LLC converter and 500kHz LLC converter is marked for comparison. The resonant frequency is normally selected below 130kHz for commercial products, which means that the D_{Burst_max} will be large than 50% and there will enough burst mode operation range.

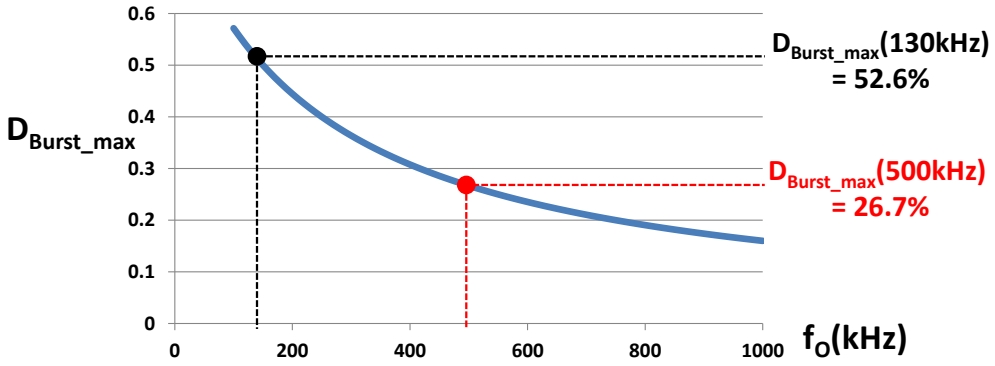

Fig. 4.5. Relationship between maximum burst duty cycle D_{Burst_max} and resonant frequency f_O

However, when the switching frequency is pushed higher, for example 500kHz, the D_{Burst_max} decreases to 26.7% and there will be a problem in the burst mode operation range if the fixed 3-pulse pattern of OTC is not changed. Fig. 4.6 takes a 500kHz LLC converter as an example. The peak efficiency is at 60% load condition. With a maximum burst duty cycle D_{Burst_max} of 26.7%,

the maximum average power $P_{average\_max\_1}$ is only 16% of full load condition. So burst mode can be applied from no load to only 16% load.

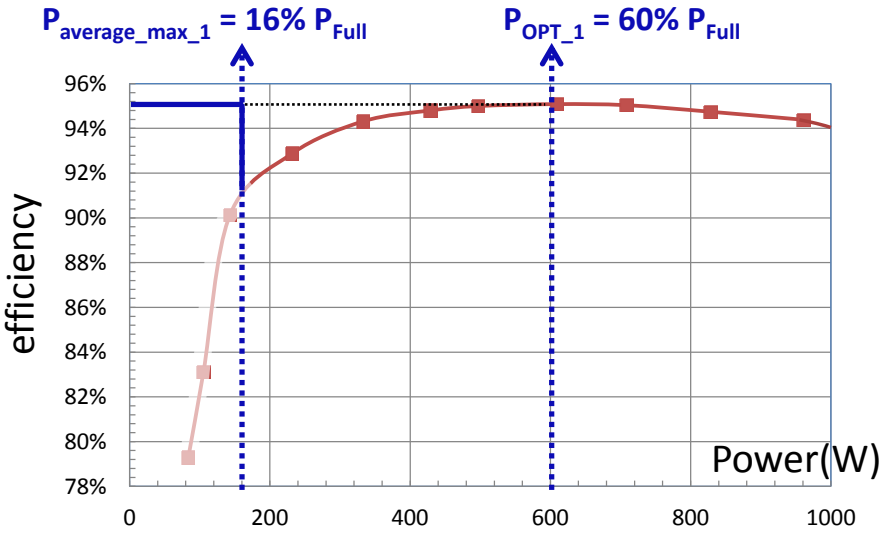

Fig. 4.6. Expected efficiency curve of OTC for burst mode with fixed 3-pulse pattern on a 500kHz LLC converter

When the OTC for burst mode of LLC converter is implemented by digital controller, there is always the limitation of the maximum burst duty cycle caused by digital delay and fixed 3-pulse pattern. And for given controller, the higher the switching frequency of LLC, the smaller this maximum burst duty cycle is. Corresponding to the maximum burst duty cycle and the burst on-power, the burst mode operation range is limited by the maximum average power. To solve this problem, the Simplified Optimal Trajectory Control (SOTC) for burst mode with adaptive burst on-power and adaptive multi-step is proposed in the followings.

4.3 Proposed Simplified Optimal Trajectory Control (SOTC) for Burst Mode with Adaptive Burst On-power and Adaptive Multi-step

The operation range of OTC for burst mode is determined by the maximum average power, which is the product of the maximum burst duty cycle and the burst on-power. To increase the maximum average power, one obvious method is to increase the burst on-power. Since the first pulse of the 3-pulse pattern in OTC for burst is used to settle resonant tank to certain power level, the controller can easily adjust the length of this first pulse to change the burst on-power.

In the OTC for burst mode, the burst on-power is chosen as the peak efficiency point. If the burst on-power is selected to be full power instead of peak efficiency point, then the maximum average power can be increased as shown in Fig. 4.7. The solid line is corresponding to the case with burst on-power of peak efficiency point, and the dash line is corresponding to the case with burst on-power of full power.

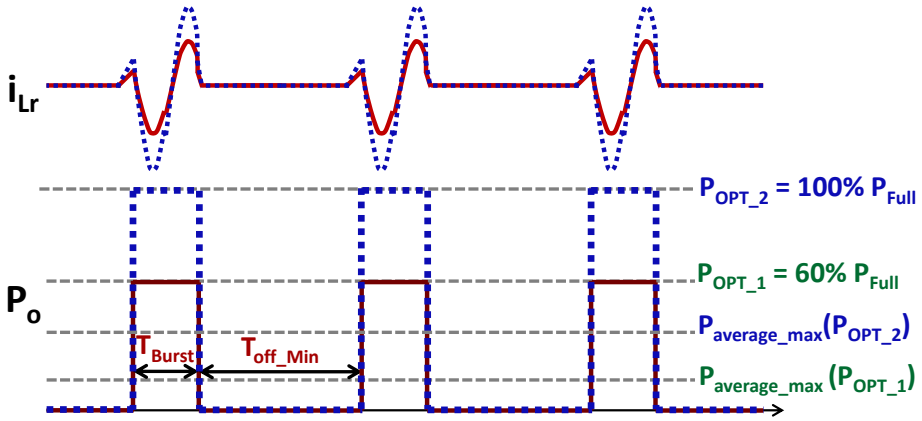

Fig. 4.7. Increase burst on-power to increase the corresponding maximum average power

Following the concept of increasing burst on-power, the SOTC for burst mode with adaptive burst on-power is proposed, whose expected efficiency curve is illustrated in Fig. 4.8. Firstly, the burst on-power is selected to be the peak efficiency point for the load range of from no load condition to the peak efficiency corresponding maximum average power, which is $P_{average\_max\_1}$ in Fig. 4.8. Then, the burst on-power is selected to be the full power for the load range of from

$P_{average\_max\_1}$ to the full power corresponding maximum average power, which is $P_{average\_max\_2}$ in Fig. 4.8.

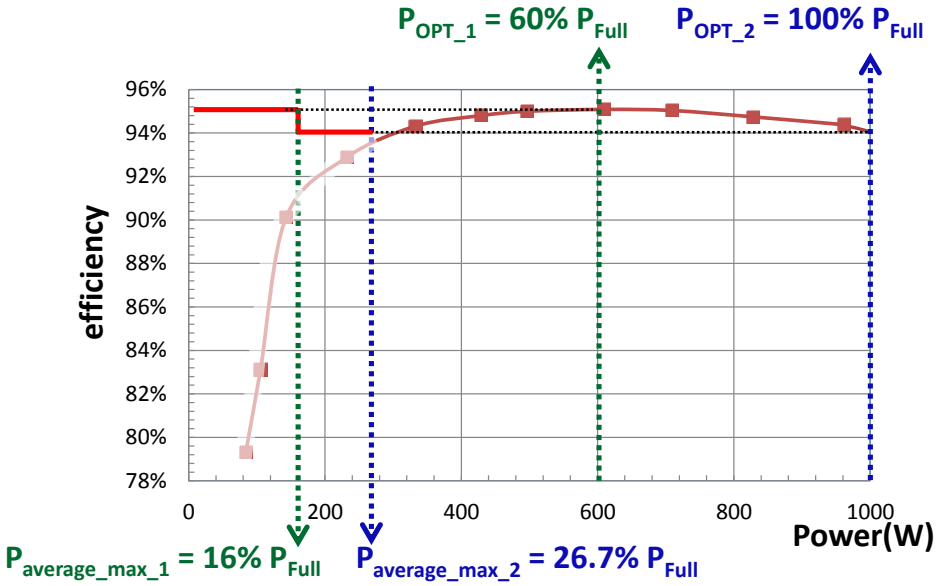

Fig. 4.8. Expected efficiency curve of the proposed SOTC for burst mode with adaptive burst on-power on a 500kHz LLC converter

The proposed SOTC for burst mode with adaptive burst on-power uses different burst on-power under different load condition to increase the burst operation range. It still uses 3-pulse pattern, but the length of the first pulse, which is used to settle resonant tank to certain power level, is dependent on load condition. For very light load (below $P_{average\_max\_1}$), it can still achieve the peak efficiency ideally. But as the load increases (between $P_{average\_max\_1}$ and $P_{average\_max\_2}$), there is a little sacrifice in the burst mode efficiency.

The maximum average power is the product of the maximum burst duty cycle and the burst on-power. The first proposed method uses larger burst on-power to increase the maximum average power. The second proposed method uses large burst on-time to increase the maximum average power.

Fig. 4.9 is the comparison of burst mode with 3-pulse pattern (top waveforms) and 5-pulse pattern (bottom waveforms). For the burst mode with 5-pulse pattern, the first pulse is still used to settle resonant tank, which is the same as the first pulse of the 3-pulse pattern. And the following 4 pulses follow the highest-efficiency load trajectory, which are same as the later 2 pulses in the 3-pulse pattern. Since the minimum off-time are the same for both cases and the burst on-time of the 5-pulse pattern is larger, the maximum burst duty cycle of the 5-pulse pattern is larger, resulting in larger maximum average power.

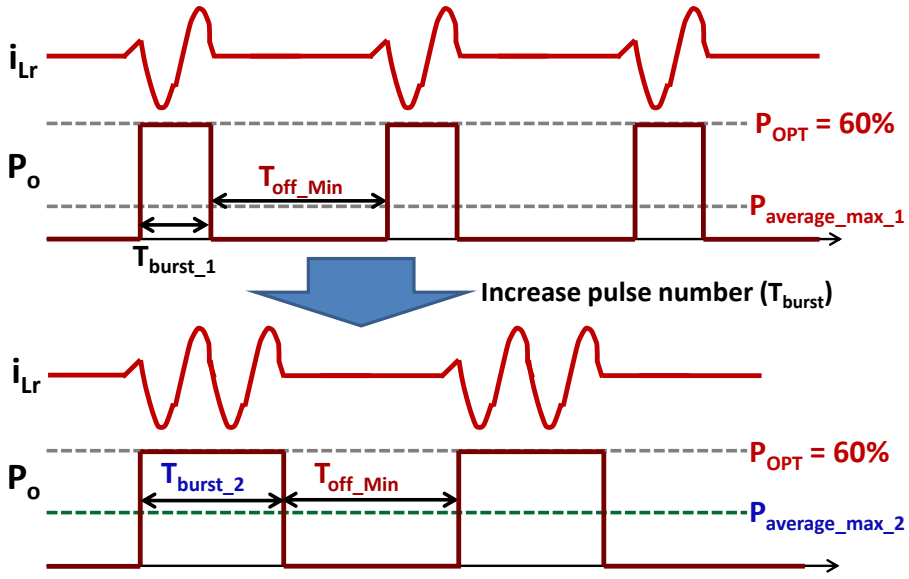

Fig. 4.9. Comparison of burst mode with 3-pulse pattern (top waveforms) and 5-pulse pattern (bottom waveforms)

Following the concept of increasing burst on-time, the SOTC for burst mode with adaptive multi-step is proposed, as illustrated in Fig. 4.10. The first pulse is always the same as that in the fixed 3-pulse pattern in OTC for burst mode, in order to settle the burst on-power to the highest-efficiency point. The pulses following the first pulse always have the length of around half resonant period. The number of pulses can be selected as 3, 5, 7, and 9 … depending on load condition.

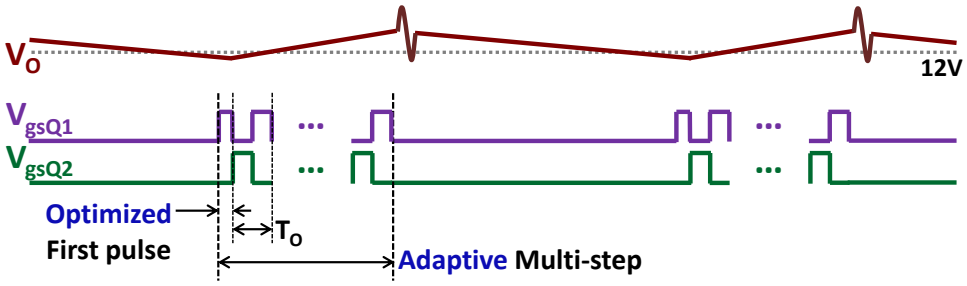

Fig. 4.10. Concept of SOTC for burst mode with adaptive multi-step

Take a 500kHz LLC converter as an example, the table of pulse number, T_{Burst}, D_{Burst_max} and $P_{Average\_max}$ is shown in Table 4.1. For different load condition, the pulse number can be selected according to P_{Aveage_max}.

Pulse #	3	5	7	9	N
T_{Burst}	2us	4us	6us	8us	…
D_{Burst_max}	26.7%	42.1%	52.2%	59.3%	…
$P_{Average\_max}$	16%	25.3%	31.3%	35.6%	…

Table 4.1. $P_{average\_max}$ vs. pulse number on a 500kHz LLC converter

The expected efficiency curve of the proposed SOTC for burst mode with adaptive multi-step on a 500kHz LLC converter is illustrated in Fig. 4.11. 3-pulse pattern is used from no load to 16% load; 5-pulse pattern is used from 16% load to 25.3% load; 7-pulse pattern is used from 25.3% load to 31.3% load; and same analogy applies until load reaches the highest-efficiency point in ideal case.

Since the pulse number is dependent on load condition, the output voltage ripple is still very small at very light load condition with 3-pulse pattern, and has little variations as pulse number increases due to the increase of load current.

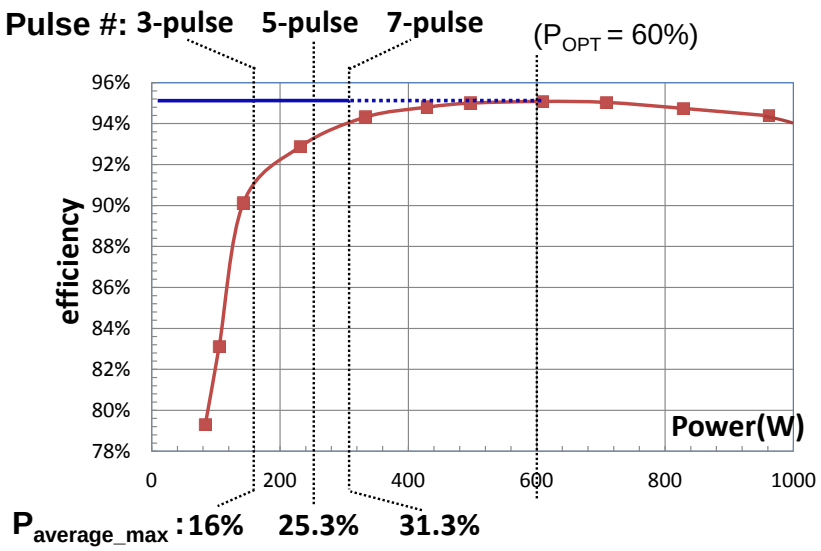

Fig. 4.11. Expected efficiency curve of the proposed SOTC for burst mode with adaptive multi-step on a 500kHz LLC converter

In this section, the SOTC for burst mode with adaptive burst on-power and adaptive multi-step are proposed to solve the limitation in OTC for burst mode with digital implementation. The SOTC for burst mode with adaptive burst on-power always uses 3-pulse pattern, but adjusts the length of the first pulse to change the burst on-power. The SOTC for burst mode with adaptive multi-step always uses the same first pulse, but adjusts the pulse number to change the burst on-time. From expected efficiency curves, it shows that the SOTC for burst mode with adaptive-multi-step has better efficiency performance and large burst operation range.

4.4 Optimized Transition between Burst Mode and Normal Operation

When burst mode is combined with normal operation, the transition between burst mode and normal operation needs to be well controlled to prevent large current and voltage stresses. To solve this problem, an optimized transient process from burst mode to normal operation is proposed. Firstly the LLC converter works at burst mode; when load current becomes larger than

burst mode limit, the controller will generate first 2 pulses of burst mode 3-pulse pattern, as shown in Fig. 4.12(a) from t_0 to t_3. Then the state is settled to i_{OPT} equivalent trajectory (i_{OPT} is the efficiency-optimal load current). After that, the controller can use SOTC to settle resonant tank from i_{OPT} equivalent trajectory to i_H equivalent trajectory, as shown in Fig. 4.12(a) from t_2 to t_4. Fig. 4.12(b) is the corresponding state trajectory.

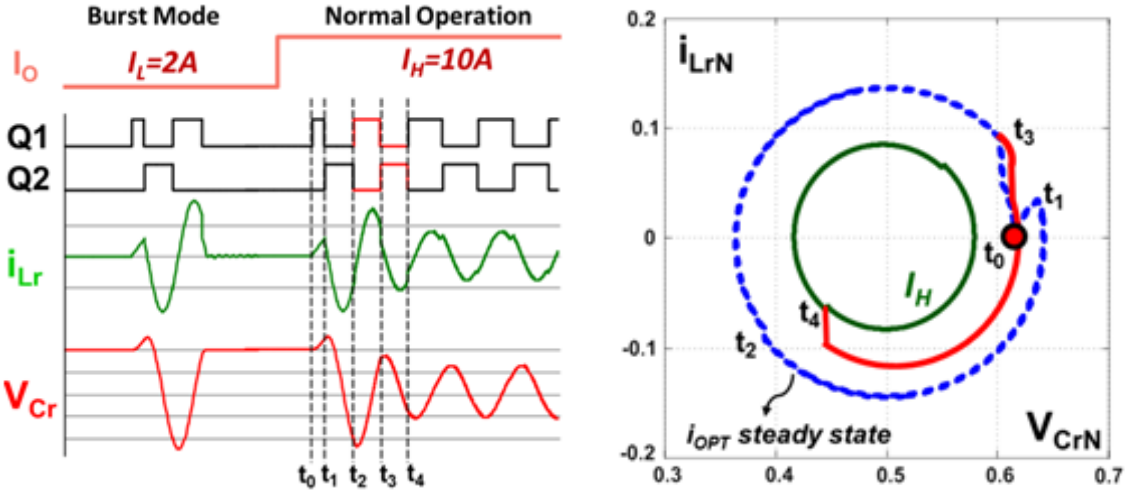

(a) Time-domain waveform; (b) State-trajectory

Fig. 4.12. Optimized transient process from burst mode to normal operation

After this, the controller can use frequency control with PI compensator and SOTC to ensure the circuit works at steady state. With the proposed method, the whole transient process does not involve much calculation burden for MCU, and there is no dynamic oscillation.

Besides the optimized transient process from burst mode to normal operation, an optimized transient process from normal operation to burst mode is proposed. Firstly the circuit works at normal operation; when load current becomes smaller than burst mode limit, the controller will generate extra one pulse, as shown in Fig. 4.13(a) from t_0 to t_1, to settle resonant tank within one step. Then after t_2, the state stays at burst mode initial point. Fig. 4.13(b) is the corresponding state trajectory. This extra one pulse is calculated using the concept of one-step SOTC.

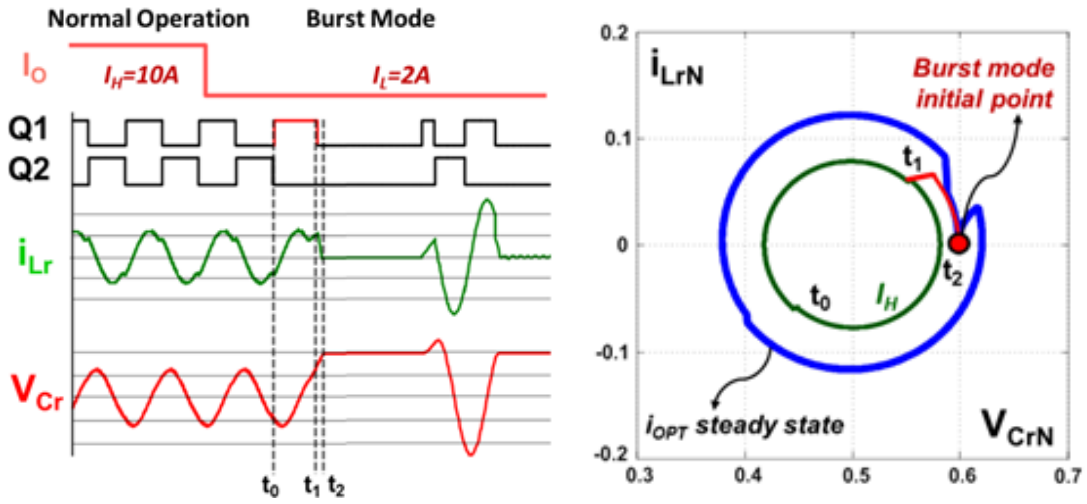

(a) Time-domain waveform; (b) State-trajectory

Fig. 4.13. Optimized transient process from normal operation to burst mode

After this, the controller can use constant burst on time control. With the proposed method, the whole transient process does not involve much calculation burden for MCU, and the performance is quite good.

Below are approximate equations for one-step SOTC. The first equation is for the case $I_H < I_{initial}$, and the extra one step would be $\frac{1}{2}T + \Delta T_{UP}$. The second equation is for the case $I_H > I_{initial}$, and the extra one step would be $\frac{1}{2}T - \Delta T_{DOWN}$. Where $I_{initial}$ is burst mode initial point equivalent trajectory, which may vary for different power stage.

$$\Delta T_{UP} = 2 \cdot \frac{L_m \cdot (I_{initial} - I_H)/n}{V_{in}} \tag{4.5}$$

$$\Delta T_{DOWN} = (1 - \frac{I_{initial}}{I_H}) \cdot \frac{T}{4} \tag{4.6}$$

4.5 Experimental Results of Burst Mode

The SOTC for burst mode with adaptive multi-step is verified on the 500kHz LLC converter referred in the Chapter 2. The waveforms of the proposed SOTC for burst mode with adaptive

multi-step are shown in Fig. 4.14, including: 3-pulse pattern @ load = 4A; 5-pulse pattern @ load = 12A; and 7-pulse pattern @ load = 18A. It is shown clearly that the resonant current fixes to the same power level during burst on-time and the output voltage ripple has little variations under different conditions.

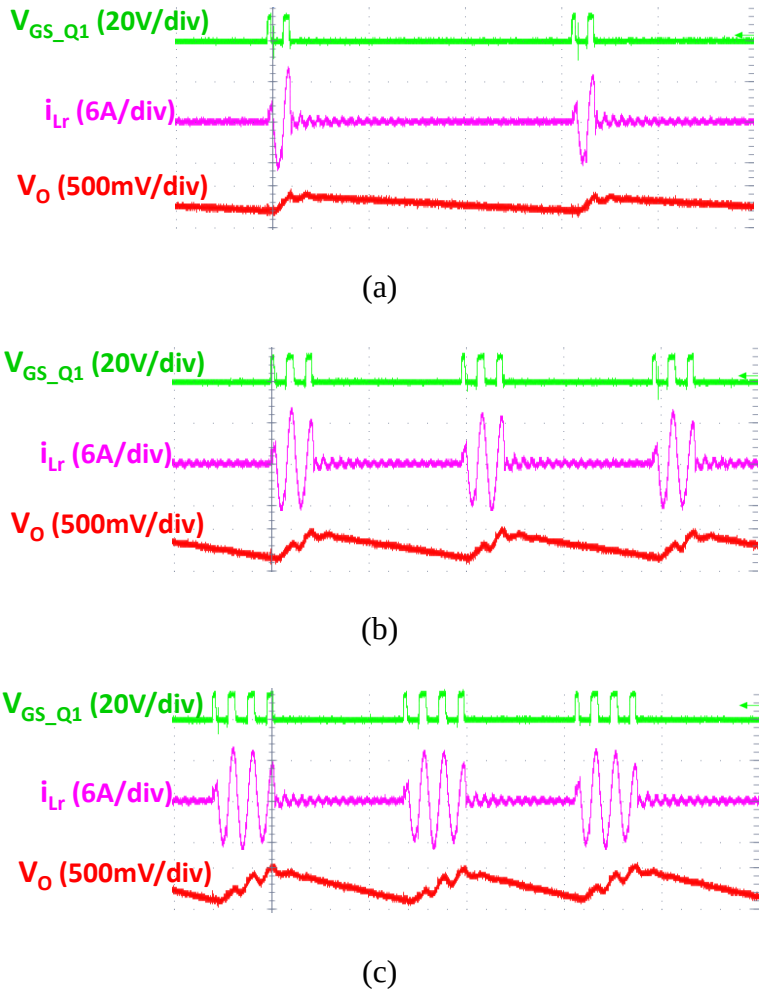

Fig. 4.14. Waveforms of the proposed SOTC for burst mode with adaptive multi-step: (a) 3-pulse pattern @ load = 4A; (b) 5-pulse pattern @ load = 12A; (c) 7-pulse pattern @ load = 18A

The efficiency curve of the proposed SOTC for burst mode with adaptive multi-step is shown in Fig. 4.15. The efficiency curves of the normal operation and the state-of-art burst mode are also drawn in Fig. 4.15 as comparison. The efficiency curves show that the light load efficiency

improvement of the proposed SOTC for burst mode with adaptive multi-step is significant. The converter enters burst mode when load condition is below 26% load. And it can achieve 91.8% efficiency at even 2.4% load.

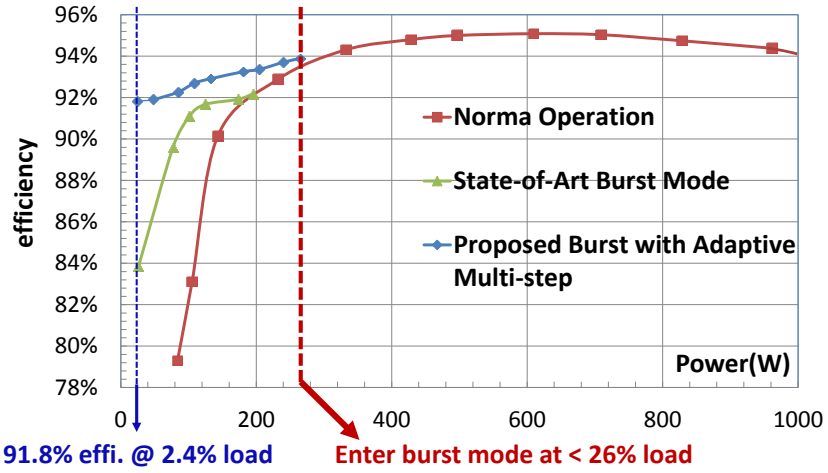

Fig. 4.15. Efficiency comparison of the proposed SOTC for burst mode with adaptive multi-step

There is some difference between the experimental efficiency curve and the expected ideal efficiency curve; this is because even the first pulse settles resonant tank to highest-efficiency point, it's still different from normal operation at highest-efficiency point. Then reasons include: the first pulse is hard switching turn-on; the energy in the first pulse is circulating energy and there is no power delivered to the secondary side; the oscillation between Lr, Lm and Coss after last pulse turn-off will induce extra loss.

The optimized transition between burst mode and normal operation is verified on the 130kHz LLC converter referred in Chapter 2. Fig. 4.16 is the experimental results of optimized transient processes between burst mode and normal operation. The left side is from normal operation (load = 10A) to burst mode (load = 2A), and the right side is from burst mode (load = 2A) to normal operation (load = 10A). It is shown clearly that the resonant tank is settled immediately in both cases.

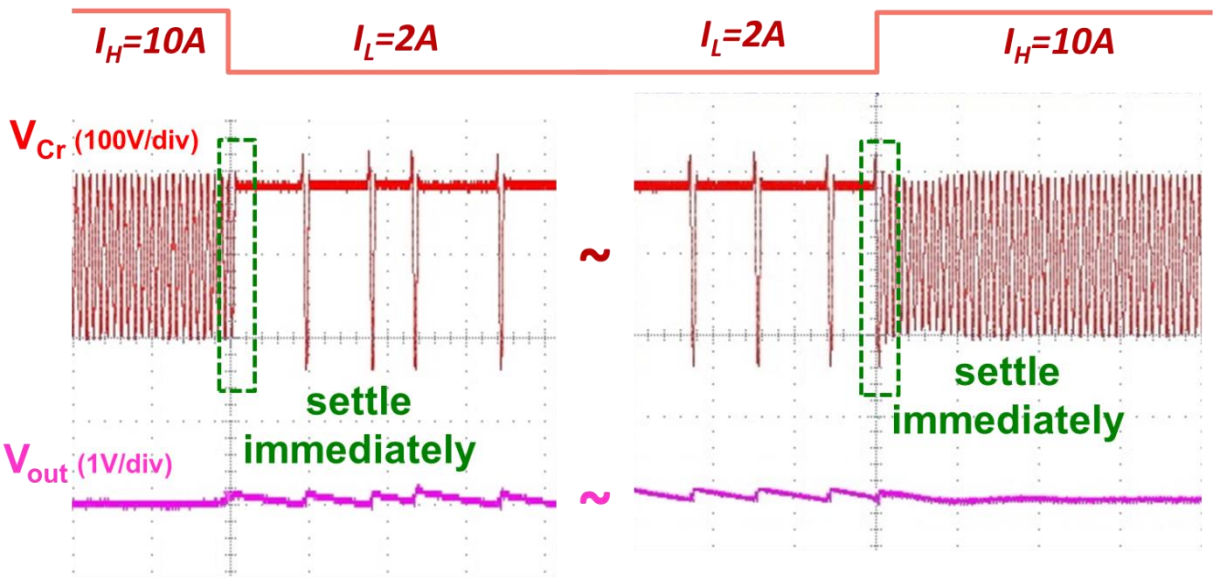

Fig. 4.16. Optimized transient processes from normal operation to burst mode and from burst mode to normal operation

4.6 Conclusions

In this chapter, the Optimal Trajectory Control (OTC) for the burst mode of the LLC converter is investigated and its limitation in the high frequency LLC converter with digital implementation is explained in detail. The burst operation range is limited when applied to the high frequency LLC converter due to the small minimum off-time caused by digital delay and the small burst on-time caused by high switching frequency.

To solve this challenge, the Simplified Optimal Trajectory Control (SOTC) for burst mode with adaptive burst on-power and adaptive multi-step are proposed. The proposed burst mode with adaptive burst on-power adjusts burst on-power based on load condition to extend burst operation range. The proposed burst mode with adaptive multi-step adjusts pulse number for burst on-time based on load condition to extend burst operation range. The second proposed

method has better efficiency and larger operation range, with which the expected burst mode can be extended to the highest-efficiency point. Besides, the optimized transition process between burst mode and normal operation is proposed to combine burst mode with normal operation.

Experimental results of SOTC for burst mode with adaptive multi-step are demonstrated on a 500kHz 1kW 400V/12V LLC converter controlled by a 60MHz microcontroller (TMS320F28027). And light load efficiency improvement is significant, with burst mode extended to 26% load and 91.8% efficiency at even 2.4% load. The optimized transition process is verified on a 130kHz LLC converter.

Chapter 5. Adaptive Synchronous Rectifier (SR) Driving Scheme for LLC Resonant Converters

5.1 Introduction

Since most of the IT applications require the DC-DC converters to provide a low-voltage high-current output, diode rectifiers will induce very large conduction loss. Synchronous rectifiers (SR) are critical for the LLC converters to improve the efficiency by tremendously reducing the conduction loss of the diode rectifiers. However, the SR driving scheme is quite challenging due to the discrepancy between primary driving signal and SR driving signal as shown in Fig. 5.1. If the switching frequency is below the resonant frequency, the SR on-time is smaller than the primary switch on-time; if the switching frequency is above the resonant frequency, the SR on-time is larger than the primary switch on-time; if the switching frequency is equal to the resonant frequency, the SR on-time is equal to the primary switch on-time. Besides, the SR on-time is also dependent on the load condition.

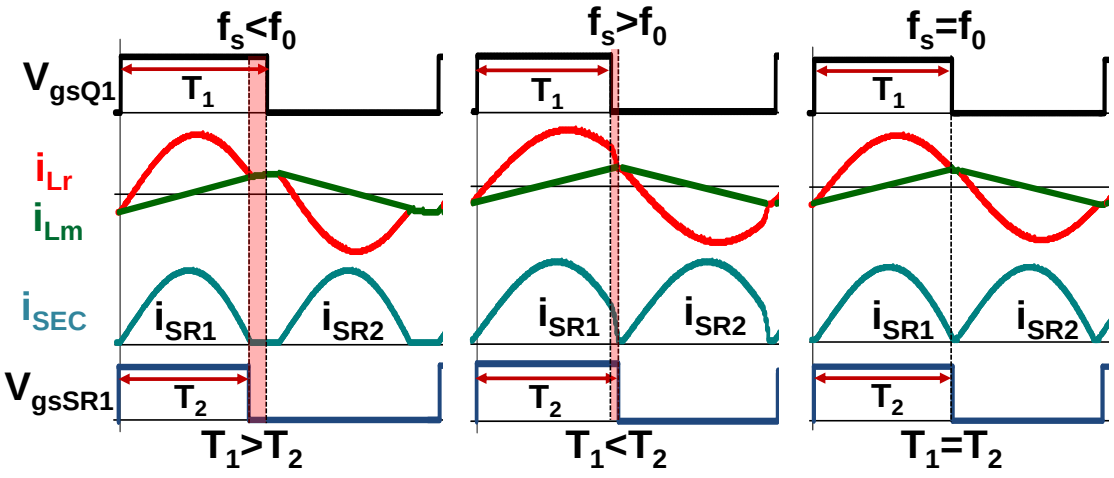

Fig. 5.1. SR on-time of LLC converter with different switching frequency

Several SR driving methods have been proposed, most of which can be sorted into three categories. The first category of SR driving is based on current sensing. One solution [53] is to use current transformer to sense SR current i_{SEC}, and generate corresponding driving signal, which is accurate but induces large loss due to the large current in SRs. Another solution [54] using CLL topology senses primary current to generate SR driving signal, but it requires an inductor with large inductance. Another SR driving method by sensing the primary resonant current was proposed in [55], but it requires complex current-compensating winding in current transformer to cancel out the magnetizing current and generate suitable driving signals for SR. The second category of SR driving is independent driving circuit based on SR drain to source voltage V_{ds_SR}, which works in the following principle: at the beginning, the SR is in off-state; when there is body diode conduction, it would result in a large forward voltage drop; then the controller would compare the V_{ds_SR} with the turn-on threshold voltage; if the V_{ds_SR} is larger than the threshold, the controller would turn on the SR; in the LLC converter, during SR on-time, the current in SR will first increase and then decrease until zero; as the current approaches zero, the V_{ds_SR} also becomes very small, which is compared with the turn-off threshold voltage to determine when to turn off the SR. Most of the solutions in the second category of SR driving are smart ICs [56][57][58]. However, the accuracy of the SR driving methods in the second category is affected by the SR package. The actual SR on-time is shorter than the expected value due to the inevitable package inductance of SR. This problem is extremely severe in high frequency application. A compensation network can be connected to the sensed terminals to solve this problem [59]. The third category of SR driving is adaptive SR driving scheme. The drain to source voltage of SR V_{ds_SR} is detected to tune the gate driving signal. If there is body diode conduction, the large forward voltage drop in V_{ds_SR} will be sensed and the SR on-time

will be increased accordingly. One solution [60] proposes to use a compensator to generate the SR on-time. Another solution [61] proposes to detect the body diode conduction just at the SR turn-off moment, and tune the SR on-time step-by-step until it reaches around the optimal point.

The digital controllers are gradually taking the place of the analog controllers in the control of the LLC resonant converter. Among the digital controllers, cost-effective microcontrollers (MCU) are preferred in industrial applications. So it is very necessary to integrate the SR driving within the cost-effective digital controllers while at the same time utilizing very little controller resources. Furthermore, it is even more challenging to apply the SR driving to the high frequency LLC converter without sacrificing the performance and increasing the cost. Compared with the first and second categories of SR driving methods, which are independent solutions, the third category of adaptive SR driving is more suitable to be integrated within the digital controllers.

5.2 Limitation of Previous Adaptive SR Driving Methods and Proposed Adaptive SR Driving Scheme Based on Ripple Detection

The implementation and limitation of two adaptive SR driving methods will be introduced in this section. Then the proposed SR driving method will be explained in detail.

The control scheme and waveforms of the adaptive SR driving method using linear compensator [60] are shown in Fig. 5.2. The SR body diode forward voltage drop is detected and compared with a threshold voltage. The output of the comparator is connected to the input of a linear compensator. The control signal of the linear compensator is connected to the positive input of the PWM generator, and a triangular waveform generated from primary driving signal is connected to the negative input of the PWM generator.

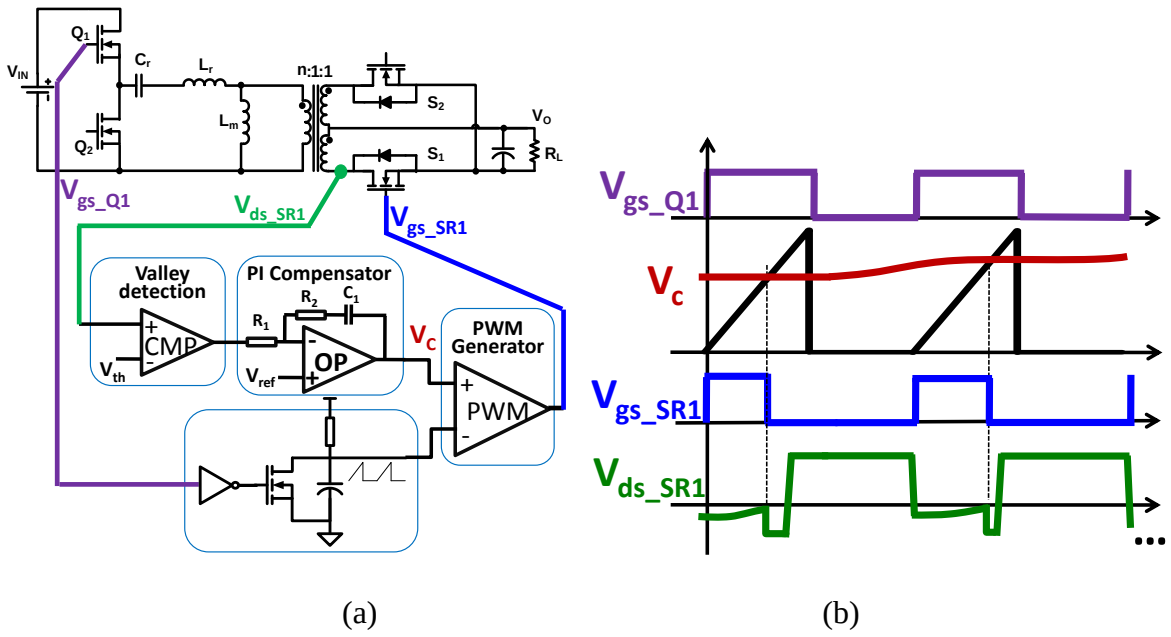

(a) (b)

Fig. 5.2. Adaptive SR driving method using linear compensator: (a) control scheme; (b) waveform

There would be two main limitations if this SR driving method is integrated within the cost-effective digital controllers. The first limitation is that it requires a linear compensator, which would either require additional circuit or occupy a lot of CPU resources. The second limitation is that since the negative input of PWM generator is from primary driving signal, the maximum SR on-time cannot be large than the on-time of primary switch, which is not suitable when switching frequency is larger than resonant frequency.

The control scheme and control flowchart of the adaptive SR driving method based on digital tuning [61] are shown in Fig. 5.3. The SR body diode forward voltage drop is detected and compared with a threshold voltage. The turn-on of SR in LLC converter is synchronized with primary switch. The on-time of SR is tuned step by step to be around the optimal point.

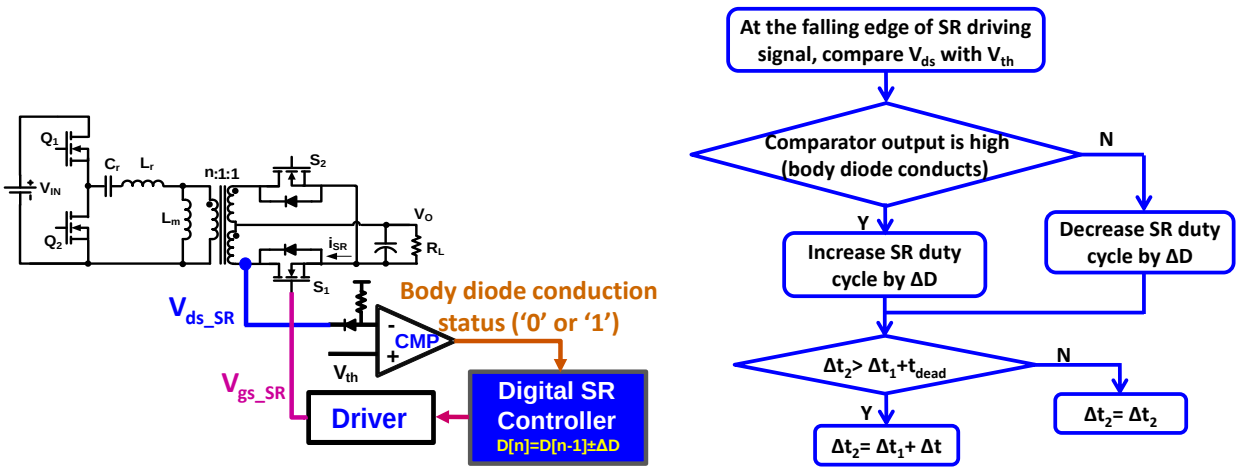

(a) (b)

Fig. 5.3. Adaptive SR driving method based on digital tuning: (a) control scheme; (b) control flowchart

The limitation with this SR driving method is that it requires comparing the V_{ds_SR} with the threshold voltage (which means sensing the output of comparator) just at the falling edge of SR driving signal. The implementation of function requires additional logic circuit or FPGA controller, which cannot be integrated within the cost-effective digital controllers.

The proposed adaptive SR driving method based on ripple detection is shown in Fig. 5.4(a). The V_{ds} of SR is sensed and compared with the threshold voltage and the output of the comparator is connected to the ripple detection function of the digital controller, i.e. the external interrupt of the microcontrollers. Since this proposed adaptive SR driving method is integrated within the digital controller, the primary driving signal is used to control the enable/disable of the ripple detection.

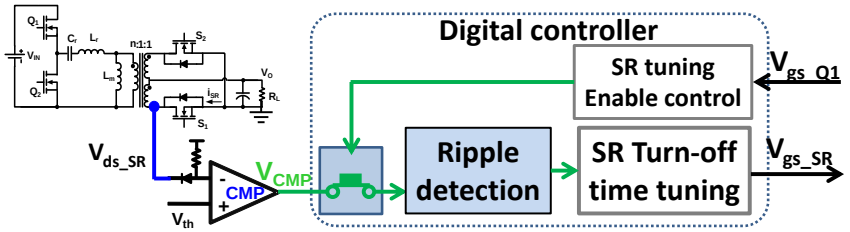

(a)

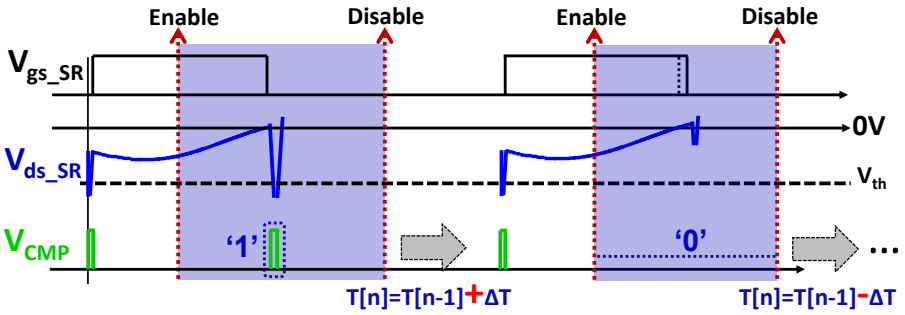

(b)

Fig. 5.4. Proposed adaptive SR driving based on ripple detection: (a) control scheme; (b) waveform around steady state

The control principle is explained in the followings. The turn-on time of the SR is synchronized with the turn-on of the primary switch, and there is a very small time of body diode conduction. After that, the ripple detection is enabled. And before the next SR turn-on moment, the ripple detection is disabled. If there is body diode conduction, the controller would detect the ripple at the output of the comparator, and will increase the SR on-time by ΔT for the next switching cycle. If there is no body diode conduction, the controller cannot detect the ripple, and will decrease the SR on-time by ΔT for the next switching cycle. The tuning process is the same with the previous adaptive SR driving method. And Fig. 5.4(b) shows the waveforms in steady state.

Compared with other adaptive SR driving method, this proposed adaptive SR driving method can be easily integrated within the digital controller. It only requires a comparator in addition to

the digital controller. And It takes very little controller resources. For a 130kHz LLC converter with a 60MHz digital controller (TMS320F28027), the execution of the proposed adaptive SR driving method requires maximum of 50 CPU cycles at each switching cycle, which corresponds to only 11% CPU utilization.

5.3 Proposed Generalized Adaptive SR Driving Using Ripple Counter Concept for High Frequency LLC Converter

The proposed adaptive SR driving method based on ripple detection is suitable for the conventional LLC converter (resonant frequency is below 150kHz) with cost-effective digital controller. However, when the method is applied to high frequency LLC converter, there would be a problem caused by the dramatically increased CPU utilization. For a given 60MHz digital controller (TMS320F28027), the execution of the proposed adaptive SR driving method requires maximum of 50 CPU cycles; if this is applied to a 500kHz LLC converter, it would take 42% CPU utilization, which means the controller has little spare time for other control functions.

To solve the challenge of the SR driving for high frequency LLC converter, a generalized adaptive SR driving method using ripple counter concept is proposed for high frequency LLC converter. The control scheme and waveform of the proposed method are shown in Fig. 5.5. Compared with the previous adaptive SR driving based on ripple detection, the digital controller does not need to provide the ripple detection function, while a ripple counter is required to be added to the control scheme.

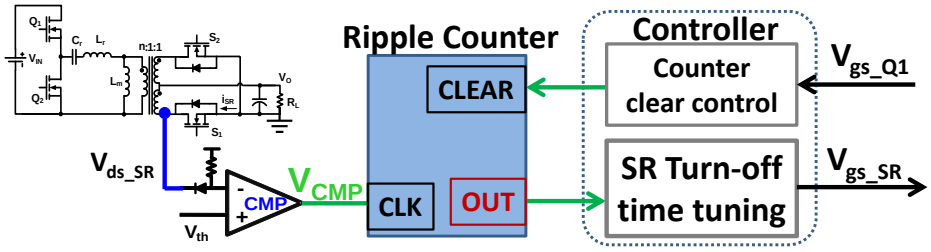

(a)

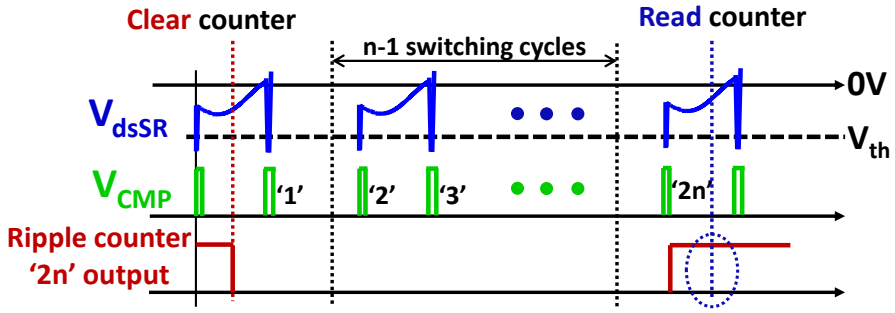

(b)

Fig. 5.5. Proposed adaptive SR driving scheme using ripple counter concept: (a) control scheme; (b) waveforms

By using the ripple counter, the proposed method can tune the SR on-time every $(n+1)^{th}$ switching cycle (n = 1, 2, 3…), as shown in Fig. 5.5(b). The turn-on time of the SR is still synchronized with the primary switch, so there is always a very small time of body diode conduction at the turn-on moment. The proposed method counts the ripples at the output of comparator to determine if there is extra body diode conduction after the SR turn-off. The controller clears the ripple counter after the SR turn-on of the first switching cycle; then after the SR turn-on of the $(n+1)^{th}$ switching cycle (n = 1, 2, 3 …), the controller reads the ripple counter. If the output is '2n', it means that there is body diode conduction after the SR turn-off. Otherwise, there is no body diode conduction.

The tuning process is shown in Fig. 5.6. The SR tuning cycle is n+1 switching cycles (n = 1, 2, 3…). At the beginning, there is large body diode conduction after SR turn-off, and the ripple counter indicates 2n ripples. So the controller keeps increasing SR on-time. Every n+1 switching cycles, the SR on-time is increased by ΔT, which continues until when the ripple counter indicates that there is only n ripples. Then the controller decreases SR on-time by ΔT. In the next n+1 switching cycles, there are 2n ripples again. Thus, the SR on-time is tuned step-by-step to eliminate the body diode conduction, and finally it's around the optimal point.

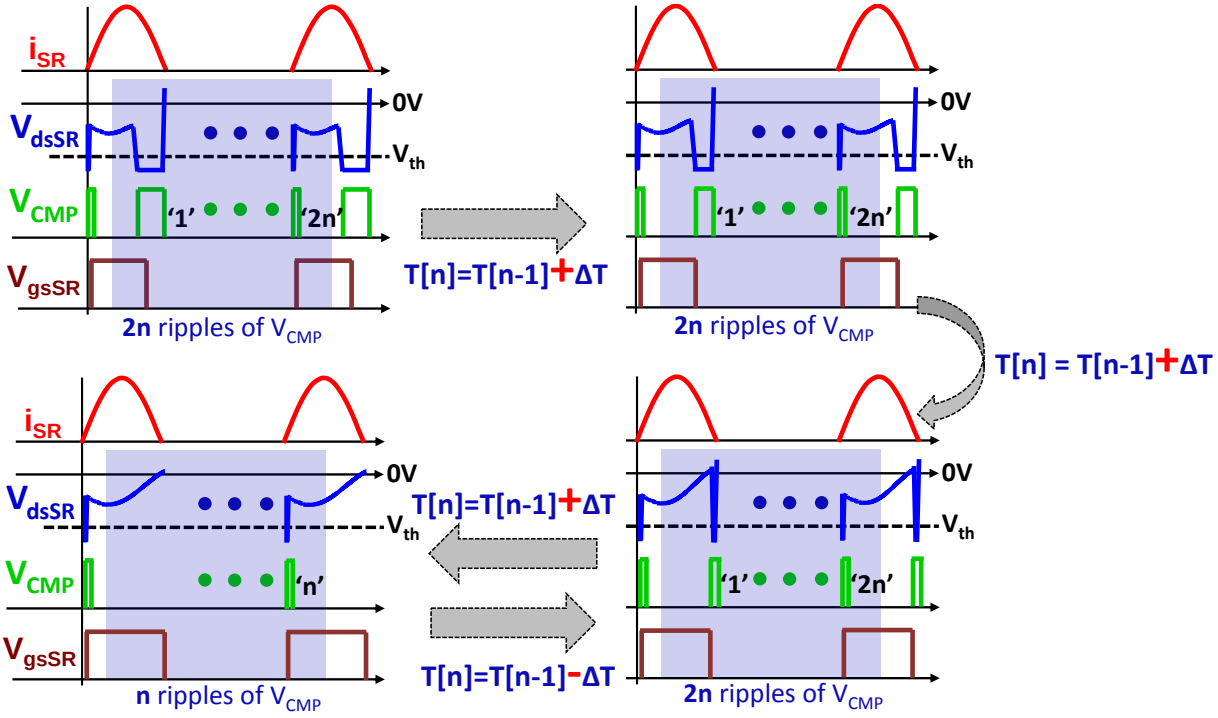

Fig. 5.6.Tuning process of the proposed adaptive SR driving scheme using ripple counter concept

For the proposed generalized adaptive SR driving scheme using ripple counter concept, the ripple counter could be cleared at k^{th} switching cycle in the SR tuning cycle and read at the m^{th} switching cycle in the SR tuning cycle, as long as k < m < n+1 and '$2 \cdot (m-k)$' ripples mean extra body diode conduction after the SR turn-off.

There are two major benefits from the proposed method. The first benefit is that it does not require the digital controller to provide ripple detection function, which means less resources and CPU utilization of the digital controllers. Now every execution of the proposed method takes less than 20 CPU cycles with TI's microcontroller TMS320F28027. The second benefit is that the SR tuning can be selected to be executed every $(n+1)^{th}$ switching cycle to further reduce the CPU utilization. For a 500kHz LLC converter with a 60MHz MCU, if the SR tuning is selected to be executed every third switching cycle, the CPU utilization is significantly reduce to 5%.

5.4 Experimental Results of Adaptive SR Driving

The first proposed adaptive SR driving method based on ripple detection is verified on the 130kHz LLC converter referred in Chapter 2. The experimental waveform is shown in Fig. 5.7. It is shown clearly that the body diode conduction is minimized in steady state.

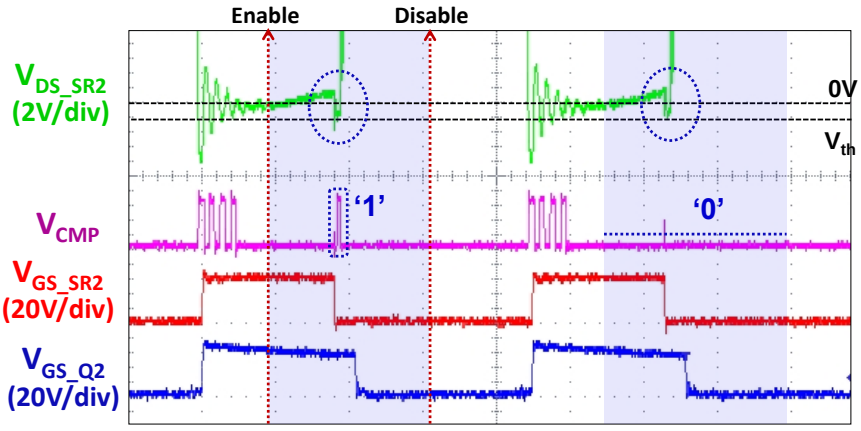

Fig. 5.7. Steady state waveform of the proposed adaptive SR driving method based on ripple detection on the 130kHz LLC converter

The second proposed adaptive SR driving method based on ripple counter concept is verified on the 500kHz LLC converter referred in Chapter 2. The controller is 60MHz microcontroller TMS320F28027.

The tuning process of the proposed adaptive SR driving method based on ripple counter concept on the 500kHz LLC converter is shown in Fig. 5.8. At the beginning, the converter works at burst mode (load = 4A), then load step-up happens, and the converter begins to work at normal operation mode with adaptive SR driving. The initial SR on-time is relatively small, which means body diode conduction time is very large and the adaptive SR driving would tune the SR on-time step-by-step until finally the body diode conduction is around the minimum point.

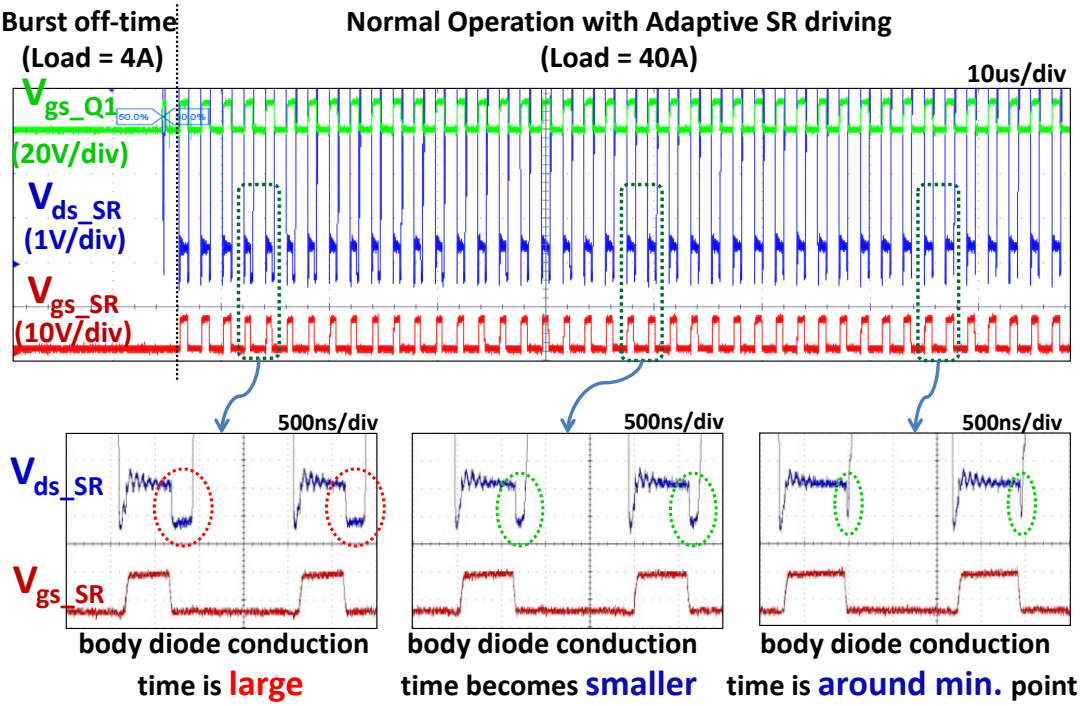

Fig. 5.8. Tuning process of the proposed adaptive SR driving method based on ripple counter concept on the 500kHz LLC converter

5.5 Conclusions

In this chapter, the adaptive SR driving for the LLC converter is investigated and its limitation with digital implementation is explained in detail. The previous adaptive SR driving methods require either additional circuit or high-performance digital controller.

To solve this challenge, the adaptive SR driving method based on ripple detection and the adaptive SR driving method based on ripple counter concept are proposed. The first proposed method is suitable for conventional LLC converter (resonant frequency is below 150kHz). It can be implemented with low-cost digital controllers and very little CPU utilization. The second proposed method is suitable for high frequency LLC converter. With the help of a ripple counter and by tuning SR on-time every $(n+1)^{th}$ switching cycle (n = 1, 2, 3…), it can also be implemented with low-cost digital controllers and minimum CPU utilization.

The first proposed method is verified on a 130kHz LLC converter with 100MHz microcontroller. And the second proposed method is verified on a 500kHz LLC converter with 60MHz microcontroller and a ripple counter. Both methods require little CPU utilization and can stable at around the optimal point.

Chapter 6. Summary and Future Work

The LLC resonant converter is widely used as the DC/DC converter in front-end converter due to its hold-up capability, high efficiency and high power density. And it is becoming more and more popular in other applications. However, there are many challenges in the control of the LLC converter due to the complexity of the resonant tank. The Optimal Trajectory Control (OTC) for LLC resonant converter can solve these challenges, but it requires high-performance digital controllers, which is not feasible for industrial applications.

In this thesis, the digital implementation and limitation of the Optimal Trajectory Control (OTC) for LLC resonant converter is investigated, and OTC is further simplified so that Simplified Optimal Trajectory Control (SOTC) can be achieved with cost-effective digital controllers. Methodology of applying SOTC to high frequency LLC converter with given controller is also provided.

The Simplified Optimal Trajectory Control (SOTC) is investigated and improved to increase the maximum switching frequency limitation for given cost-effective controller. Then the Multi-step Simplified Optimal Trajectory Control (SOTC) is proposed to further increase the maximum switching frequency limitation. The Simplified Optimal Trajectory Control (SOTC) for soft start-up of LLC converter with only sensing Vo is proposed. The Optimal Trajectory Control (OTC) for the burst mode of the LLC converter is investigated and its limitation in the high frequency LLC converter with digital implementation is explained in detail. The Simplified Optimal Trajectory Control (SOTC) for burst mode with adaptive burst on-power and adaptive multi-step is proposed to extend burst operation range. The adaptive SR driving method based on ripple detection and the adaptive SR driving method based on ripple counter concept are proposed. The first proposed method is suitable for conventional LLC converter (resonant frequency is below

150kHz). The second proposed method is suitable for high frequency LLC converter. Both methods can be achieved with low-cost digital controllers and very little CPU utilization.

A complete control system solution based on the concept of the Simplified Optimal Trajectory Control (SOTC) is demonstrated on a 500kHz 1kW 400V/12V LLC converter with 60MHz Microcontroller (MCU) TMS320F28027, which integrates Multi-step SOTC for fast load transient response, SOTC for soft start-up with only sensing Vo, SOTC for burst mode with adaptive multi-step, and adaptive SR driving using ripple counter concept. The whole system resource utilization of the 60MHz MCU for the 500kHz LLC converter is shown in Fig. 6.1.

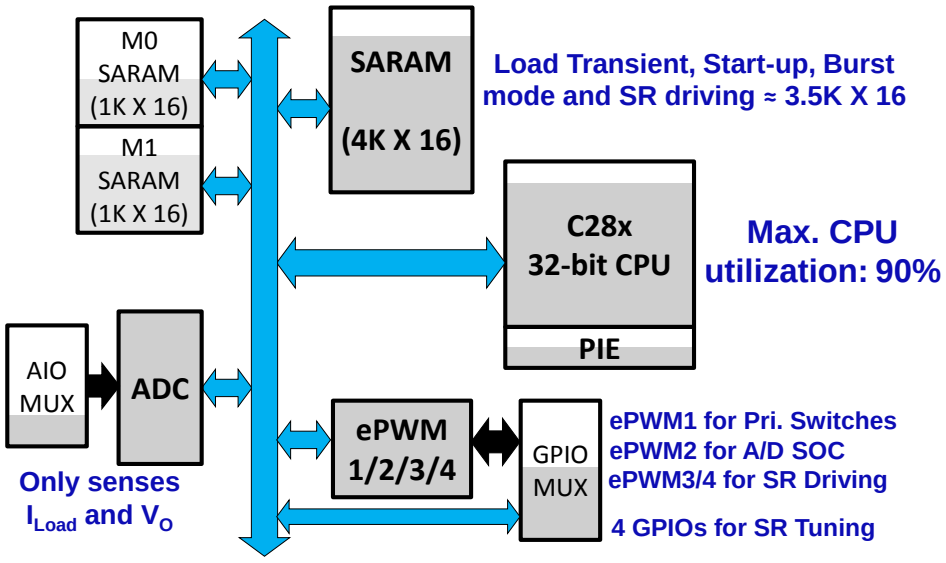

Fig. 6.1. Resource utilization of the 60MHz MCU for the 500kHz LLC converter

The concept of SOTC is calculating trajectory based on output voltage and load current. It is proved to have significant advantages over conventional linear control methods for server power supply application with fixed output voltage requirement.

One aspect of future work is to investigate how to apply SOTC to the applications which have even faster transient response requirement such as LLC converter used as intermediate bus

converter or voltage regulate module with strict transient response requirement. In these applications, the digital delay need to be further minimized to achieve faster response.

Another aspect is the wide output voltage range applications, such as battery charger and telecom power supply. It is necessary to investigate how to optimize SOTC and reduce controller resource utilization for a wide range of output voltage.

Another aspect is to achieve SOTC with mixed-signal controller. By adding some sensing of resonant tank and analog auxiliary circuit, the requirement for digital controller can be further reduced and performance can be improved.

References

[1] W. A. Tabisz, M. M. Jovanovic, and F. C. Lee. "Present and future of distributed power systems." IEEE Applied Power Electronics Conference, 0-7803-0485-3/92. 1992.

[2] G. C. Hua, W. A. Tabisz, C. S. Leu, N. Dai, R. Watson, and F. C. Lee. "Development of a DC distributed power system." In Applied Power Electronics Conference and Exposition, 1994. APEC'94. Conference Proceedings 1994., Ninth Annual, pp. 763-769. IEEE, 1994.

[3] F. C. Lee, P. Barbosa, P. Xu, J. Zhang, B. Yang, and F. Canales. "Topologies and design considerations for distributed power system applications." Proceedings of the IEEE 89, no. 6 (2001): 939-950.

[4] M. M. Jovanović. "Technology Drivers and Trends in Power Supplies for Computer/TELECOM Applications." (2006).

[5] F. C. Lee, S. Wang, P. Kong, C. Wang, and D. Fu. "Power architecture design with improved system efficiency, EMI and power density." In Power Electronics Specialists Conference, 2008. PESC 2008. IEEE, pp. 4131-4137. IEEE, 2008.

[6] A. Pratt, P. Kumar, and T. V. Aldridge. "Evaluation of 400V DC distribution in telco and data centers to improve energy efficiency." In Telecommunications Energy Conference, 2007. INTELEC 2007. 29th International, pp. 32-39. IEEE, 2007.

[7] B. Fortenbery, E. C. EPRI, and W. Tschudi. "DC power for improved data center efficiency." (2008).

[8] D. J. Becker, and B. J. Sonnenberg. "400Vdc power distribution: Overcoming the challenges." In Telecommunications Energy Conference (INTELEC), 32nd International, pp. 1-10. IEEE, 2010.

[9] 80Plus Program [Online]. Available: http://www.plugloadsolutions.com/80PlusPowerSupplies.aspx , Nov. 2014.

[10] D. Reusch, F. C. Lee, D. Gilham, and Y. Su. "Optimization of a high density gallium nitride based non-isolated point of load module." In Energy Conversion Congress and Exposition (ECCE), 2012 IEEE, pp. 2914-2920. IEEE, 2012.

[11] X. Huang, Z. Liu, Q. Li, and F. C. Lee. "Evaluation and application of 600V GaN HEMT in cascode structure." In Applied Power Electronics Conference and Exposition (APEC), 2013 Twenty-Eighth Annual IEEE, pp. 1279-1286. IEEE, 2013.

[12] S. Ji, D. Reusch, and F. C. Lee. "High-frequency high power density 3-D integrated gallium-nitride-based point of load module design." Power Electronics, IEEE Transactions on 28, no. 9 (2013): 4216-4226.

[13] Y. Su, Q. Li, and F. C. Lee. "Design and Evaluation of a High-Frequency LTCC Inductor Substrate for a Three-Dimensional Integrated DC/DC Converter." Power Electronics, IEEE Transactions on 28, no. 9 (2013): 4354-4364.

[14] D. Huang, S. Ji, and F. C. Lee. "LLC resonant converter with matrix transformer." In Applied Power Electronics Conference and Exposition (APEC), 2014 Twenty-Ninth Annual IEEE, pp. 1118-1125. IEEE, 2014.

[15] G. Hua, and F. C. Lee. "Soft-switching techniques in PWM converters." Industrial Electronics, IEEE Transactions on 42, no. 6 (1995): 595-603.

[16] W. Chen, F. C. Lee, M. M. Jovanovic, and J. A. Sabate. "A comparative study of a class of full bridge zero-voltage-switched PWM converters." In Proc. IEEE APEC, vol. 95, pp. 893-899. 1995.

[17] J. G. Cho, J. A. Sabate, G. Hua, and F. C. Lee. "Zero-voltage and zero-current-switching full bridge PWM converter for high-power applications." Power Electronics, IEEE Transactions on 11, no. 4 (1996): 622-628.

[18] W. Chen, P. Xu, and F. C. Lee. "The optimization of asymmetric half bridge converter." In Applied Power Electronics Conference and Exposition, 2001. APEC 2001. Sixteenth Annual IEEE, vol. 2, pp. 703-707. IEEE, 2001.

[19] V. Vorperian. "Analysis of Resonant Converters." PhD dissertation in California Institute of Technology (1984).

[20] F-S. Tsai, and F. C. Lee. "A complete DC characterization of a constant-frequency, clamped-mode, series-resonant converter." In Power Electronics Specialists Conference, 1988. PESC'88 Record., 19th Annual IEEE, pp. 987-996. IEEE, 1988.

[21] R. Liu, and C. Q. Lee. "The LLC-type series resonant converter-variable switching frequency control." In Circuits and Systems, 1989., Proceedings of the 32nd Midwest Symposium on, pp. 509-512. IEEE, 1989.

[22] B. Yang. "Topology investigation for front end DC/DC power conversion for distributed power system." PhD dissertation, Virginia Polytechnic Institute and State University, 2003.

[23] B. Lu. "Investigation of high-density integrated solution for AC/DC conversion of a distributed power system." PhD dissertation, Virginia Polytechnic Institute and State University, 2006.

[24] Y. Liu. "High efficiency optimization of LLC resonant converter for wide load range." M.S. thesis, Virginia Polytechnic Institute and State University, 2007.

[25] D. Fu. "Topology investigation and system optimization of resonant converters." PhD dissertation, Virginia Polytechnic Institute and State University, 2010.

[26] C. Prasantanakorn. "Current Sharing Method for Resonant DC-DC Transformers." M.S. thesis, Virginia Polytechnic Institute and State University, 2011.

[27] B. Yang, F. C. Lee, A. J. Zhang, and G. Huang. "LLC resonant converter for front end DC/DC conversion." In Applied Power Electronics Conference and Exposition, 2002. APEC 2002. Seventeenth Annual IEEE, vol. 2, pp. 1108-1112. IEEE, 2002.

[28] B. Lu, W. Liu, Y. Liang, F. C. Lee, and J. D. Van Wyk. "Optimal design methodology for LLC resonant converter." In Applied Power Electronics Conference and Exposition, 2006. APEC'06. Twenty-First Annual IEEE, pp. 6-pp. IEEE, 2006.

[29] R. J. King, and T. A. Stuart. "Small-signal model for the series resonant converter." Aerospace and Electronic Systems, IEEE Transactions on 3 (1985): 301-319.

[30] E. X. Yang, F. C. Lee, and M. M. Jovanovic. "Small-signal modeling of series and parallel resonant converters." In Applied Power Electronics Conference and Exposition, 1992. APEC'92. Conference Proceedings 1992., Seventh Annual, pp. 785-792. IEEE, 1992.

[31] E. X. Yang, F. C. Lee, and M. M. Jovanovic. "Small-signal modeling of LCC resonant converter." In IEEE power electronics specialists conference, pp. 941-941. INSTITUTE OF ELECTRICAL ENGINEERS INC (IEE0, 1992.

[32] B. Yang, F. C. Lee, and M. M. Jovanovic. "Small-signal analysis for LLC resonant converter." In CPES Seminar, vol. 7, pp. 144-149. 2003.

[33] Y. Jang, and M. M. Jovanovic. "Light-load efficiency optimization method." Power Electronics, IEEE Transactions on 25, no. 1 (2010): 67-74.

[34] X. Zhang, and D. Maksimovic. "Digital PWM/PFM controller with input voltage feed-forward for synchronous buck converters." In Applied Power Electronics Conference and Exposition, 2008. APEC 2008. Twenty-Third Annual IEEE, pp. 523-528. IEEE, 2008.

[35] J. Sun, M. Xu, Y. Ren, and F. C. Lee. "Light-load efficiency improvement for buck voltage regulators." Power Electronics, IEEE Transactions on 24, no. 3 (2009): 742-751.

[36] B. Wang, X. Xin, S. Wu, H. Wu, and J. Ying. "Analysis and implementation of LLC burst mode for light load efficiency improvement." In Applied Power Electronics Conference and Exposition, 2009. APEC 2009. Twenty-Fourth Annual IEEE, pp. 58-64. IEEE, 2009.

[37] R. Oruganti, and F. C. Lee. "Resonant Power Processors, Part I---State Plane Analysis." Industry Applications, IEEE Transactions on 6 (1985): 1453-1460.

[38] R. Oruganti, and F. C. Lee. "Resonant power processors, Part II-Methods of control." Industry Applications, IEEE Transactions on 6 (1985): 1461-1471.

[39] R. Oruganti, J. J. Yang, and F. C. Lee. "Implementation of optimal trajectory control of series resonant Converter." Power Electronics, IEEE Transactions on 3, no. 3 (1988): 318-327.

[40] W. Feng, F. C. Lee, and P. Mattavelli. "Simplified optimal trajectory control (SOTC) for LLC resonant converters." Power Electronics, IEEE Transactions on 28, no. 5 (2013): 2415-2426.

[41] W. Feng, and F. C. Lee. "Optimal Trajectory Control of LLC Resonant Converters for Soft Start-Up." Power Electronics, IEEE Transactions on 29, no. 3 (2014): 1461-1468.

[42] W. Feng, F. C. Lee, and P. Mattavelli. "Optimal trajectory control of burst mode for LLC resonant converter." Power Electronics, IEEE Transactions on 28, no. 1 (2013): 457-466.

[43] H. De Groot, E. Janssen, R. Pagano, and K. Schetters. "Design of a 1-MHz LLC resonant converter based on a DSP-driven SOI half-bridge power MOS module." *Power Electronics, IEEE Transactions on* 22, no. 6 (2007): 2307-2320.

[44] Z. Hu, Y. Qiu, L. Wang, and Y. Liu. "An interleaved LLC resonant converter operating at constant switching frequency." In *Energy Conversion Congress and Exposition (ECCE), 2012 IEEE*, pp. 3541-3548. IEEE, 2012.

[45] J. Jung, H. Kim, J. Kim, M. Ryu, and J. Baek. "High efficiency bidirectional LLC resonant converter for 380V DC power distribution system using digital control scheme." *In Applied Power Electronics Conference and Exposition (APEC)*, 2012 Twenty-Seventh Annual IEEE, pp. 532-538. IEEE, 2012.

[46] C. Adragna, A. V. Novelli, and C. L. Santoro. "Charge-mode control device for a resonant converter." U.S. Patent No. 8,699,240. 15 Apr. 2014.

[47] J. Jang, M. Joung, S. Choi, Y. Choi, and B. Choi, "Current mode control for LLC series resonant DC-to-DC converters," in *Proc. IEEE Appl. Power Electron. Conf*., Mar. 2011, pp. 21–27.

[48] Z. Hu, Y. F. Liu and P. C. Sen, " Bang-Bang charge control for LLC resonant converters.." *Power Electronics, IEEE Transactions on.*, VOL. 30, NO. 2, pp. 1093-1108 , Feb. 2013.

[49] NXP Semiconductors, (Sep. 2011). AN10881: TEA1713 resonant power supply control IC with PFC [online]. Available: http://www.nxp.com/documents/application_note/AN10881.pdf

[50] STMicroelectronics, (Feb. 2009). L6599: High-voltage resonant controller [online]. Available: http://www.st.com/st-web-ui/static/active/en/resource/technical/document/datasheet/CD00108892.pdf

[51] Texas Instruments, (Jul., 2011). UCC25600: 8-Pin High-Performance Resonant Mode Controller [online]. Available: http://www.ti.com/lit/ds/symlink/ucc25600.pdf

[52] Infineon Technologies AG, (May, 2011). ICE2HS01G: High Performance Resonant Mode Controller [online]. Available: http://www.infineon.com/dgdl/Infineon-ICE2HS01G-DS-v02_01-en.pdf?fileId=db3a30432a40a650012a458289712b4c

[53] X. Xie, J. Liu, F. N. K. Poon, and M. Pong, "A novel high frequency current-driven SR applicable to most switching topologies," *IEEE Trans. Power Electron.*, vol. 16, no. 5, pp. 635–648, Sep. 2001.

[54] D. Huang, D. Fu, and F. C. Lee, "High switching frequency, high efficiency CLL resonant converter with synchronous rectifier," In *Proc. IEEE Energy Convers. Congr. Expo.*, 2009, pp. 804–809.

[55] X. Wu, G. Hua, J. Zhang, and Z. Qian, "A new current-driven synchronous rectifier for series–parallel resonant (LLC) DC-DC converter," *Industrial Electronics, IEEE Transactions on*, vol. 58, no. 1, pp. 289–297, Jan. 2011.

[56] NXP Semiconductors, "TEA1795T: GreenChip synchronous rectifier controller" (Nov. 2010). [Online]. Available: http://www.nxp.com/documents/data_sheet/TEA1795T.pdf

[57] International Rectifier, "IR11682S: DUAL SmartRectifier DRIVER IC" (Jul. 2011). [Online]. Available: http://www.irf.com/product-info/datasheets/data/ir11682spbf.pdf

[58] STMicroelectronics, "Synchronous rectifier smart driver for LLC resonant converters" (Aug. 2013). [Online]. Available: http://www.st.com/st-web-ui/static/active/en/resource/technical/documen t/datasheet/CD00282226.pdf

[59] D. Fu, Y. Liu, F. C. Lee, and M. Xu, "A novel driving scheme for synchronous rectifiers in LLC resonant converters," *Power Electronics, IEEE Transactions on*, vol. 24, no. 5, pp. 1321–1329, May 2009.

[60] L. Cheng, T. Liu, H. Gan, and J. Ying, "Adaptive synchronous rectification control circuit and method thereof," U.S. Patent 7.495.934, Feb. 24, 2009

[61] W. Feng, F. C. Lee, P. Mattavelli, and D. Huang, "A universal adaptive driving scheme for synchronous rectification in LLC resonant converters," *Power Electronics, IEEE Transactions on*, vol. 27, no. 8, pp.3775-3781, Aug. 2012